Characterization of human breast cancer cells affected by coculture conditions and kisspeptin-10

Doctoral Thesis

In partial fulfillment of the requirements for the degree

"Doctor rerum naturalium (Dr. rer. nat.)"

in the Molecular Medicine Study Program

at the Georg-August University Göttingen

submitted by

Elke Ziegler

born in Darmstadt, Germany

Göttingen, March 2013

Thesis Committee

Supervisor

Prof. Dr. Carsten Gründker

Department of Gynecology and Obstetrics
Laboratory for Molecular Gynecology
University Medicine Göttingen

Second member of the thesis committee

Prof. Dr. Matthias Dobbelstein

Department of Molecular Oncology
Georg-August University Göttingen

Third member of the thesis committee

Prof. Dr. Sigrid Hoyer-Fender

Department of Developmental Biology
Georg-August University Göttingen

Date of Disputation:

Affidavit

I hereby declare that my doctoral thesis entitled "Characterization of human breast cancer cells affected by coculture conditions and kisspeptin-10" has been written independently with no other sources and aids than quoted.

_____

Elke Ziegler

Göttingen, March 2013

Publications

E. Ziegler, T. Olbrich, G. Emons, and C. Gründker. Antiproliferative effects of kisspeptin-10 depend on artificial GPR54 (KISS1R) expression levels. *Oncol Rep*, 29(2):549-554, Feb 2013.

T. Olbrich, E. Ziegler, G. Türk, A. Schubert, G. Emons, and C. Gründker. Kisspeptin-10 inhibits bone-directed migration of GPR54-positive breast cancer cells: Evidence for a dose–window effect. *Gynecol Oncol,* 119(3):571–578, Dec 2010.

Congress participations

126th Meeting of the North German Society for Gynecology and Obstetrics 2010, Schwerin (Germany)

Poster: E. Ziegler, T. Olbrich, G. Emons, and C. Gründker. Der Einfluss von Kisspeptin-10 auf die Expression migrationsrelevanter Gene beim Mammakarzinom (Influence of kisspeptin-10 on gene expression of genes involved in migration in breast cancer).

34th Annual Meeting of the German Society for Cell Biology 2011, Bonn (Germany)

Poster: E. Ziegler, T. Olbrich, G. Emons, and C. Gründker. EMT marker expression in breast cancer cells during bone-directed migration.

30th German Cancer Congress of the German Cancer Society 2012, Berlin (Germany)

Poster: E. Ziegler, G. Emons, and C. Gründker. Kisspeptin-10 reduces tumor growth and metastasis in a breast cancer model in vivo.

128th Meeting of the North German Society for Gynecology and Obstetrics 2012, Kiel (Germany)

Poster: E. Ziegler, T. Olbrich, G. Emons, and C. Gründker. Die antiproliferative Wirkung von Kisspeptin-10 ist abhängig vom GPR54-Expressionsstatus (Antiproliferative effects of kisspeptin-10 depend on GPR54 expression levels).

Contents

Acknowledgments

Abstract

Breast cancer is the most common type of cancer in women. Lethality is mainly attributed to a severe metastatic spread in patients. Research in new therapeutic treatments demands the understanding of the metastatic processes and the interaction of tumor cells with the distant organ microenvironment. Therefore, a coculture cell system was studied on relations between human breast cancer cells and osteoblast-like osteosarcoma cells mimicking an important metastasis environment in bone. Kisspeptin-10, a peptide derived from the metastasis suppressor gene KISS1, interferes within this cell system by inhibition of invasion. An influence of kisspeptin-10 *in vivo* was further investigated to evaluate its effect as a possible therapeutic option in the metastatic breast cancer disease.

Human breast cancer cells were classified by morphology, motility marker expression and their individual invasiveness. In coculture, epithelial-like cells showed a dramatic increase in invasion. Microarray gene analysis revealed potential factors of cell motility processes and immune response mechanisms, which were regulated by the interaction of breast cancer cells and osteosarcoma cells. An involvement of EMT was shown partially by upregulation of mesenchymal gene markers without an altered epithelial marker expression. CXCL12 was identified as one important factor in invasive progression: the "coculture effect" may trigger invasion by an autocrine CXCL12/CXCR4 loop. Factors as EGF and interferons are possible new targets of investigations on the interaction of breast cancer cells and osteosarcoma cells.

Kisspeptin-10 was studied in breast cancer xenografts for an influence on metastatic spread and tumor growth. Treatment with the peptide inhibited tumor growth. But investigations on cell proliferation *in vitro* revealed no antiproliferative effect. The role of kisspeptin-10 in angiogenetic processes is an interesting option as possible mechanism leading to decreased tumor size in treated animals. A conclusion could not be offered on an antimetastatic effect of kisspeptin-10 as possible therapeutic option in breast cancer based on the poor metastasis model in mice.

List of figures

List of tables

List of abbreviations

Ala	alanine
APS	ammonium persulfate
Arg	arginine
Asn	asparagine
BRCA	breast cancer (proteins)
BSA	bovine serum albumin
BW	body weight
Ca^{2+}	calcium ion
CAF	cancer-associated fibroblast
CAT	collective to amoeboid transition
CD44	cluster of differentiation 44
CDH1	cadherin 1, epithelial cadherin
CDH2	cadherin 2, neuronal cadherin
cDNA	complementary DNA
CIS	carcinoma *in situ*
CO_2	carbon dioxide
COX-2	cyclooxygenase 2
CSF1	colony stimulating factor 1
CTC	circulating tumor cell
CTGF	connective tissue growth factor
CXCL12 (SDF-1)	chemokine (C-X-C motif) ligand 12 (stromal cell derived factor 1)
CXCR4	chemokine (C-X-C motif) receptor 4
DCIS	ductal carcinoma *in situ*
DKP-10	DK6-Kisspeptin-10
DMEM	Dulbecco's Modified Eagle Medium
DMSO	dimethyl sulfoxide
DNA	deoxyribonucleic acid
dNTPs	deoxyribonucleotides
(D)PBS	phosphate buffered saline
DTC	disseminated tumor cell

DTT	dithiothreitol
ECM	extracellular matrix
EDTA	ethylenediaminetetraacetic acid
EGF	epidermal growth factor
EMT	epithelial to mesenchymal transition
ER	estrogen receptor
ERK1/2	extracellular signal regulated kinases 1/2
ET1	endothelin 1
EtOH	ethanol
FAK	focal adhesion kinase
FC	fold change
FCS	fetal calf serum
FGF	fibroblast growth factor
FN1	fibronectin 1
Gly	glycine
GPR	G-protein coupled receptor
GRK2	GPR serine/threonine kinase 2
GSK3β	glycogen synthase kinase 3β
HCl	hydrochloric acid
hDNA	human deoxyribonucleic acid
HER2	human epidermal growth factor receptor 2
HGF	hepatocyte growth factor
H_2O	water
H_2O_2	hydrogen peroxide
IFIT	interferon induced protein with tetratricopeptide repeats
KCl	potassium chloride
KP-10	kisspeptin-10
L7	ribosomal protein L7
LCIS	lobular carcinoma *in situ*
IGF	insulin-like growth factors
Leu	leucine
MAP	mitogen activated protein
MAT	mesenchymal to amoeboid transition
mDNA	murine deoxyribonucleic acid
MEM	minimum Essential Medium
MeOH	methanol
mGPR	murine G-protein coupled receptor
MMP	matrix metalloproteinase

NaCl	sodium chloride
OAS	2'-5'-oligoadenylate synthetase
NaOH	sodium hydroxide
PAGE	polyacrylamide gel electrophoresis
PARP9	poly (ADP-ribose) polymerase 9
PCR	polymerase chain reaction
PDGF	platelet derived growth factor
Phe	phenylalanine
PIP_2	phosphatidylinositol 4,5-bisphosphate
PLC	phospholipase C
PR	progesterone receptor
PTHrP	parathyroid hormone-related protein
qPCR	quantitative polymerase chain reaction
Rac	Ras-related C3 botulinum toxin substrate
RANKL	receptor activator of nuclear factor kappa-B ligand
Rho	Ras homolog gene family
RNA	ribonucleic acid
ROCK	Rho-associated protein kinase
S100A4 (FSP1)	S100 calcium binding protein A4 (fibroblast-specific protein-1)
SDS	sodium dodecyl sulfate
SEM	standard error of the mean
SER	serine
SerpinE2	serpin peptidase inhibitor, clade E, member 2
SPARC (ON)	secreted protein, acidic, cysteine-rich (osteonectin)
STAT1	signal transducer and activator of transcription 1
TACC1	transforming acidic coiled-coil containing protein 1
TAM	tumor associated macrophage
TBE	Tris-borate-EDTA buffer
TBS	tris buffered saline
TBST	tris buffered saline tween
TCF21	transcription factor 21
TEMED	tetramethylethylenediamine
$TGF\beta_1$	transforming growth factor β_1
TJP1 (ZO1)	tight junction protein 1 (zona occludens 1)
TNF	tumor necrosis factor
Trp	tryptophan
Tyr	tyrosine
UV	ultraviolet light

VCAM-1	vascular cell adhesion protein 1
VEGF	vascular endothelial growth factor
VIM	vimentin
YWHAZ	14-3-3 protein zeta/delta

1 Introduction

1.1 Breast cancer

1.1.1 Epidemiology and etiology

Breast cancer is the most occurrent type of cancer in women with an incidence of 23 % of all cancers in the female population worldwide in 2008. Over the last decades, mortality rates were continuously decreasing to approximately 6-19 per 100,000 cases by improved therapies and an optimized screening especially in the developed countries [Ferlay et al., 2010]. In Germany, about 72,000 women contract with breast cancer every year and the mortality was about 17,000 in 2008. Most of the patients are of 60-70 years of age, when cancer was diagnosed. The absolute 5-years overall survival is about 78 % [RKI. Robert Koch-Institut, 2012].

The main risk factors for the disease are an older age, an early age at menarche and a late age at menopause. Childlessness or age at first birth of 40 years and more are also associated with breast cancer. In addition, there is evidence that breast density is a strong risk factor. The risk of diagnosis raises by an extended use of hormone-replacement therapies in the climacteric period, whereas the risk by using oral contraceptives is almost reversible after ten years of stopping the taking. General obesity together with low physical activity, alcohol consumption and smoking seems to be involved in a higher risk of breast cancer diagnosis. Genetic factors as mutations in the breast cancer (BCRA) genes are involved in less than 10 % of the cases. Having relatives suffering from breast cancer is another risk factor for the disease [WHO. World Health Organization, 2003, Veronesi et al., 2005, RKI. Robert Koch-Institut, 2012].

1.1.2 Classification and etiopathology

Breast cancer is classified by its histopathologic appearance in carcinoma *in situ* (CIS) and invasive carcinoma. CIS is differentiated in ductal (DCIS) and lobular (LCIS) depending on its origin. Both types are associated with the invasive kind of breast cancer and are considered as precancerous.

Invasive carcinoma is defined as a malignant tumor penetrating partly or completely the basement membrane of the site of origin [WHO. World Health Organization, 2002].

Prognosis and treatment of patients suffering from breast cancer is addicted to time-dependent variables influencing tumor stage and intrinsic characteristics related to the inherent biology of the individual tumor. The stage of the tumor is characterized by the histological tumor size (T) and the existence and dimension of lymph node (N) and systemic metastasis (M) classified as TNM status. The intrinsic aspects describe the histological grade by evaluating tubule and gland formation, nuclear pleomorphism and mitotic counts (grade 1: well differentiated, grade 2: moderately differentiated, grade 3: poorly differentiated), the histological tumor type and molecular properties as receptor status of the hormone and growth factor receptors, estrogen receptor (ER), progesterone receptor (PR) and human epidermal growth factor receptor 2 (HER2), and the presence of Ki-67 as a marker for cell proliferation [WHO. World Health Organization, 2002, Veronesi et al., 2005]. Knowledge of these factors enables a classification by the intrinsic subtypes of breast cancer in luminal A, luminal B (HER2 positive/negative), HER2 positive (non-luminal) and triple negative (ductal)/basal-like (see table 1.1).

Intrinsic subtype	Definition		
luminal A	ER and/or PR positive	HER2 negative	Ki67 low
luminal B (HER2 negative)	ER and/or PR positive	HER2 negative	Ki67 high
luminal B (HER2 positive)	ER and/or PR positive	HER2 overexpressed	any Ki67
HER2 positive (non-luminal)	no ER and/or PR	HER2 overexpressed	
triple negative (ductal)/basal-like	no ER and/or PR	HER2 negative	

Table 1.1: Intrinsic subtypes of breast cancer
Definitions of the intrinsic subtypes of breast cancer by Goldhirsch et al. 2011, modified.

Lethality is mainly depending on the grade of the tumor showing a 90 % death rate within eight years of diagnosis in patients with grade 3 tumors, within 13 years in patients with grade 2 tumors and within 30 years in patients with grade 1 tumors. A less differentiated tumor seems to be an important factor for a systemic metastatic disease and the risk of death is mainly based on the extend of metastasis rather than on the characteristics of the primary tumor [WHO. World Health Organization, 2002].

The breast cancer disease is characterized by a high rate of metastases. The primary tumor is the second common primary cancer with more than 11 % of all cancers and causes the most metastatic sites with up to 24 % of all metastases. The ratio of metastases per primary tumor is more than five. The preferred organs for metastasis are lymph nodes, lung, liver and bone. According to the great number of metastases, treatment of the breast cancer disease is difficult. Thus, the major cause of death for breast cancer patients is related to their individual systemic disease [Disibio and French, 2008].

1.1.3 Therapy

Therapeutic options for breast cancer treatment cover surgery, radiotherapy and systemic treatments. Surgeries with breast-conserving strategies are a common treatment for cancers having a restricted size. Large primary tumors are often reduced in size by primary chemotherapy before removal. The surgery is often followed by a postoperative radiotherapy. Systemic treatments are differentiated in cytotoxic chemotherapy consisting of mainly anthracyclines and taxanes, endocrine therapy with aromatase inhibitors, tamoxifen as competitive ER-antagonist and GnRH-analogs, and therapies against molecular targets as HER2 with trastuzumab as antibody against the receptor [Veronesi et al., 2005, DKG. Deutsche Krebsgesellschaft. DGGG. Deutsche Gesellschaft für Gynäkologische und Geburtshilfe, 2012]. The kind of therapy is dependent on the intrinsic subtype (see chapter 1.1.2). ER and/or PR positive tumors are treated primarily with an endocrine therapy, optionally supported by a cytotoxic regime. ER and/or PR negative tumors get a cytotoxic therapy. All of the HER2 positive tumors are treated with an anti-HER2 therapy [Goldhirsch et al., 2011].

During therapy of metastatic breast cancer, additional treatment of bone metastases can be carried out by surgery, radiotherapy or therapy with bisphosphonates and receptor activator of nuclear factor kappa-B ligand (RANKL)-inhibitors [DKG. Deutsche Krebsgesellschaft. DGGG. Deutsche Gesellschaft für Gynäkologische und Geburtshilfe, 2012].

1.2 Metastasis

Cancer diseases are often characterized by primary tumors and secondary tumor sites formed by metastasizing tumor cells. Mechanisms, which allow tumor cells to arise from a solid tumor, disseminate and colonize distant organs, are summarized as metastatic processes. The earliest hypothesis on metastasis, the "seed and soil" hypothesis, was proposed by Paget in 1889 describing a cross-talk between selected tumor cells, the "seed", and specific organ microenvironments, the "soil". Metastatic processes require both, the intrinsic properties of the tumor cells and the response of the host environment for efficient metastasis [Paget, 1889]. Later studies improved this hypothesis by differentiating three principles: tumor cells and host cells are both forming primary tumors and metastases, metastasis includes different mechanisms all necessary for building metastases and metastasis is depending on the organ microenvironment [Fidler, 2003].

The focus of the following information is based on the distant metastasis processes. Regional metastasis commonly depends on mechanical and anatomical conditions.

1.2.1 Metastasis cascade

Metastasis is a multi-step process. First, tumor cells have to break through the cell structure of the solid primary tumor before they can invade the extracellular matrix (ECM) and connecting cell layers. The metastatic cells intravasate into blood and lymphatic vessels. There, they are transported through the vasculature. Before they extravasate into distant organ tissue, the cells adhere to the vessels. The metastatic cells have to adapt to the microenvironment of the local tissue. Then, they proliferate and form micrometastases. By developing a vascular network, the metastases grow and are clinically detectable after time [Fidler, 2003, Valastyan and Weinberg, 2011]. This process is illustrated in figure 1.1.
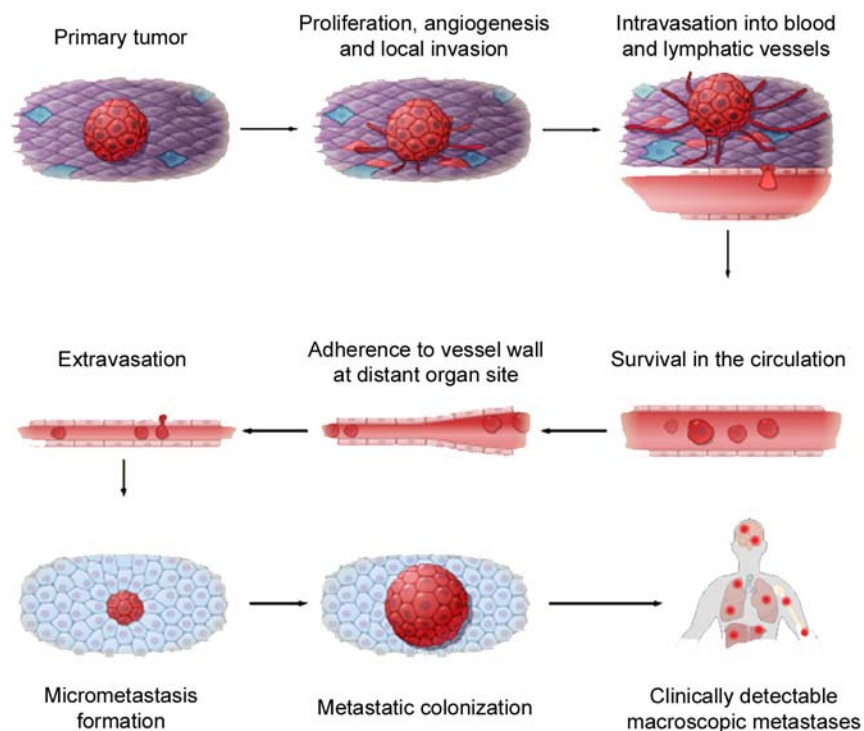
Figure 1.1: Metastasis cascade
The invasion-metastasis cascade describes the exit of tumor cells from the primary site by local invasion and intravasation, the systemic translocation requiring survival in the circulation, adaption to distant tissues by extravasation and metastases formation [Valastyan and Weinberg, 2011], modified.

The metastasis cascade covers some very complex and insufficient processes. Local invasion of single tumor cells requires the ability to defy the barriers of normal epithelium of the surrounding tissue. Different kinds of cellular invasion are possible (see chapter 1.2.3). Intravasation depends on the structural properties of the vessels. The tumor itself releases diverse growth factors to extend its vascular supply. This process is called neoangiogenesis. The formed vessels show differences compared to physiological vasculature. They are more permeable and leaky and allow an easier intravasation. When the cells reach the circulation, they have to survive the transport.

Normally, the adhesion to the ECM is essential for epithelial cells and loss of this interaction leads physiologically to apoptosis. In addition, the circulating tumor cells (CTCs) are exposed to hemodynamic shear forces and cells of the immune system. The CTCs have to overcome these conditions, for example by passing the blood stream only for a short time or by masking themselves by interaction with blood platelets in order to arrive at distant organs. The location of settlement of the CTCs is not arbitrary. Arrest at distant sites can be influenced by physical conditions as limited diameters of the vessels or by interaction of liberated molecules of the target tissue with the CTCs and directed "homing" (see chapter 1.2.4). Extravasation of the disseminated tumor cells (DTCs) is characterized by the properties of the cells and the site of metastasis. Tissue as bone or liver are more permeable for penetrating, whereas extravasation into the brain requires overcoming the blood-brain barrier. Thus, the tumor cells need different mechanisms to enter distant organs. After extravasation, the tumor cells have to adapt to the foreign microenvironment to survive and form micrometastases. The microenvironment of the distant organ itself can be changed by factors released by the primary tumor to optimize the settlement of the DTCs. For further proliferation and colonization of the metastases, the target tissue and the tissue of the primary tumor are important. Macrometastases can only develop, if the interaction of host and occupying cells facilitates the active growth of metastases. Most of the DTCs remain dormant by either attrition or a continuous proliferation which does not exceed the apoptotic rate of the micrometastases [Valastyan and Weinberg, 2011].

The metastasis cascade is are very inefficient process and it needs continuous changes of physiological cellular behavior to generate clinically detectable macrometastases.

1.2.2 Progression of metastasis

The dissemination process of tumor cells leading to a systemic disease is mainly described by two models: the linear progression model and the parallel progression model. The major difference between these models is the temporal development and the beginning of metastasis and dissemination.

The linear progression model describes a late dissemination of tumor cells at distant organs. Development of aggressive tumor cells takes place within the primary tumor of advanced cancers by mutation and selection processes. When these tumor cell clones reach an autonomous growth as a small fraction of fully malignant cells, they are able to leave the primary tumor and colonize at distant sites [Hunter et al., 2008]. Evidence for this model is given by a correlation between tumor size and frequency of metastasis as basis of the TNM classification system (see chapter 1.1.2). The death rates of patients with T2 tumors is higher than of patients with T1 tumors [Klein, 2009].

The parallel progression model defines an early dissemination of tumor cells. Premalignant cells

disseminate to distant sites before and during the primary tumor develops. All of the cells expand genetic and epigenetic changes independently and in parallel. They show discrepancies in their gene expression profiles. Diagnosis of metastases in early stage cancers and cancer diseases of unknown primary sites are evident for this progression model [Pantel and Brakenhoff, 2004, Klein, 2009].

Progression of metastasis shows various clinical events which can not be described by one single model. The individual aspects of metastasis can be explained by either the linear or the parallel progression model but not for cancer metastasis in general.

1.2.3 Motility mechanisms of cells

One initial step of the metastasis cascade (see chapter 1.2.1) is dissemination of tumor cells. Therefore, changes of the cellular plasticity have to be performed to gain motile cells which can invade into the circulating system. Different kinds of motility mechanisms are known: migration of single cells via mesenchymal-like or amoeboid-like migration and collective cell migration. The choice of migration mode is depending on present cell-cell and cell-matrix adhesions, ability of ECM remodeling and the constitution of the surrounding ECM.

Mesenchymal and amoeboid migration of individual cells is characterized by a loss of cell-cell adhesions. Mesenchymal-like cells have a polarized cell structure and a spindle-shaped and fibroblast-like morphology. They are able to form cell-matrix interactions by integrins and cytoskeletal protrusions. These cells move by pulling of an ECM substrate via generation of traction forces. Thereby, they interact with focal adhesions in the front of the cell and contractions of the retraction fibres in the cell tail. Invasion through the ECM is afforded by proteolysis with matrix metalloproteinases (MMPs) (see figure 1.2). In contrast, cell migration in an amoeboid-like manner lacks focal adhesions and stress fibres. The rounded cells move without cell-matrix adhesions by cytoskeletal contractions in a "push-and-squeeze" type. Cell propulsions allow a forward pushing of the cell body through gaps in the ECM without its proteolytic degradation (see figure 1.2). Collective migration is characterized by migrating cell clusters with active cell-cell adhesions. These clusters move by membrane protrusions, integrin-mediated focal adhesions and contractions via the actin-myosin apparatus. The cells use pulling forces on their neighboring cells and keep connection by adherent junctions (see figure 1.2). The collectively migrating cells degrade the ECM for invasion by proteolysis. All kinds of motility mechanisms are described for tumor cells. Single-cell migration is important for metastasis to distant organs whereas collective cell migration is observed during cancer progression by local invasion [Friedl and Wolf, 2010, Yilmaz and Christofori, 2010, Parri and Chiarugi, 2010, van Zijl et al., 2011].

The change from one motility mechanism to another is reversible and dependent on the structure of the ECM, the availability of proteases for remodeling the surrounding tissue and the existence

of cell-cell adhesion. These factors can alter during cell movement. In figure 1.2, the different conversions are graphed. Collectively migrating cells can change their motility mode to individual cell migration by epithelial to mesenchymal transition (EMT) to become mesenchymal-like cells or by collective to amoeboid transition (CAT) to become amoeboid-like cells. The reverse processes are named MET for mesenchymal to epithelial transition respectively amoeboid to collective transition (ACT). The conversion of mesenchymal-like cells to amoeboid-like cells is described as mesenchymal to amoeboid transition (MAT) respectively AMT for amoeboid to mesenchymal transition for the reverse process.
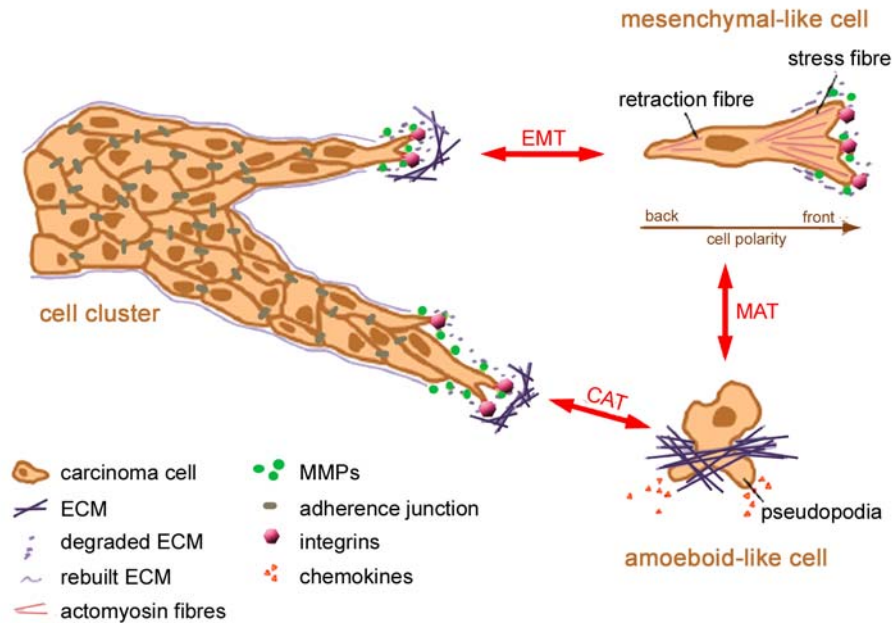
Figure 1.2: Mechanisms of cell invasion

Plasticity of invading cells is illustrated for cell clusters, mesenchymal-like and amoeboid-like cells. The conversions from one mode to another are reversible. EMT, epithelial-mesenchymal-transition; MAT, mesenchymal-amoeboid-transition; CAT, collective-amoeboid-transition; ECM, extracellular matrix; MMPs, matrix metalloproteinases [van Zijl et al., 2011], modified.

EMT is characterized by a loss of epithelial markers important for cell-cell adhesions as epithelial cadherin (CDH1) and an increase in mesenchymal markers as neuronal cadherin (CDH2), the so-called "cadherin-switch", and vimentin (VIM), an intermediate filament. EMT occurs physiologically during implantation, embryogenesis and organ development (type 1 EMT). In addition, EMT is associated with tissue regeneration and organ fibrosis (type 2 EMT). Evidence for a type 3 EMT involved in cancer progression and metastasis is given [Kalluri and Weinberg, 2009].

During MAT and CAT, mesenchymal respectively collective migrating cells become amoeboid-like. These cells show less cell-ECM interactions and invade by squeezing through gaps in the ECM without use of proteases and ECM degradation. CAT is characterized by a loss CDH1-mediated adhesions and develops mainly after integrin inhibition [van Zijl et al., 2011]. MAT is often

induced by reduced Ras-related C3 botulinum toxin substrate (Rac) activity and an increased Ras homolog gene family - Rho-associated protein kinase (Rho/ROCK) signaling. The Rac pathway is responsible for extensions of the leading edge of the cells, for focal adhesions by integrins as basis for mesenchymal-like migration and for an elongated cell morphology. The Rho/ROCK pathway controls actomyosin retractions of the trailing cell edge leading to a nonadhesive amoeboid-like migration and a rounded cell morphology. These two pathway are counterbalancing each other [Friedl and Wolf, 2010, Parri and Chiarugi, 2010, van Zijl et al., 2011].

The kind of cell motility differs depending on the molecular genetics of the tumor cells and the constitution of the surrounding tissue. Thus, changes of the motility mode happen constantly and reversibly.

1.2.4 Microenvironmental dependency of metastatic settlement

With regard to Paget's "seed and soil" hypothesis and clinical observations, evidence is given for a dependency of metastasis to specific organs by certain tumor types. Typical sites of metastases are lung, liver, bone and brain. Some sites of metastatic settlement can be explained by physical and physiological forces as mechanical lodgement of CTCs and high vascularization rates characteristic for liver. But in contrast, the spleen is rarely affected by metastases, while it is also highly vascularized. Additionally, there are millions of tumor cells circulating the blood and less than 0.01 % of the CTCs are successfully forming metastases [Paget, 1889, Fidler, 2003, Mathot and Stenninger, 2012]. Beside these "passive" criteria of metastatic formation, molecular processes as homing in preferential sites and a favorable environment for growth are required for an "active" and selective metastasis. The distant organ site itself and the primary tumor are considered as activators of the conditioning of the so-called "premetastatic/metastatic niche". On the one hand, proinflammatory proteins and chemotactic factors are released of the host organ for promoting the attachment and homing of the CTCs. On the other hand, the primary tumor changes the host microenvironment by signaling factors and CTCs. The CTCs, which were previously arrested at the distant site, can modify the microenvironment for a favorable establishment of metastases by later CTCs [Bidard et al., 2008].

There are some homing mechanisms respectively factors known for metastasizing tumor cells to lung, liver, bone and brain. In lung metastasis, organ specific upregulation of vascular cell adhesion protein 1 (VCAM-1) is described to support metastases growth. Upregulation of cyclooxygenase 2 (COX-2) in the liver leads to a resistance of the immune response of the CTCs and allows a better settlement for liver metastases. An important mechanism in bone metastasis is the chemokine (C-X-C motif) receptor 4/chemokine (C-X-C motif) ligand 12 (CXCR4/CXCL12) interaction. It is characterized by a receptor expression in the tumor cells and a release of CXCL12 at target organs leading to a directed metastasis. Furthermore, the tumor cells are able to release parathy-

roid hormone-related protein (PTHrP), which interacts with the bone formation and resorption processes, leading to better angiogenesis and immune suppression via transforming growth factor β (TGFβ). In metastasis of the brain, the vascular endothelial growth factor (VEGF) seems to be involved in angiogenesis and growth [Mathot and Stenninger, 2012].

1.3 KISS1

The KISS1 gene and its peptides are involved in physiological and pathophysiological mechanisms as neuroendocrine regulation of reproduction, pregnancy and tumor metastasis. The focus of the following work lies in the antimetastatic properties of the gene.

1.3.1 KISS1 and its receptor GPR54

The KISS1 gene was discovered as metastasis suppressor gene. The antimetastatic effect was first identified in vivo. Mice showed less metastases after injection of melanoma and breast cancer cell lines, if cells were transfected with KISS1 [Welch et al., 1994, Lee et al., 1996, Miele et al., 1996, Lee and Welch, 1997a,b]. The KISS1 gene encodes a peptide of 145 amino acids, which is cleaved proteolytically in shorter peptides, the kisspeptins (KP). KP-54, KP-14, KP-13 and KP-10 are characterized by their common amidated C-terminal. The kisspeptins are agonists binding to the KISS1 receptor GPR54. KP-10 shows the highest potency upon the kisspeptins in receptor activation [Kotani et al., 2001, Muir et al., 2001, Ohtaki et al., 2001].

GPR54 is a $G_{q/11}$-protein coupled receptor responsible for phospholipase C (PLC) activation and phosphatidylinositol 4,5-bisphosphate (PIP$_2$) hydrolysis, Ca^{2+} mobilization, arachidonic acid release, extracellular signal regulated kinases 1 and 2 (ERK1/2) and p38 mitogen activated protein (MAP) kinase phosphorylation and stress fibre formation [Kotani et al., 2001, Stafford et al., 2002, Navenot et al., 2005]. The receptor is involved in cell cycle arrest and apoptosis [Becker et al., 2005]. Its signaling is regulated by GPR serine/threonine kinase 2 (GRK2) and β-arrestin [Pampillo et al., 2009, Szereszewski et al., 2010].

The role of KISS1 and GPR54 expression in cancer tissue is not yet clear. In healthy tissue, KISS1 is expressed predominantly in the placenta, testis, pancreas and liver, whereas the receptor is detected mainly in brain, pancreas and placenta [Muir et al., 2001, Ohtaki et al., 2001]. In clinical samples, loss of KISS1 and GPR54 expression correlated with lymph node metastasis in esophageal squamous carcinoma [Ikeguchi et al., 2004]. In ovarian carcinomas, KISS1 and GPR54 expression was associated with a good overall survival [Prentice et al., 2007]. Related results were observed in patients with pancreatic cancer [Nagai et al., 2009] and endometrial cancer [Kang et al., 2011]. Reduced KISS1 mRNA was detected in breast cancer tissue compared to normal

tissue [Mooez et al., 2011]. In contrast, upregulated levels of KISS1 and GPR54 expression led to shorter relapse free survival in breast cancer patients [Martin et al., 2005, Marot et al., 2007]. High GPR54 expression was also found in breast, ovarian, small intestine and colon cancer compared to normal tissue [Ohtaki et al., 2001] and overexpression of KISS1 and GPR54 correlated with hepatocellular carcinoma progression [Ikeguchi et al., 2003]. In summary, there is conflicting data comparing the expression of KISS1 and GPR54 with cancer progression.

1.3.2 Cell motility and metastasis affected by kisspeptins

Several studies in literature show an involvement of the KISS1/GPR54 system in cell motility mechanisms. KISS1 transfection led to reduced invasion and migration in ovarian and gastric carcinoma cells [Jiang et al., 2005, Li et al., 2012]. Treatment with KP-10 showed similar effects in trophoblasts and cancer cell lines as renal, pancreatic, breast and endometrial carcinoma cells [Bilban et al., 2004, Masui et al., 2004, Shoji et al., 2009, Olbrich et al., 2010b, Chen et al., 2011, Kang et al., 2011, Roseweir et al., 2012]. Additionally, invasion of cells transfected to overexpress GPR54 was also inhibited by KP-10 [Hori et al., 2001].

The KISS1/GPR54 system seems to be participating in chemokinetic and chemotactic processes. The activation of GPR54 by KP-10 affects the Rho-ROCK axis leading to changes in the actin cytoskeleton and alterations of the cell shape [Takino et al., 2003, Navenot et al., 2009, Shoji et al., 2009]. Evidence is given for a regulation of focal adhesions by an ERK1/2 - glycogen synthase kinase 3β (GSK3β) - focal adhesion kinase (FAK) feedback loop via EGFR transactivation in trophoblasts by KP-10 and GPR54 [Roseweir et al., 2012]. Chemotactic responses of the CXCR4/CXCL12 system are inhibited by KP-10 treatment in cells transfected with GPR54 and in breast cancer cells with an endogenous GPR54 expression [Navenot et al., 2005, Olbrich et al., 2010b]. Another aspect for the reduced invasion by the KISS1/GPR54 system is a negative regulation of MMP expression [Yan et al., 2001, Yoshioka et al., 2008, Li et al., 2012] (see chapter 1.2.3).

The first experiments on KISS1 identified the gene as metastasis suppressor in xenografts with melanoma cells transfected to overexpress KISS1 [Lee et al., 1996, Lee and Welch, 1997a]. Continuing studies verified the effect in *in vivo* experiments with KISS1 transfected breast, ovarian and pancreatic cancer cells [Lee and Welch, 1997b, Jiang et al., 2005, McNally et al., 2010]. Peripherally administered KP-10 also reduced metastasis in xenografts with melanoma, prostate and endometrial cancer cells [Ohtaki et al., 2001, Cho et al., 2009b, Kang et al., 2011].

1.3.3 Kisspeptin analogs

The kisspeptins are related to the RF-amide family. These peptides share a common Arg-Phe-amide C-terminal and prolactin-releasing peptide and neuropeptide FF belong to this group. The most potent kisspeptin is KP-10. Its amino acid structure is Tyr-Asn-Trp-Asn-Ser-Phe-Gly-Leu-Arg-Phe-NH$_2$. The C-terminal Arg-Phe is critical for its biologic activity at GPR54 [Clements et al., 2001, Kotani et al., 2001, Orsini et al., 2007]. Several kisspeptin analogs were developed. One aim was to enhance the low stability of the kisspeptins and another, to increase the activation potency or antagonize their effects.

Kisspeptins have a very short lifetime especially in serum [Tomita et al., 2008]. This is due to a rapid degradation by MMPs, which inactivate the peptides by cleavage of the Gly-Leu peptide bond in the C-terminal region [Takino et al., 2003]. Gly-Leu isosteres were developed showing a resistance against MMP mediated digestion and a prolonged half-life [Tomita et al., 2008]. Enantiomer changes from L-amino acids to D-amino acids are another possibility to stabilize secondary structures [Curtis et al., 2009].

Receptor activation is mainly based on the five amino acids at the C-terminal [Niida et al., 2006, Gutierrez-Pascual et al., 2009, Roseweir et al., 2009]. A higher potency is reached by replacement of Phe at position ten by Trp. This peptide is known as the murine KP-10 [Clements et al., 2001]. The aromatic group at position six seems to be important for agonistic activity [Tomita et al., 2007, 2006]. A correlation between membrane binding and agonist activity of the peptides was shown [Lee et al., 2009]. Experiments on different structures than analogs of kisspeptin revealed agonistic and antagonistic substances with an peptidic form and also small molecules [Kobayashi et al., 2010, Kuohung et al., 2010].

1.4 Outline of the thesis

One aim of this project was to characterize human breast cancer cell lines according to their behavior in coculture. The experimental setting was established in the laboratory by a former member. Breast cancer cells were cocultivated with osteoblast-like osteosarcoma cells to study a possible interaction of both cell kinds. Coculture conditions led to changes of breast cancer cell invasion properties [von Alten et al., 2006]. In continuing experiments, this effect should be further investigated. Therefore, different breast cancer cell lines were studied in monoculture and coculture for their invasion and migration. Cells were classified morphologically and on molecular levels to identify a possible cell motility mechanisms. The main focus was set upon EMT and additional experiments were done with TGFβ_1, which is known as important activator of EMT processes.

In earlier works, it was shown, that the increased invasion during cocultivation was inhibited by kisspeptin-10, a peptide derived from the metastasis suppressor gene KISS1 [Olbrich et al., 2010b, Olbrich, 2010a]. The coculture system was developed originally as an *in vitro* model to mimic a bone metastasis microenvironment based on the preferred metastasis to bone in breast cancer patients. During this project, it should be checked, if a comparable effect of kisspeptin-10 could be detected in *in vivo* experiments. Studies in literature investigated the antimetastatic effect mainly in xenografts with cancer cells transfected with the KISS1 gene (see chapter 1.3.2). A peripheral administration of kisspeptin was only investigated for melanoma [Ohtaki et al., 2001], prostate [Cho et al., 2009b] and endometrial cancer cells [Kang et al., 2011] and up to date not for a breast cancer xenograft. Therefore, different breast cancer cell lines were used in mouse xenografts. Spontaneous metastasis was studied under treatment with kisspeptin-10 after intracardiac respectively orthotopic tumor cell injection. An effect of kisspeptin-10 on tumor growth was not expected, but observed during the experiments. Thus, further studies on proliferation *in vitro* were carried out to verify an antiproliferative effect of KP-10.

KISS1 and its peptides are an interesting aim of research and the kisspeptins may be a potent tool in treatment of metastatic diseases especially in patients suffering from breast cancer. Further studies on kisspeptin are required with regard to more potent and more stable analogs. Therefore, first experiments with a kisspeptin-10 analog were done *in vitro* under coculture conditions.

2 Material and methods

2.1 Material

2.1.1 Biological substances, chemicals, commercial reagents and kits

The used biological substances, chemicals, commercial reagents and kits are shown in the following tables.

Biological substances	Manufacturer
Bovine serum albumin (BSA)	Sigma, Steinheim, Germany
DK6-Kisspeptin-10; peptide Tyr-Asn-Trp-Asn-Ser-dLys-Gly-Leu-Arg-Phe	PSL, Heidelberg, Germany
Fetal calf serum (FCS)	Biochrom, Berlin, Germany
Fetal calf serum (FCS), charcoal treated	PAN Biotech, Aidenbach, Germany
Instant skimmed milk powder, spray-dried	Saliter, Obergünzburg, Germany
Insulin, Insuman® rapid®	Sanofi-Aventis, Frankfurt, Germany
Kisspeptin-10; peptide Tyr-Asn-Trp-Asn-Ser-Phe-Gly-Leu-Arg-Phe	PSL, Heidelberg, Germany
L-Glutamine	Biochrom, Berlin, Germany
Matrigel^{TM} Basement Membrane Matrix	BD Biosciences, Bedford, MA, USA
Pen Strep, Gibco®	Life Technologies, Darmstadt, Germany
TGFβ1	Sigma-Aldrich, Saint Louis, MO, USA
Trypsin-EDTA (1x)	PAA, Pasching, Austria

Table 2.1: Biological substances

Chemicals	Manufacturer
Agarose, peqGOLD universal	Peqlab, Erlangen, Germany
6-Aminohexanoic acid	Roth, Karlsruhe, Germany
Ammonium persulfate (APS)	AppliChem, Darmstadt, Germany
Boric acid	Roth, Karlsruhe, Germany
Bio-Rad Protein Assay	BIO-RAD, München, Germany
Chloroform	Merck, Darmstadt, Germany
Dimethyl sulfoxide (DMSO)	Merck, Darmstadt, Germany
Ethylenediaminetetraacetic acid (EDTA)	Sigma, Steinheim, Germany
Ethanol (EtOH)	Merck, Darmstadt, Germany
Ethidium bromide	Roth, Karlsruhe, Germany
G418 sulfate	PAA, Pasching, Austria
Glycine	USB, Cleveland, OH, USA
Haematoxylin	Merck, Darmstadt, Germany
holo-Transferrin human	Sigma, Steinheim, Germany
Hydrochloric acid (HCl), 1 M	Merck, Darmstadt, Germany
Hydrogen peroxide (H_2O_2)	Merck, Darmstadt, Germany
Isopropyl alcohol	Th.Geyer, Renningen, Germany
2-Mercaptoethanol	Sigma, Steinheim, Germany
Methanol (MeOH)	Th.Geyer, Renningen, Germany
Sodium hydroxide (NaOH), 1 M	Merck, Darmstadt, Germany
Paraformaldehyde	Roth, Karlsruhe, Germany
Potassium chloride (KCl)	Roth, Karlsruhe, Germany
Sodium chloride (NaCl)	USB, Cleveland, OH, USA
Sodium dodecyl sulfate (SDS)	Merck-Schuchardt, Hohenbrunn, Germany
Tetramethylethylenediamine (TEMED)	BIO-RAD, München, Germany
Tris	USB, Cleveland, OH, USA
Tween	Sigma, Steinheim, Germany

Table 2.2: Chemicals

Reagent or kit	Manufacturer
AEC substrate chromogen	Dako, Carpinteria, CA, USA
alamarBlue®	AbD Serotec, Oxford, UK
Aquatex®	Merck, Darmstadt, Germany
CelLytic™ buffer	Sigma, St. Lois, MO, USA
Chromatography paper 3MM Chr	Whatman, GE Healthcare, Freiburg, Germany
DNA Ladder, 100 bp	Life Technologies, Darmstadt, Germany
dNTPs	Roche Diagnostics, Mannheim, Germany
ECL Immobilon® Western	Millipore, Schwalbach
Histostain® Bulk Kit	Life Technologies, Darmstadt, Germany
KAPA2GTM Fast, 2x ReadyMix with Dye	Peqlab, Erlangen, Germany
NucleoSpin® Tissue Kit and Filters	Macherey-Nagel, Düren, Germany
NuPAGE® 4x LDS sample buffer	Life Technologies, Darmstadt, Germany
NuPAGE® 10x sample reducing agent	Life Technologies, Darmstadt, Germany
p(dT)15 primer	Roche Diagnostics, Mannheim, Germany
ProSieve® 50 Gel solution	Lonza, Rockland, ME, USA
Protease Inhibitor	Sigma, St. Lois, MO, USA
Protein Assay Reagent	BIO-RAD, München, Germany
Protein-Marker I and V	Peqlab, Erlangen, Germany
PVDF membranes	Millipore, Billerica, MA, USA
RNase inhibitor, RNasin®	Promega, Madison, WI, USA
RNeasy® Mini Kit	Qiagen, Hilden, Germany
SensiFAST SYBR No-ROX One-Step Kit	Bioline, Luckenwalde, Germany
18S rRNA Control Kit	Eurogentec, Köln, Germany
TaqMan® Universal PCR Master Mix	Life Technologies, Darmstadt, Germany
TriFast™, peqGOLD	Peqlab, Erlangen, Germany

Table 2.3: Commercial reagents and kits

2.1.2 Buffers, solutions and media

Commonly used buffers, solutions and media are shown in the following tables.

Liquid	Receipt or manufacturer
Agarose (1.5 %; 2 %)	1.50 %/2 % (w/v) Agarose in $\frac{1}{2}$x TBE
Ammonium persulfate (APS) (10 %)	10 % (w/v) APS in H_2O
Anode buffer	30 mM Tris, 20 % MeOH in H_2O; pH 10.4
Anode buffer (conc.)	300 mM Tris, 20 % MeOH in H_2O; pH 10.4
Blocking solution	5 % (w/v) instant skimmed milk powder in TBST
Cathode buffer	40 mM 6-aminohexanoic acid, 25 mM Tris, 20 % MeOH in H_2O; pH 9.4
Ethanol (70 %)	70 % (v/v) EtOH in H_2O
Ethidium bromide staining bath	1,72 µM ethidium bromide in H_2O
Hydrogen peroxide (3 %)	3 % (v/v) H_2O_2 in H_2O
Ketamine, Ketavet®	Bayer Animal Health GmbH, Leverkusen, Germany
Kisspeptin-10 solutions	KP-10 (initially dissolved in DMSO) was diluted in water for injection to get the used concentrations for *in vitro* experiments; KP-10 (initially dissolved in DMSO) was diluted in PBS with HAc [10 mM] to get the solutions for *in vivo* experiments
Paraformaldehyde (4 %)	4 % (v/v) paraformaldehyde in H_2O
Phosphate buffered saline (DPBS)	PAN Biotech, Aidenbach, Germany
SDS electrophoresis buffer	25 mM Tris, 192 mM Glycin, 0.1 % (w/v) SDS in H_2O
Sodium chloride (NaCl), 0.9 %	B. Braun Melsungen AG, Melsungen, Germany
Sol B	1.5 M Tris in H_2O; pH 8,8 (HCl)
Sol C	10 % (w/v) SDS in H_2O
Sol D	0,5 M Tris in H_2O; pH 6,8 (HCl)
TBE	8.4 mM Tris, 90 mM boric acid, 2.8 mM EDTA in H_2O
TBS	137 mM NaCl, 2.7 mM KCl, 24.8 mM Tris in H_2O; pH 7.4
TBST	0.1% Tween in TBS
Transfer buffer	25 mM Tris, 192 mM Glycin, 20 % (v/v) MeOH in H_2O
Xylazine, Rompun®	Bayer Animal Health GmbH, Leverkusen, Germany

Table 2.4: Buffers and solutions

Medium	Receipt and manufacturers
Cell culture medium for breast cancer cell lines	MEM with stable glutamine, phenol red (Biochrom, Berlin, Germany) 10 % (v/v) FCS 100 U/ml penicillin and 100 µg U/ml streptomycin 0.05 IU/ml insulin 1 µg/ml transferrin
Cell culture medium for osteosarcoma cell line	DMEM with stable glutamine, phenol red (Gibco®, Life Technologies, Darmstadt, Germany) 10 % (v/v) FCS 100 U/ml penicillin and 100 µg/ml streptomycin
Cell culture medium for transfected B35 cell clones	DMEM with stable glutamine, phenol red (Gibco®, Life Technologies, Darmstadt, Germany) 10 % (v/v) FCS 1 mg/ml G418 sulfate
Experimental medium for breast cancer and osteosarcoma cell lines	DMEM, without phenol red (Gibco®, Life Technologies, Darmstadt, Germany) 10 % (v/v) charcoal treated FCS 100 U/ml penicillin and 100 µg/ml streptomycin 2 µmol/ml L-glutamine
Experimental medium for transfected B35 cell clones	DMEM, without phenol red (Gibco®, Life Technologies, Darmstadt, Germany) 10 % (v/v) charcoal treated FCS 100 U/ml penicillin and 100 µg/ml streptomycin 2 µmol/ml L-glutamine
Freezing medium	Cell culture medium containing 5 % (v/v) DMSO

Table 2.5: Media

2.1.3 Enzymes

Enzyme	Manufacturer
DNase I recombinant, RNase-free	Roche Diagnostics, Mannheim, Germany
RNase A	Qiagen, Hilden, Germany
SuperScript^{TM} II Reverse Transcriptase	Life Technologies, Darmstadt, Germany
Trypsin-EDTA (0,05 %/0,02 % in DPBS)	PAA, Pasching, Austria

Table 2.6: Enzymes

2.1.4 Oligonucleotides

Gene	Sequence	Product length	Use
ALU	sense 5' CAT GGT GAA ACC CCG TCT CTA 3' antisense 5' CC TCA GCC TCC CGA GTA 3'	-	*In vivo* studies, qPCR
ALU probe	5' [YY]-ATT AGC CGG GCG TGG TGG CG-[BHQ-1] 3'	-	*In vivo* studies, qPCR
CDH1	sense 5' ACA TTT CCC AAC TCC TCT CC 3' antisense 5' CAG CCA TCC TGT TTC TCT TTC 3'	222 bp	EMT marker, standard PCR
CXCL12	sense 5' CCG CGC TCT GCC TCA GCG ACG GGA 3' antisense 5' CTT GTT TAA AGC TTT CTC CAG GTA 3'	227 bp	qPCR
FN1	sense 5' TGA AGA GGG GCA CAT GCT GAA C 3' antisense 5' AAT GCC ACG GCC ATA GCA GTA G 3'	178 bp	qPCR
GPR54	sense 5' CGA CTT CAT GTG CAA GTT CGT C 3' antisense 5' CAC ACT CAT GGC GGT CAG AG 3'	82 bp	Breast cancer cell lines, standard PCR
GPR54	sense 5' TGA CCG CCA TGA GTG TGG AC 3' antisense 5' GCG GAG TGG CTG TAG GAC AT 3'	553 bp	GPR54 transfected cell clones, standard PCR
L7	sense 5' AGA TGT ACA GAA CTG AAA TTC 3' antisense 5' ATT TAC CAA GAG ATC GAG CAA 3'	357 bp	Housekeeping gene, standard PCR
MMP2	sense 5' CTC CTG ACA TTG ACC TTG GCA C 3' antisense 5' TCA CAG TCC GCC AAA TGA ACC 3'	150 bp	qPCR
PARP9	sense 5' CAG CAA CAA AAA ACC CAA GAC 3' antisense 5' GAA AGG CAG CCA TAA GGA C 3'	166 bp	qPCR
S100A4	sense 5' TCT CTC CTC AGC GCT TCT TC 3' antisense 5' GCT GTC CAA GTT GCT CAT CA 3'	238 bp/ 239 bp	EMT marker, standard PCR
SPARC	sense 5' TGC TTC GGC ATC AAG CAG AAG G 3' antisense 5' ACA TTG GGG GAA ACA CGA AGG G3'	111 bp	qPCR
TACC1	sense 5' CTC AGC GAA TCA GAC AAG AC 3' antisense 5' TCA TCT CCA AAA CTT CTT GCC 3'	124 bp	qPCR
TCF21	sense 5' CCT TCT CCA GAC TCA AGA CCA C 3' antisense 5' TGG TTC CAC ATA AGC GGC TC 3'	237 bp	qPCR
TJP1	sense 5' TTC AAA AAC TCC CAC TTC TCC 3' antisense 5' CCA TTG CTG TTA AAT ATG CCT C 3'	240 bp	EMT marker, standard PCR
VIM	sense 5' GCT GCT AAC TAC CAA GAC AC 3' antisense 5' TCA GGT TCA GGG AGG AAA AG 3'	208 bp	EMT marker, standard PCR and qPCR
YWHAZ	sense 5' CTG GTG ATG ACA AGA AAG GG 3' antisense 5' GAA CAC AGA GAA GTT AAG GGC 3'	131 bp	Housekeeping gene, qPCR

Table 2.7: Oligonucleotides

2.1.5 Antibodies

Description	Use	Manufacturer
ECL Anti-rabbit IgG, horseradish peroxidase-linked species-specific whole antibody	Western blot analysis, secondary antibody; dilution 1:33000	GE Healthcare, Freiburg, Germany
Monoclonal rabbit actin antibody	Western blot analysis; dilution 1:1000	Epitomics, Burlingame, CA, USA
Polyclonal rabbit anti-GPR54 (AKR-001)	Western blot analysis; dilution 1:1000	Alomone Labs, Jerusalem, Israel
Polyclonal rabbit anti-human GPR54 (SP4238P)	Immunocytochemical staining; dilution 1:250	Acris, Herford, Germany

Table 2.8: Antibodies

2.1.6 Biological material

Cell lines were obtained from the American Type Culture Collection (ATCC; Manassas, VA, USA) and the German Collection of Microorganisms and Cell Cultures (DSMZ; Braunschweig, Germany).

Cell line	Source	Histology	Reference
HCC70	Primary tumor	Primary ductal carcinoma	Gazdar et al. 1998
HCC1806	Primary tumor	Primary acantholytic squamous cell carcinoma	Gazdar et al. 1998
HCC1937	Primary tumor	Primary ductal carcinoma	Gazdar et al. 1998
MCF-7	Pleural effusion	Adenocarcinoma	Soule et al. 1973
MDA-MB-231	Pleural effusion	Adenocarcinoma	Cailleau et al. 1974
MDA-MB-435s	Pleural effusion	Ductal carcinoma	Cailleau et al. 1978
MDA-MB-453	Pericardial effusion	Metastatic carcinoma	Cailleau et al. 1978
T47D	Pleural effusion	Ductal carcinoma	Keydar et al. 1979
ZR75-1	Ascites	Ductal carcinoma	Engel et al. 1978

Table 2.9: Human breast cancer cell lines

The cell line MDA-MB-435 was originally established as human breast cancer cell line. Over the last years several studies suggested a gene expression profile most compatible with a melanoma origin [Rae et al., 2004, Ross et al., 2000]. Others showed evidence for MDA-MB-435 original derived from breast cancer [Chambers, 2009, Sellappan et al., 2004]. According to this, the MDA-MB-435 cell line was used as breast cancer cell line.

Cell line	Origin	Histology	Reference
MG63	Bone	Osteosarcoma	Billiau et al. 1977

Table 2.10: Osteosarcoma cell lines

Transfected cell clones were kindly provided by Prof. Millar, Edinburgh, UK.

Cell line	Origin	Histology	Reference	Transfection	Clones
B35	Central nervous system	Neuroblastoma	Schubert et al. 1974	mGPR54	1, 2, 3, 4, 5, 6

Table 2.11: Transfected cell clones

2.1.7 Animals

Animals used in *in vivo* experiments were obtained from Charles River, Wilmington, MA, USA.

Strain	Genotype
CD1 nude mouse	Crl:CD1-Foxn1^{nu}

Table 2.12: Animals

2.1.8 Consumable supplies

Consumable supplies were obtained from BD (Franklin Lakes, NJ, USA), Biozym (Hessisch Old-enburg, Germany), Eppendorf (Hamburg, Germany), Greiner Bio-One (Frickenhausen, Germany), Merck Millipore (Billerica, MA, USA), Sarstedt (Nümbrecht, Germany), Starlab (Hamburg, Germany) and Thermo Fisher Scientific, Nunc (Langenselbold, Germany).

2.1.9 Equipment

Standard laboratory equipment was used. Special instruments are listed below. They were run with the recommended software for each instrument.

Instrument	Manufacturer
Applied Biosystems 7500 Real Time PCR System	Life Technologies, Darmstadt, Germany
BioPhotometer	Eppendorf, Hamburg, Germany
IX51, inverted microscope	Olympus, Hamburg, Germany
Mikro-Dismembrator S	Sartorius, Göttingen, USA
Mini-PROTEAN System, electrophoresis	BIO-RAD, München, Germany
qTower, Real Time PCR System	Analytik Jena, Jena, Germany
Semi-dry electroblotter	Peqlab, Erlangen, Germany
Synergy HT, plate reader	BIO-TEK, Bad Friedrichshall, Germany
Thermocycler T3000	Biometra, Göttingen, Germany
UV-Transilluminator	Biometra, Göttingen, Germany
X-Ray processor, SRS-101A	Konica Minolta, Langenhagen, Germany

Table 2.13: Equipment

2.2 Methods

2.2.1 Cell biology

Cell culture works were carried out under aseptic conditions in a laminar air flow work station.

2.2.1.1 Cell cultivation

Cells were grown in medium (see table 2.5) in culture flasks in a 5 % CO_2 atmosphere saturated with H_2O at 37 °C. Reaching a confluency up to 90 %, cells were passaged. Thus, medium was removed and cells were washed with PBS. Trypsin was added and cells were incubated at 37 °C for detachment. Culture medium was added to inactivate trypsin. Cell suspension was centrifuged and resuspended in experimental medium for experiments or in cell culture medium in dilutions for further cultivation (see table 2.5).

2.2.1.2 Freezing and thawing of cells

After harvesting, cells were resuspended in freezing medium (see table 2.5) and aliquoted in cryo vials. Vials were put in a freezing device containing isopropyl alcohol for slow cooling and freezing at -80 °C. Thereafter, vials were stored in liquid nitrogen.

Starting with a new stock of cells, a cryo vial was taken from liquid nitrogen. Cells were thawn by resuspension in warm culture medium (see table 2.5). Freezing medium was removed by centrifugation. Cells were resuspended in culture medium and transferred to culture flasks for cultivation.

2.2.1.3 Determination of cell density

Cell density was measured by a Neubauer counting chamber. 10 µl of cell suspension was added and cells were counted. Cell number was given by the following equation:

$$\frac{number\ of\ cells}{number\ of\ squares} \times 10^4 = \frac{cells}{ml}$$

2.2.2 Cocultivation

For studying bone metastasis *in vitro*, cell culture models for bone-directed invasion and migration were used.

2.2.2.1 Invasion assay

As *in vitro* model for bone directed invasion, breast cancer cells were cocultivated with osteoblast-like osteosarcoma cells without direct cell-cell contact in modified Boyden chambers (see figure 2.1). Matrigel^{TM} was used to represent the extracellular matrix [von Alten et al., 2006].
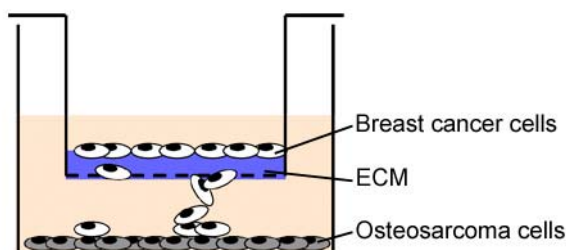
Figure 2.1: *In vitro* model for invasion studies under coculture conditions

Invasion was studied in a modified Boyden chamber assay. In the bottom well, osteosarcoma cells were grown. On top, breast cancer cells were seeded on an insert with a Matrigel^{TM} coated filter membrane. Both cell kinds were cultivated without direct cell-cell contact. An interaction was only possible by exchange of substrates through medium. ECM, extracellular matrix.

Cell culture inserts (Ø 8 μm) were coated with Matrigel^{TM} (1:1 solution in DMEM) on ice. For hardening, inserts were incubated at 37 °C for 30 min. Thereafter, breast cancer cell suspension was placed on top. Osteosarcoma cells were seeded separately in well plates. All of the cells were cultured in experimental medium (see table 2.5) at 37 °C over night. The next day, inserts with breast cancer cells were set on top the osteosarcoma cells in well plates. Cells were cocultured up to 96 h at 37 °C.

Experiments were done in 6-well plates for generating RNA samples and in 12-well plates for invasion studies. Every experimental setting included monoculture controls, where the insert was put on top medium without osteosarcoma cells. For TGFβ_1 studies, inserts were incubated with 2 μM TGFβ_1. The enzyme was added at coculture begin. For KP-10 studies, inserts were incubated with different concentrations twice daily starting at coculture begin.

RNA samples were taken of the cells in the upper well. Therefore, Matrigel^{TM} together with the cells was collected and RNA was isolated (see chapter 2.2.3.1.1).

For invasion studies, inserts were washed with PBS and H$_2$O. Cells were fixed with MeOH and stained with haematoxylin. Matrigel^{TM} and cells on top the filter membrane were removed. Filters with the remaining cells at the bottom were cut of the inserts and placed on a microscope slide. Cells were counted.

2.2.2.2 Wound healing assay

Migration was studied under coculture conditions. Therefore, petri dishes with a center well were used (see figure 2.2).
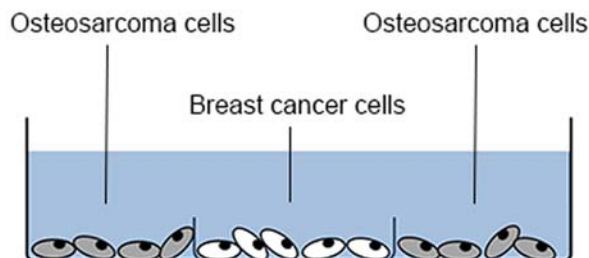
Figure 2.2: *In vitro* model for migration studies under coculture conditions

Migration was studied in a petri dish with a center well. In the outer circle, osteosarcoma cells were grown. In the middle, breast cancer cells were seeded. Both cell kinds were cultivated without direct cell-cell contact. An interaction was only possible by exchange of substrates through the medium.

Osteosarcoma cells were grown in the outer circle and breast cancer cells in the inner one. Cell suspension was filled in, so that it did not reached the inner wall. All of the cells were cultured in experimental medium (see table 2.5). Cells were incubated without contact at 37 °C until the breast cancer cell layer was confluent. Then, a scratch was done by the bottom end of a pipette tip. Pictures of the scratch were taken directly after the scratch and 8 h, 24 h and 48 h later. The width of the scratch was measured. Monoculture controls were prepared comparably without osteosarcoma cells in the outer circle.

2.2.3 Molecular biology

2.2.3.1 Isolation of ribonucleic acids (RNA)

RNA was isolated by two different methods according to the requirements of further applications. A spin-column based method was used for isolation of mRNA for PCR analysis. The TriFast$^{\text{TM}}$ reagent (PeqLab, Erlangen, Germany) was used for isolation of mRNA for gene array analysis.

2.2.3.1.1 Spin-column method

Total RNA was prepared by the RNeasy Mini Kit protocol according to the manufacturer's description (Qiagen, Hilden, Germany).

Cell culture samples and cell samples in Matrigel^{TM} were lysed and cleaned up in columns and RNA was purified by selective binding to silica membranes. After several washing steps, RNA was eluted from the membrane.

The concentration of RNA in each sample was determined by photospectroscopy. Protein contamination were detected by the ratio of the optical densities of nucleic acids (OD_{260}) and of proteins (OD_{280}). Samples were further used, when the value was between 1.8 and 2.0.

RNA samples were stored at -80 °C.

2.2.3.1.2 TriFast^{TM} reagent

For genearray analysis, isolation of RNA from invasion experiments was handled by a phenol-chloroform based extraction [Chomczynski and Sacchi, 1987] with TriFast^{TM} reagent.

Cells below the filter membrane (see chapter 2.2.2.1) were washed with PBS after removal of medium and Matrigel^{TM}. Membranes were cut out of the cell culture inserts and put in TriFast^{TM} reagent. After a few minutes, membranes were removed and the samples were directly delivered to the Transkriptomanalyselabor (TAL) in Göttingen for microarray analysis.

After return, RNA samples were stored at -80 °C.

2.2.3.2 Reverse transcription

The RNA samples were treated with DNase I for digestion of DNA. For further analysis, RNA was reverse transcribed in complementary DNA (cDNA).

During synthesis of cDNA, a poly-T oligonucleotide primer hybridizes with a single strand RNA molecule. The enzyme reverse transcriptase synthesizes a complementary DNA strand depending on the RNA template [Verma et al., 1974].

DNA digestion was carried out by incubation of 1 µg total RNA with 10 U DNase I and 40 U RNase inhibitor at 37 °C for 30 min. After 3 min at 70 °C, a reaction mixture was added to a final volume of 40 µl containing 90 pmol Primer p(dT)15, 40 nmol dNTPs and 400 U Superscript^{TM} II reverse transcriptase, 5x First-Strand buffer, 400 nmol DTT. The preparation was heated up to 37 °C for 60 min for elongation and transcription followed by 95 °C for 5 min for enzyme inactivation. Negative controls were carried along with the samples.

cDNA samples was stored at -20 °C.

2.2.3.3 Polymerase chain reaction (PCR)

PCR is a method for amplifying a certain gene product [Mullis et al., 1986]. It is organized in three steps: denaturation, annealing and elongation. During denaturation, double stranded DNA is separated in single strands by high temperature. Lower temperatures allows sequence-specific oligonucleotide primers to anneal to the certain gene product (template). Elongation of

the primer-DNA structure is carried out by a polymerase by heating and a double strand DNA is generated. One PCR cycle is run through and the next begins again with denaturation. According to this, the amount of PCR product doubles with each cycle.

cDNA templates were amplified in a 15 µl reaction volume containing 0.3 U KAPA2GTM Fast (2x ReadyMix with Dye) and 0.5 µM of the appropriate primers in a thermal cycler (T3000, Biometra). The initial denaturation step was carried out for 3 min at 95 °C. The cycles were performed at 95 °C for 15 s, 15 s at the primer-specific temperature and 5 s at 72 °C. The number of cycles was adjusted to the amount of PCR product. End of the program was performed for 2 min at 72 °C. No template controls were carried along with the samples.

For semi quantitative analysis, each sample was analyzed for the amount of L7. L7 was used as ribosomal housekeeping gene for standardization.

2.2.3.4 Agarose gel electrophoresis

For separation of DNA fragments, agarose gel electrophoresis was used.

DNA molecules are sorted by molecule based size and charge. By applying an electric field, molecules move through the gel in a proper buffer system. Smaller ones move faster than larger DNA fragments. The separated bands can be visualized by ethidium bromide staining an UV radiation, which intercalates into double stranded DNA.

The density of the agarose gel was adapted to the expected product length and varied between 1.5 % and 2 % (w/v) in $\frac{1}{2}$x TBS buffer (see table 2.4). Gels were casted 30 min for use. A proper DNA ladder was applied to the gels for length determination. Electrophoresis was performed in $\frac{1}{2}$x TBS buffer at 80-90 V for 30-75 min. PCR products were visualized by ethidium bromide staining and UV photometric detection. Bands were analyzed using the Biometra BioDoc Analyze System (Biometra, Göttingen, Germany).

2.2.3.5 Microarray analysis

Microarray analysis was performed by the Transkriptomanalyselabor (TAL) in Göttingen. Therefore, RNA samples were prepared (see chapter 2.2.3.1.2). Analysis were done by Affymetrix GeneChip® and raw data were prepared by TAL
(see http://www.microarrays.med.uni-goettingen.de/; last page view on March 2013).

2.2.3.6 Isolation of deoxyribonucleic acid (DNA)

DNA was isolated by the NucleoSpin® Tissue Kit protocol according to the manufacturer's description (Macherey-Nagel, Dueren, Germany).

For preparation of DNA from mouse tissue, bone samples were homogenized by a dismembrator. Lung and liver were cut by scalpel. Blood and cell samples were used directly. RNase was added. Lysates from bone, lung and liver were separated by NucleoSpin® Filters (Macherey-Nagel, Düren, Germany).

The concentration of DNA in each sample was measured by photospectroscopy and contamination were detected by the ratio of the optical densities of nucleic acids (OD_{260}) and of proteins (OD_{280}). A value between 1.8 and 2.0 was optimal. Because of a limited sample yield, all samples were used for further analysis. The results were interpreted based on the quality of the DNA samples.

DNA samples were stored at -80 °C.

2.2.3.7 Quantitative real-time PCR

Quantitative real-time PCR is a method for amplifying DNA molecules according to the principles of a standard PCR (see chapter 2.2.3.3) and simultaneous quantification of the product. Compared to the standard PCR, where the product is detected in the end, real-time PCR enables detection as the reaction progresses. The accumulation of DNA product is measured by the increase of fluorescent dyes for every cycle. The dyes can be divided in groups with different detection methods. The intercalating dyes are non-specific fluorescent dyes, which intercalate with double stranded DNA [Higuchi et al., 1993]. The other group is characterized by sequence-specific probes that are labeled. Three methods are used. The TaqMan method uses a sequence-specific probe. The probe is labeled with a reporter dye and a quencher, which permits detection until the target is elongated. During elongation the reporter dye and the quencher are cut of and fluorescence can be detected [Livak et al., 1995]. Molecular beacon probes are characterized by complementary 5'- and 3'-ends, which form hairpin structures and offers low distances between reporter and quencher. A fluorescent signal is only detectable during hybridization of the molecular beacon with the target DNA [Tyagi and Kramer, 1996]. The method hybridization probes is based on two oligonucleotides, one having the acceptor at its 3'-end, the other having the donor at its 5'-end. Both oligonucleotides bind the same DNA strand with a maximum distance of five nucleotides. During hybridization, the fluorescent signal of the donor is detectable.

2.2.3.7.1 SYBR green method

For validation of the results of the micro array, the RNA samples were analyzed by real-time PCR and DNA products were quantified. Reverse transcription and real-time PCR were performed in one step.

10 ng RNA was added to 10 µl 2x SensiFAST SYBR No-ROX One-Step Mix, 0.2 µl reverse transcriptase, 0.4 µl RNase inhibitor, 10 µM sense and antisense primer respectively, in a final volume

of 20 µl. The real-time PCR program was the following: 10 min at 45 °C (reverse transcription), 2 min at 95 °C (polymerase activation), followed by 40 cycles of 5 s at 95 °C (denaturation) and 20 s at 59 °C (annealing and elongation). The qTower (AnalytikJena) was used. One real-time PCR run was done in three replicates for each sample on 96-well plates. No template controls were performed for every primer.

Because of the limited RNA samples, no DNA digestion was performed. To avoid replication of DNA next to RNA, only primers with exon overlapping sequences were used.

The data were analyzed by qPCRsoft. Threshold and baseline were set automatically for each gene. Data were standardized to the expression of YWHAZ and normalized to the sample without treatment using the ddCt method. YWHAZ belongs to the 14-3-3 family and mediates signal transduction by binding to phosphoserine-containing proteins. It was used as housekeeping gene according to studies in literature showing stable expression in MCF-7 cells [Curtis et al., 2010, Chua et al., 2011, Ferreira and Cronjé, 2012].

2.2.3.7.2 TaqMan method

Samples of the *in vivo* studies were analyzed by real-time PCR using the TaqMan assay. The amount of human DNA in murine tissue was quantified by a duplex real-time PCR.

Target sequence was the ALU element, which is specific for primate genomes [Batzer and Deininger, 2002]. The ALU probe was labeled with VIC (Yakima Yellow) and quenched by a non-fluorescent dye, Black Hole Quencher 1 [Munoz et al., 2005]. As endogenous reference the 18S rRNA sequence was used for both, human and murine DNA. The 18S rRNA probe was flagged with FAM (6-carboxyfluorescein) and TAMRA (carboxytetramethylrhodamine) as quencher.

Amplifications were carried out in a 25 µl reaction mixture containing 12.5 µl 2x TaqMan® Universal PCR Master Mix, 22.5 pmol of ALU sense and antisense primer respectively, 6.25 pmol ALU probe, 15 pmol 18S rRNA primer pair, 3.125 pmol 18S rRNA probe and 50 ng DNA sample. Reactions were run on a thermal cycler (ABI 7500, Life Technologies) and conditions were set as 50 °C for 2 min and 95 °C for 10 min followed by 40 cycles of 95 °C for 15 s and 60 °C for 1 min. One real-time PCR run was done in three replicates for each sample on 96-well plates and standard solutions for ALU and 18s rRNA were carried along. No template controls were performed.

The fluorescence intensity for VIC and FAM was aligned with ROX (6-carboxy-X-rhodamine) as passive reference. Data was analyzed by SDS software. Baseline and threshold were verified manually. The baseline was set a few cycles (2-3) before the cycle number where increasing fluorescence was detected. The threshold was placed in the exponential phase according to the fluorescent noise. Standard curves for ALU and 18s rRNA were calculated and the data were standardized.

2.2.4 Protein biochemistry

2.2.4.1 Immune cytochemical staining

Cells were grown up to 70 % confluency on two-well chamber slides in culture medium (see table 2.5). Before each treatment, cells were rinsed with PBS. Cells were fixed in 4 % paraformaldehyde, treated with 3 % H_2O_2 and incubated with blocking solution (Histostain® Bulk Kit). Antibody dilution was added and cells were incubated at 4 °C overnight before they were again treated with Histostain® Bulk Kit according to the manufacturer's description. As detection reagent AEC substrate chromogen (Dako) was used. Controls were performed by omission of the primary antibody.

2.2.4.2 Western blot analysis

2.2.4.2.1 Preparation of cell lysates

Cell samples were collected from cultivated cells. Cell pellets were washed with PBS and resuspended in CelLytic™ buffer containing protease inhibitor. Samples were stored at -80 °C.

For further preparation, lysates were thawn. Thereafter, samples were centrifuged at 4 °C for 5 min and supernatants were collected. Protein concentration was determined (see chapter 2.2.4.2.2).

Equal amounts of protein per sample were diluted with 4x LDS sample buffer supplemented with 10x sample reducing agent. Samples were denatured at 95 °C for 10 min. Protein samples were directly applied to gel electrophoresis (see chapter 2.2.4.2.3) or stored at -20 °C.

2.2.4.2.2 Protein determination

The concentration of solubilized protein was determined with the Bio-Rad Protein Assay based on the Bradford method [Bradford, 1976]. Adding a specific dye to a protein solution changes the color by binding to the protein. Color shift occurs in response to the concentration of protein.

Bio-Rad Protein Assay reagent was diluted in H_2O (1 : 5) and filled in 96-well plates. On top, samples and BSA standards were added. The plates were measured by a microplate reader at 590 nm. BSA standard curve was calculated and protein concentrations of the samples were detected. Experiments were done in three replicates for each sample and standard.

2.2.4.2.3 Polyacrylamide gel electrophoresis

Proteins were separated by sodium dodecyl sulfate polyacrylamide gel electrophoresis (SDS-PAGE) [Laemmli, 1970]. Proteins bind to SDS and the resulting complexes are negatively charged in a

ratio of charge to mass. The complexes are sorted by size in the gel by applying an electric field in a proper buffer system. Smaller ones move faster than larger protein complexes.

Gels were separated in two areas: on top a gel for protein collection with 5 % density and underneath, a gel for separation, which density was adapted to the expected protein mass (10 %, 12 % or 14 %; see table 2.14).

	Collection (5 %)	Separation (10 %)	Separation (12 %)	Separation (14 %)
ProSieve® 50 Gel solution (acrylamide)	500 µl	2.0 ml	2.4 ml	2.8 ml
Sol B	-	2.5 ml	2.5 ml	2.5 ml
Sol C	50 µl	100 µl	100 µl	100 µl
Sol D	1.3 ml	-	-	-
H_2O	3.1 ml	5.3 ml	4.9 ml	4.5 ml
TEMED	5 µl	5 µl	5 µl	5 µl
APS (10 %)	50 µl	50 µl	50 µl	50 µl

Table 2.14: Composition for two gels

First, gel for separation was prepared and polymerized for 45 min. Gel for collection was casted on top and polymerized for 30 min. Gels were directly used for electrophoresis or stored in a humid atmosphere at 4 °C up to three days.

Samples in LDS sample buffer and protein markers were loaded into the gel slots. Electrophoresis was performed in SDS electrophoresis buffer for 30 min at 80 V for collection, followed by 45 min-130 min at 150 V for separation. Gels were equilibrated in transfer buffer.

2.2.4.2.4 Blotting

Proteins were transferred to a membrane after electrophoresis. A semi-dry electroblotter was used. Therefore, four chromatography papers were bathed with concentrated anode buffer. On top, four chromatography papers were placed and bathed with anode buffer. Gels were applied. PVDF membranes were activated in MeOH, washed in H_2O, equilibrated in transfer buffer and then, put on top of the gels. Again, four chromatography papers were bathed in cathode buffer and placed above. Gels were blotted for 90 min-105 min at 100 V-110 V and 4 °C. After blotting, membranes were equilibrated in TBST.

2.2.4.2.5 Immunostaining

Proteins were detected by immunostaining. Therefore, membranes were blocked for 60 min with blocking solution for saturation at all places, where no protein has been attached. Then, membranes were rinsed with TBST and incubated in a solution of the primary antibody over night at

4 °C. The next day, membranes were washed with TBST and incubated in a solution of the secondary antibody for 1 h at room temperature. The secondary antibody was coupled to horseradish peroxidase allowing chemiluminescent detection. After TBST washing steps, membranes were exposed to the Immobilion^{TM} Western detection solution. Light emission of the membranes was detected by X-ray film in a X-ray processor at the site of specific antibody binding. Bands were analyzed using the Biometra BioDoc Analyze System (Biometra, Göttingen, Germany).

2.2.5 Proliferation assay

Cells were harvested and sowed in 96 well-plates in experimental medium (see table 2.5) at 37 °C overnight. Cell density varied between $1*10^4$ and $2*10^4$ cells per well depending on the metabolism of each cell line. KP-10 solutions and vehicle (control) were added once daily. alamarBlue$^{®}$ solution was added after 72 h and cells were incubated for 4 h respectively 7 h. Then, the plates were measured by a microplate reader.

alamarBlue$^{®}$ (AbD Serotec, Oxford, UK) is an redox indicator. It is reduced by cellular metabolism processes and offers the possibility of an indirect measurement of viable cells. The colorimetric change from blue to violet is measured by the optical density of the reduced dye at 570 nm vs. 630 nm [Voytik-Harbin et al., 1998].

Experiments were done in six replicates for each sample. Changes in viability were used as marker for proliferation compared to control samples.

For transfected cell experiments, transfection stability was controlled by RT-PCR samples of cells growing in experimental or transfection media.

2.2.6 Animal experiments

Animal studies were approved and carried out according to the mandatory ethical guidelines and the German laws for protection of animals.

2.2.6.1 Keeping of animals

Six till eight weeks old female CD1 nude mice were kept in groups of three to five in cages. They were maintained in a 12 h light/dark schedule and were fed and watered *ad libitum*.

2.2.6.2 Anesthesia

Mice were anesthetized before tumor cell injection in the breast or intracardially. A mixture of ketamine [100 mg/kg BW], xylazine [4 mg/kg BW] in sodium chloride [0.9 %] was applied

intraperitoneally in a final volume of 200 µl per mouse.

2.2.6.3 Tumor cell injection

Different xenograft models were used. Therefore, breast cancer cells were injected intracardially (10^5 cells per mouse) into the left ventrical or orthotopically at the second pair of mammary glands into the fatty tissue (10^6 cells per gland).

Cells were prepared in MEM without additives. Depending on the cell line, Matrigel^{TM} was added (1:1) for optimal growth conditions in vivo.

2.2.6.4 Study design

Mice of every in vivo study were divided into three groups: the first group without tumor cell injection, the second with tumor cell injection but without treatment, and the third group with tumor cell injection and treatment with KP-10 [50 µg/mouse] daily starting the day after injection. Study end was determined by tumor volume.

2.2.6.5 Tumor volume

Tumor growth was measured as tumor volume. Equation 2.1 describes the volume of a spheroid with length, as longest dimension, and width, as the distance perpendicular to and in the same plane as the length [Richtig et al., 2004].

$$\frac{1}{6}\pi \times width^2 \times length = Tumorvolume \qquad (2.1)$$

Tumors were measured two times a week.

2.2.6.6 Section

At the end of the study, mice were euthanized with CO_2 and blood was collected by cardiocentesis. Lung, femurs and liver were taken.

For studies with no cardiocentesis, mice were euthanized with CO_2 and cervical dislocation was done.

2.2.6.7 Sample preparation

Blood samples were added by EDTA [4 mM] and stored at -20 °C.

Collected murine tissue was washed with PBS. Bones were relieved of tissue. Samples were frosted in liquid nitrogen and stored at -80 °C.

DNA was isolated (see chapter 2.2.3.6) and metastasis was measured (see chapter 2.2.3.7.2).

2.2.7 Statistical analysis

The statistical analysis was carried out by the GraphPad Prism® software 5.0. The results were graphed by mean $\pm$ standard error of the mean (SEM). Significant differences were indicated by *: $p < 0.05$, **: $p < 0.01$ and ***: $p < 0.001$. The number of samples was specified as n.

Cell culture experiments were done three times and more in independent preparations. In most of the studies, two different conditions respectively treatments were compared and the paired t-test was used for statistical analysis. Experimental settings covering more than two conditions respectively treatments, data was analyzed by a 1way ANOVA together with a multiple comparison test. Tukey's was used for comparison of all pairs of columns and Dunnett's was used, if every data column should be compared only with the control. Images were graphed in figures being representative for at least three sample preparations.

Data of the *in vivo* experiments was differently analyzed according to the compared groups. The Mann Whitney test was used for matching the control group versus the tumor group. In the control group, it was expected that no hDNA could be detected. Thus, a Gaussian distribution could not be estimated and the nonparametric test was used. In contrast, hDNA was expected to be found in the tumor group and in the treatment group. Here, the data was analyzed by the paired t-test.

3 Results

3.1 Morphology and motility marker expression of breast cancer cells

In the following chapter, breast cancer cell lines (see table 2.9) were characterized by their morphology and their intracellular configuration of markers important for EMT.

3.1.1 Morphological characteristics of breast cancer cells

Breast cancer cell lines were studied for their morphology. Therefore, images of living cells were taken. The pictures in figure 3.1 are representative for each cell line. T47D, ZR75-1, MDA-MB-453, HCC 70, HCC 1806, HCC 1937 and MCF-7 showed growth in clusters with intercell connections like epithelial cells. MDA-MB-231 and MDA-MB-435s had a more spindle shaped appearance like mesenchymal cells.
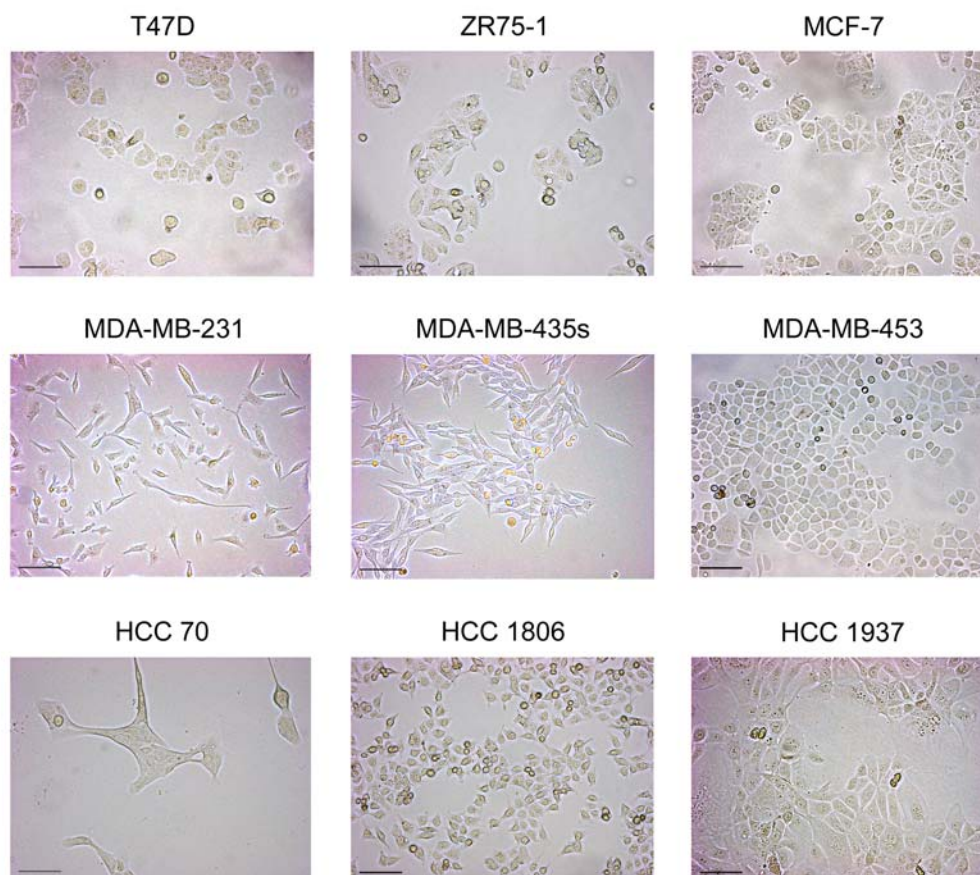
Figure 3.1: Morphology of breast cancer cells

Breast cancer cell lines T47D, ZR75-1, MCF-7, MDA-MB-231, MDA-MB-435s, MDA-MB-453, HCC 70, HCC 1806 and HCC 1937 were grown in culture flasks. Bright field images of living cells were taken (scale bar = 100 µm). Images represent the findings in at least three different passages of each cell line.

3.1.2 EMT marker expression

Breast cancer cell lines were further characterized for expression of genes involved in EMT by mRNA analysis (see chapters 2.2.3.1-2.2.3.4). As marker for the epithelial phenotype CDH1 and TJP1 were chosen. S100A4 and VIM were investigated as marker for the mesenchymal phenotype.

Figure 3.2 represents the expression levels of CDH1 and TJP1 (figure 3.2 a) and the expression levels of S100A4 and VIM (figure 3.2 b). Epithelial marker TJP1 could be detected in all of the studied cell lines. CDH1 was expressed in almost all of the breast cancer cells. In MDA-MB-231, CDH1 was detected in a small amount. In MDA-MB-435s, no CDH1 was found. Mesenchymal markers were expressed differently in the studied cell lines. S100A4 was clearly identified in T47D, ZR75-1, MDA-MB-231, HCC 70, HCC 1806, HCC 1937 and MCF-7. MDA-MB-435s cells expressed only a small amount of S100A4. In MDA-MB-453, no S100A4 could be detected. VIM

was found in MDA-MB-231, MDA-MB-435s, HCC 70, HCC 1937 and MCF-7, but not in T47D and ZR75-1. In HCC 1806 and MDA-MB-453 cells, VIM was expressed in a small amount.

(a) Epithelial marker CDH1 and TJP1   (b) Mesenchymal marker S100A4 and VIM
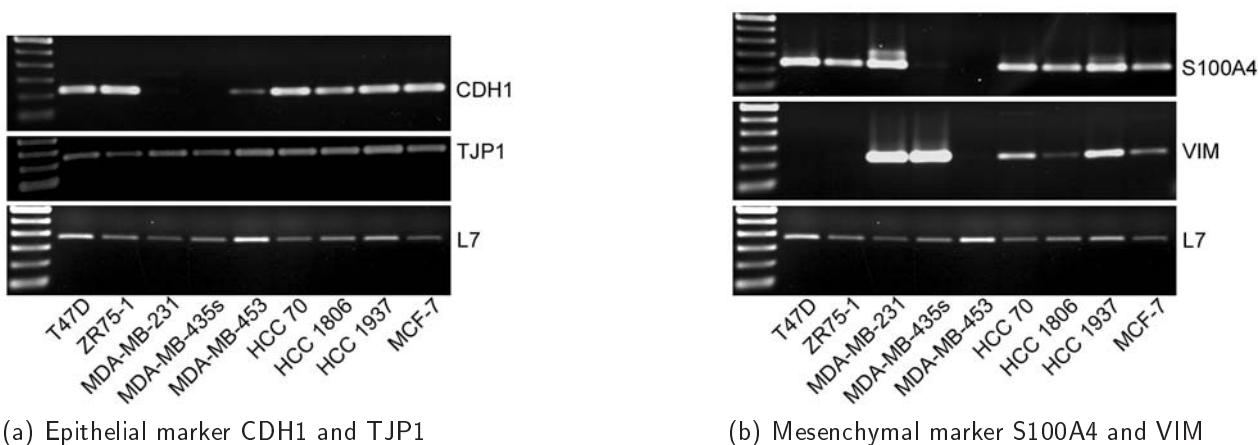
Figure 3.2: Expression of EMT marker in breast cancer cell lines

EMT marker distribution was investigated by gene expression analysis via RT-PCR. For reasons of comparison, mRNA controls were performed by proof of the housekeeping gene L7. (a) Levels of CDH1 and TJP1 were detected as marker for the epithelial phenotype. (b) S100A4 and VIM were picked as marker for the mesenchymal phenotype. Images represent the findings in at least three different passages of each cell line.

In summary, expression of epithelial marker CDH1 and TJP1 showed a different pattern within the cells lines. No differences were observed in TJP1 gene expression between the cell lines. All of the breast cancer cell lines showed a clear CDH1 expression except MDA-MB-231 and MDA-MB-435s cells. Mesenchymal marker S100A4 and VIM were expressed in HCC 70, HCC 1806, HCC 1937 and MCF-7 in detectable quantities. In T47D and ZR75-1, only S100A4 was verified. MDA-MB-231 cells had large amounts of S100A4 and VIM. MDA-MB-435s cells expressed clear amounts of VIM, but they had very low S100A4 expression. MDA-MB-453 cells showed very small quantities of VIM and no S100A4 expression.

3.2 Invasion of breast cancer cells

In this chapter, the breast cancer cell lines were analyzed for their invasion properties. Cell lines showing great differences in their invasive behavior were further analyzed.

3.2.1 Invasive properties of breast cancer cells

Invasive behavior of breast cancer cells was studied. Therefore, a modified Boyden chamber assay was chosen as model system (see chapter 2.2.2.1). Cells moved through a Matrigel^{TM} coated

filter membrane towards medium in monoculture or towards osteosarcoma cells in coculture up to 96 h.
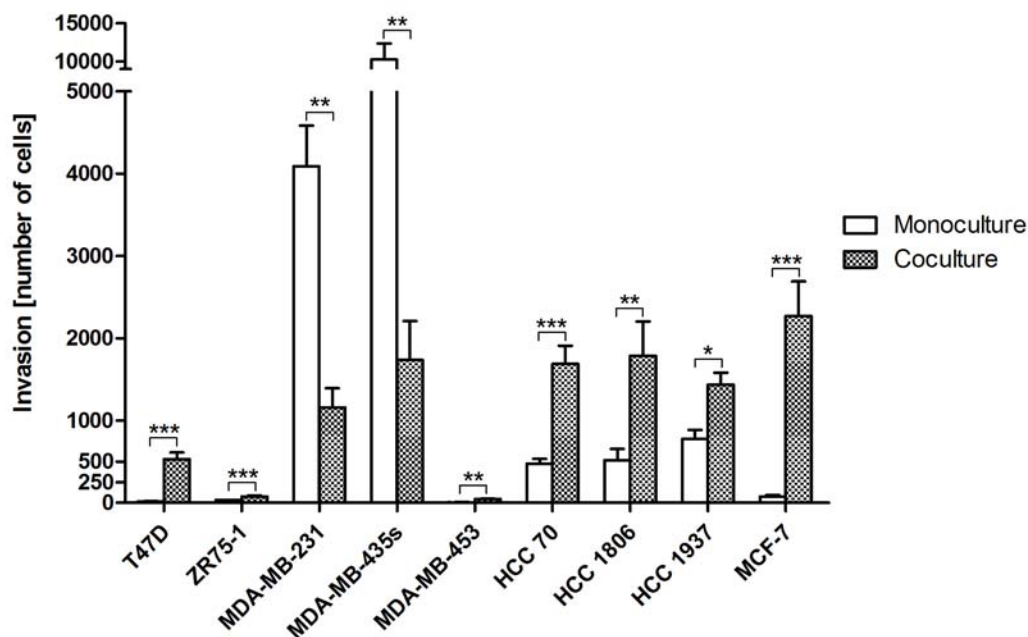
Figure 3.3: Invasive behavior of breast cancer cells

The breast cancer cell lines T47D, ZR75-1, MDA-MB-231, MDA-MB-435s, MDA-MB-453, HCC 70, HCC 1806, HCC 1937 and MCF-7 were studied on their invasive properties by a modified Boyden chamber assay. Numbers of invaded cells were collected in monoculture (white columns) and cocultivated with osteosarcoma cells (dotted columns) after 96 h. Results were analyzed by paired t-test comparing data of monoculture and coculture conditions within one cell line (mean $\pm$ SEM; *: $p < 0.05$; **: $p < 0.01$; ***: $p < 0.001$; n = 6 for MDA-MB-435s, HCC 1937; n = 8 for T47D, ZR75-1, MDA-MB-231, MDA-MB-453, HCC 70, HCC 1806; n = 17 for MCF-7).

In figure 3.3, the numbers of invaded cells are represented for all breast cancer cell lines under monoculture and coculture conditions.

In monoculture, MDA-MB-435s (10236 cells $\pm$ 2125 cells SEM) and MDA-MB-231 (4093 cells $\pm$ 493 cells SEM) showed strong invasion. T47D (16 cells $\pm$ 4 cells SEM), ZR75-1 (30 cells $\pm$ 5 cells SEM), MDA-MB-453 (5 cells $\pm$ 2 cells SEM) and MCF-7 (73 cells $\pm$ 21 cells SEM) rarely invaded. HCC 70 (473 cells $\pm$ 58 cells SEM), HCC 1806 (518 cells $\pm$ 136 cells SEM) and HCC 1937 (774 cells $\pm$ 110 cells SEM) had intermediate invasive properties.

Under coculture conditions, a significant increase of invasion was observed for T47D (528 cells $\pm$ 84 cells SEM), ZR75-1 (77 cells $\pm$ 10 cells SEM), MDA-MB-453 (46 cells $\pm$ 8 cells SEM), HCC 70 (1686 cells $\pm$ 225 cells SEM), HCC 1806 (1784 cells $\pm$ 420 cells SEM), HCC 1937 (1437 cells $\pm$ 144 cells SEM) and MCF-7 (2268 cells $\pm$ 421 cells SEM). MDA-MB-231 (1160 cells $\pm$ 232 cells SEM) and MDA-MB-435s (1736 cells $\pm$ 473 cells SEM) showed significantly reduced invasion in contrast to monoculture.
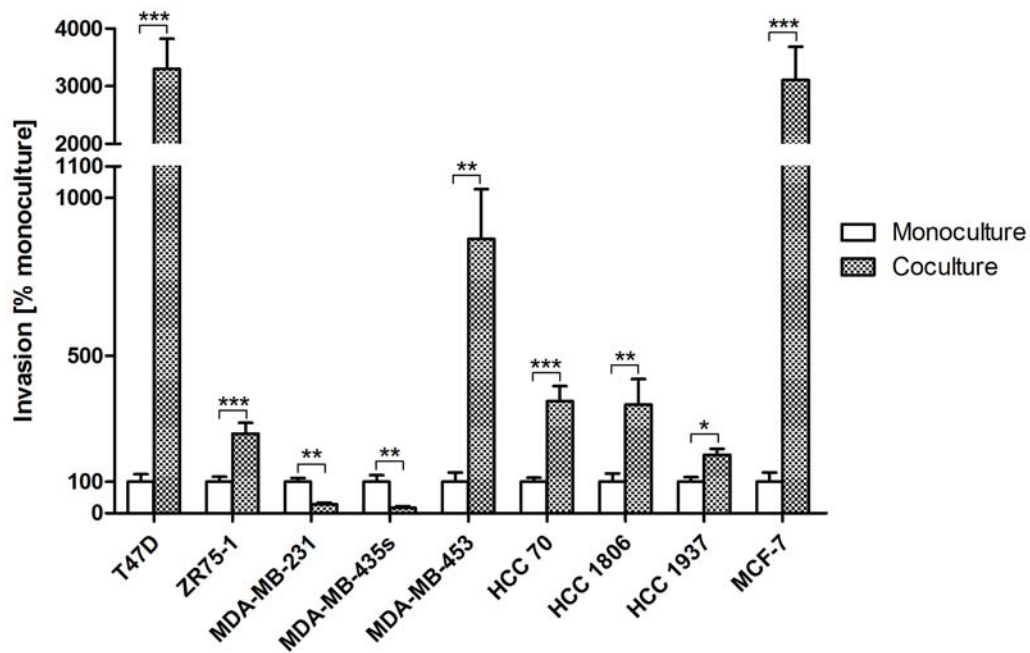
Figure 3.4: Invasion of breast cancer cells affected by cocultivation with osteosarcoma cells

The breast cancer cell lines T47D, ZR75-1, MDA-MB-231, MDA-MB-435s, MDA-MB-453, HCC 70, HCC 1806, HCC 1937 and MCF-7 were studied on their invasive properties by a modified Boyden chamber assay. Invasion of cells cocultivated with osteosarcoma cells (dotted columns) is graphed in relation to the invaded cells in monoculture (white columns) for each cell line after 96 h. Results were analyzed by paired t-test comparing data of monoculture and coculture conditions within one cell line (mean $\pm$ SEM; *: $p < 0.05$; **: $p < 0.01$; ***: $p < 0.001$; n = 6 for MDA-MB-435s, HCC 1937; n = 8 for T47D, ZR75-1, MDA-MB-231, MDA-MB-453, HCC 70, HCC 1806; n = 17 for MCF-7).

For comparison of invasion within one cell line, figure 3.4 shows the extent of invasion in coculture related to the invasion in monoculture. MDA-MB-231 (28.3 % $\pm$ 5.7 % SEM) and MDA-MB-435s (17.0 % $\pm$ 4.6 % SEM) were significantly inhibited in their invasion properties by cocultivation with osteosarcoma cells. T47D (3297.7 % $\pm$ 523.8 % SEM) and MCF-7 (3108.8 % $\pm$ 577.0 % SEM) showed the largest increase in invasion. ZR75-1 (252.3 % $\pm$ 34.5 % SEM), MDA-MB-453 (869.0 % $\pm$ 158.0 % SEM), HCC 70 (356.3 % $\pm$ 47.5 % SEM), HCC 1806 (344.5 % $\pm$ 81.1 % SEM) and HCC 1937 (185.8 % $\pm$ 18.6 % SEM) also had a significant increase in invasion.

Taken together, the breast cancer cell lines showed different invasive behavior from hardly any invasion to a strong cell movement. Coculture conditions led to increased cell invasion especially in cell lines showing almost no invasion in monoculture as T47D and MCF-7 cells. The cell lines with the strongest invasion properties in monoculture, MDA-MB-231 and MDA-MB-435s, showed decreased cell movement in coculture.

3.2.2 Progression of bone-directed invasion

Four different breast cancer cell lines were chosen for a detailed study of their invasion behavior. MDA-MD-231 and MDA-MB-435s cells were investigated as cell lines showing reduced invasion in coculture (see chapter 3.2.1). MCF-7 cells showed a strong increase in invasion by cocultivation with osteosarcoma cells. HCC 1806 cells had an intermediate increase in invasion. Invasion was studied for 24 h, 48 h, 72 h and 96 h.

3.2.2.1 Invasion of MDA-MD-231 and MDA-MB-435s

Invasion of MDA-MB-231 cells is represented as number of invaded cells in figure 3.5. For up to 48 h, cells in coculture showed significantly increased invasion compared to monocultured cells (24 h: 35 cells $\pm$ 11 cells SEM vs. 124 cells $\pm$ 38 cells SEM; 48 h: 117 cells $\pm$ 26 cells SEM vs. 296 cells $\pm$ 60 cells SEM). At 72 h, no significant difference was observable between both conditions (620 cells $\pm$ 155 cells SEM vs. 808 cells $\pm$ 244 cells SEM). At 96 h, cells in monoculture invaded stronger than cells in coculture (see chapter 3.2.1).

Figure 3.5: Invasive characteristics of MDA-MB-231 cells in coculture

Invasion of the breast cancer cell line MDA-MB-231 was studied by a modified Boyden chamber assay for cells in monoculture (white columns) and cells cocultivated with osteosarcoma cells (dotted columns). Numbers of invaded cells were counted after 24 h, 48 h, 72 h and 96 h. Results were analyzed by paired t-test comparing data of monoculture and coculture conditions within one point in time (mean $\pm$ SEM; *: $p < 0.05$; **: $p < 0.01$; n = 8 for 24 h, 48 h, 96 h; n = 10 for 72 h).

Invasion of MDA-MB-435s cells is graphed in figure 3.6. A significantly increased invasion was observed for up to 48 h (24 h: 6 cells $\pm$ 1 cells SEM vs. 27 cells $\pm$ 4 cells SEM; 48 h: 27 cells $\pm$ 7 cells SEM vs. 96 cells $\pm$ 20 cells SEM). The later measurements showed less invasion in coculture than in monoculture (72 h: 725 cells $\pm$ 228 cells SEM vs. 501 cells $\pm$ 172 cells SEM; 96 h: 10236 cells $\pm$ 2125 cells SEM vs. 1736 cells $\pm$ 473 cells SEM).
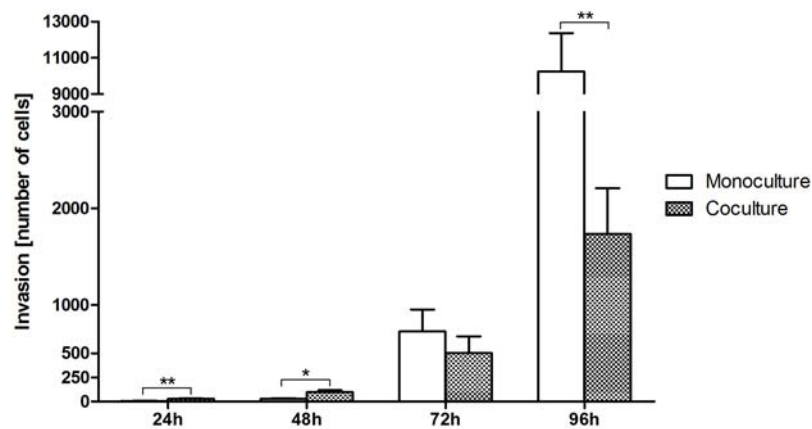
Figure 3.6: Invasive characteristics of MDA-MB-435s cells in coculture

Invasion of the breast cancer cell line MDA-MB-435s was studied by a modified Boyden chamber assay for cells in monoculture (white columns) and cells cocultivated with osteosarcoma cells (dotted columns). Numbers of invaded cells were counted after 24 h, 48 h, 72 h and 96 h. Results were analyzed by paired t-test comparing data of monoculture and coculture conditions within one point in time (mean $\pm$ SEM; *: $p < 0.05$; **: $p < 0.01$; n = 8 for 24 h; n = 7 for 48 h; n = 11 for 72 h; n = 6 for 96 h).

3.2.2.2 Invasion of HCC 1806

The cell line HCC 1806 showed a significantly increased invasion in coculture after 48 h, 72 h and 96 h graphed in figure 3.7 (24 h: 7 cells $\pm$ 1 cells SEM vs. 25 cells $\pm$ 8 cells SEM; 48 h: 40 cells $\pm$ 7 cells SEM vs. 265 cells $\pm$ 50 cells SEM; 72 h: 429 cells $\pm$ 89 cells SEM vs. 1413 cells $\pm$ 323 cells SEM; 96 h: 518 cells $\pm$ 136 cells SEM vs. 1784 cells $\pm$ 420 cells SEM).
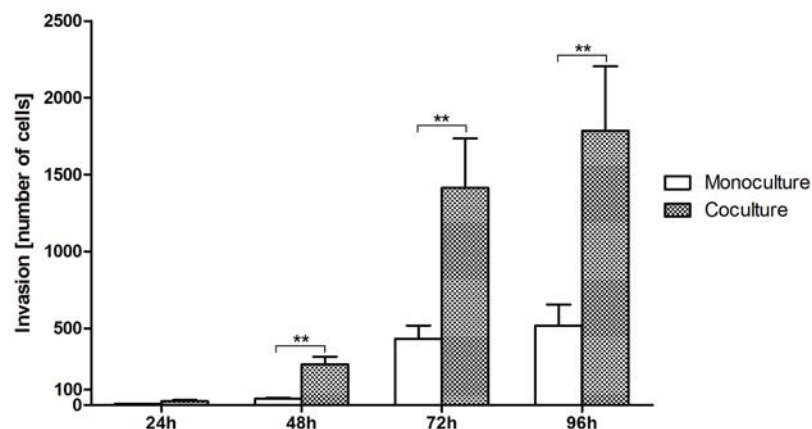
Figure 3.7: Invasive characteristics of HCC 1806 cells in coculture

Invasion of the breast cancer cell line HCC 1806 was studied by a modified Boyden chamber assay for cells in monoculture (white columns) and cells cocultivated with osteosarcoma cells (dotted columns). Numbers of invaded cells were counted after 24 h, 48 h, 72 h and 96 h. Results were analyzed by paired t-test comparing data of monoculture and coculture conditions within one point in time (mean $\pm$ SEM; **: $p < 0.01$; n = 7 for 24 h; n = 8 for 48 h, 72 h, 96 h).

3.2.2.3 Invasion and migration of MCF-7

Invasion of MCF-7 is represented in figure 3.8. The cocultured cells invaded significantly stronger after 48 h, 72 h and 96 h (24 h: 15 cells $\pm$ 4 cells SEM vs. 28 cells $\pm$ 10 cells SEM; 48 h: 21 cells $\pm$ 3 cells SEM vs. 74 cells $\pm$ 6 cells SEM; 72 h: 69 cells $\pm$ 35 cells SEM vs. 489 cells $\pm$ 103 cells SEM; 96 h: 73 cells $\pm$ 21 cells SEM vs. 2268 cells $\pm$ 421 cells SEM).
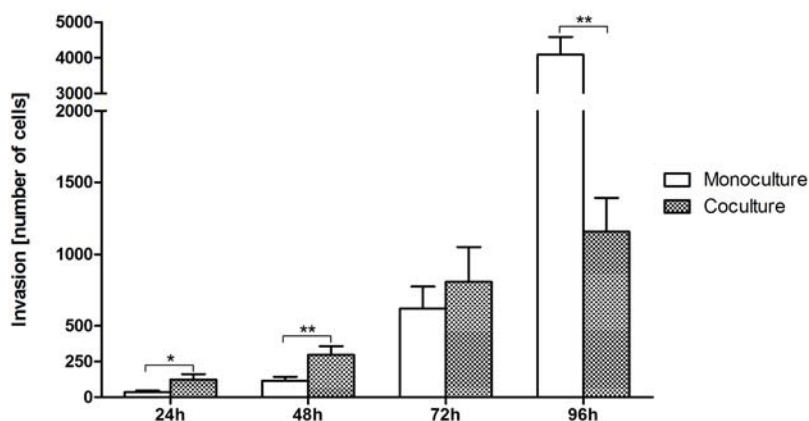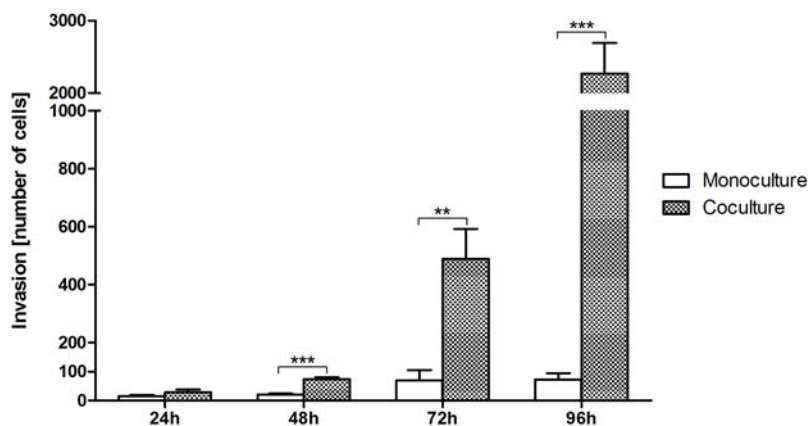

Figure 3.8: Invasive characteristics of MCF-7 cells in coculture

Invasion of the breast cancer cell line MCF-7 was studied by a modified Boyden chamber assay for cells in monoculture (white columns) and cells cocultivated with osteosarcoma cells (dotted columns). Numbers of invaded cells were counted after 24 h, 48 h, 72 h and 96 h. Results were analyzed by paired t-test comparing data of monoculture and coculture conditions within one point in time (mean $\pm$ SEM; **: $p < 0.01$; ***: $p < 0.001$; n = 8 for 24 h, 48 h, 72 h; n = 17 for 96 h).

MCF-7 cells were studied for their migration behavior in monoculture and coculture. Therefore, a wound healing assay was used (see chapter 2.2.2.2). The scratch was observed for up to 48 h.

In figure 3.9a pictures of the scratches in control and coculture samples are shown. Time point 0 h shows the scratches directly after the cell layer was wounded. The widths between the cell layers was measured after 8 h, 24 h and 48 h and the results are graphed in figure 3.9b. Cell migration is represented as decreasing width of the scratches. No difference in cell migration was seen in monocultured and cocultured cell layers.
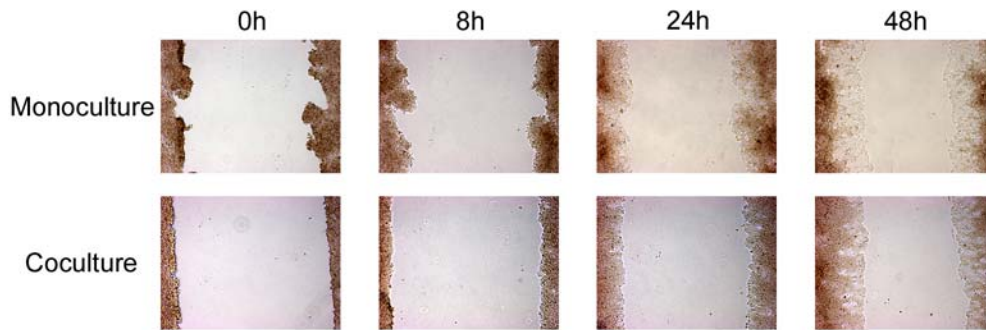
(a) Images of confluent MCF-7 cells after scratching
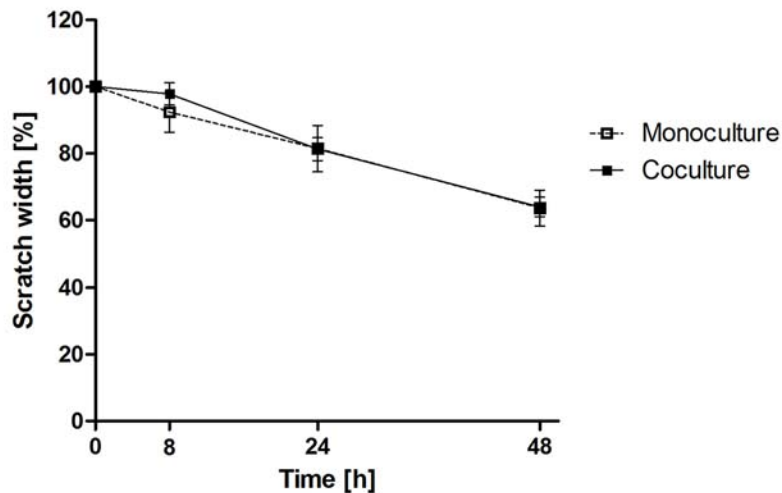
(b) Scratch width

Figure 3.9: Migratory characteristics of MCF-7 cells in coculture

Migration of the breast cancer cell line MCF-7 was studied by a wound healing assay for cells in monoculture and cells cocultivated with osteosarcoma cells. Scratching was performed after cell layers reached confluency. The scratches were studied directly after cell wounding (0 h) and after 8 h, 24 h and 48 h. (a) Bright field images show the scratches of monocultured (upper line of pictures) and cocultured cells (lower line). (b) Scratch width was measured for monocultured (white rectangles with dotted line) and cocultured cells (black rectangles with continuous line). Data is graphed in relation to the first measurement at 0 h. (White and black rectangles overlie each other in parts in the graph.) Results were analyzed by paired t-test comparing data of monoculture and coculture conditions within one point in time (mean $\pm$ SEM; n = 5).

In sum, cocultivation of breast cancer cells with osteosarcoma cells led to different effects depending on the studied cell line. MDA-MB-231 and MDA-MB-435s cells showed an increased invasive behavior up to 48 h. Then, both cell lines invaded stronger in monoculture. In HCC 1806 and MCF-7 cells, invasion in coculture increased continuously over 96 h. In contrast, cell migration in MCF-7 cells was not changed by coculture conditions.

3.2.3 Influence of TGFβ_1 treatment on breast cancer cell invasion

TGFβ_1 as one mediator of EMT was studied on breast cancer cell invasion in monocultured and cocultured cells. Invasion was studied in MDA-MB-231, HCC 1806 and MCF-7 cells treated with 2 µM TGFβ_1 for 48 h. Results are analyzed related to the invasion in monocultured cells without treatment.

In MDA-MB-231, a significantly increased invasion was observed in cocultured cells under control conditions (100 % $\pm$ 15 % SEM vs. 221 % $\pm$ 37 % SEM; see figure 3.10). Treatment with TGFβ_1 showed a trend towards more invasion in monoculture and coculture (183 % $\pm$ 74 % SEM vs. 298 % $\pm$ 42 % SEM). Direct comparison of treated and untreated samples for monoculture respectively coculture showed no significant differences.
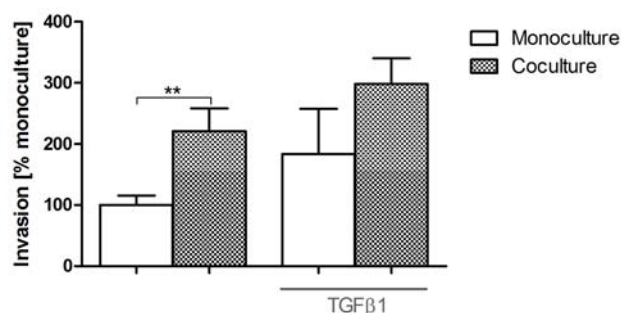
Figure 3.10: Invasion of MDA-MB-231 cells treated with TGFβ_1

Invasion of the breast cancer cell line MDA-MB-231 was studied by a modified Boyden chamber assay for cells treated with TGFβ_1 [2 µM] and controls without treatment in monoculture (white columns) and cocultivated with osteosarcoma cells (dotted columns). Invasion is graphed in relation to the invaded cells in monoculture without treatment after 48 h. Results were analyzed by paired t-test comparing data constant in culture conditions respectively treatment (mean $\pm$ SEM; **: p < 0.01; n = 6).

In figure 3.11, HCC 1806 cells invaded significantly stronger in coculture compared to monoculture under control conditions (100 % $\pm$ 16 % SEM vs. 847 % $\pm$ 252 % SEM). Cells treated with TGFβ_1 showed a stronger invasion (510 % $\pm$ 82 % SEM vs. 910 % $\pm$ 391 % SEM). The difference in invaded cells is significant for monocultured cells with and without exposition to TGFβ_1.
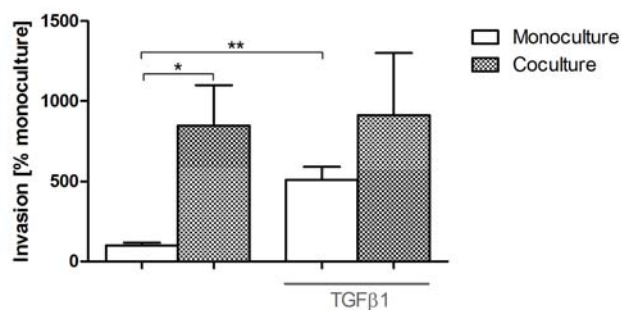
Figure 3.11: Invasion of HCC 1806 cells treated with TGFβ_1

Invasion of the breast cancer cell line HCC 1806 was studied by a modified Boyden chamber assay for cells treated with TGFβ_1 [2 µM] and controls without treatment in monoculture (white columns) and cocultivated with osteosarcoma cells (dotted columns). Invasion is graphed in relation to the invaded cells in monoculture without treatment after 48 h. Results were analyzed by paired t-test comparing data constant in culture conditions respectively treatment (mean $\pm$ SEM; *: p $<$ 0.05; **: p $<$ 0.01; n $=$ 7).

Results for MCF-7 cells are graphed in figure 3.12. Invasion of cocultured cells was significantly increased under control conditions (100 % $\pm$ 20 % SEM vs. 724 % $\pm$ 188 % SEM). Incubation with TGFβ_1 showed little effect on monocultured cells (76 % $\pm$ 8 % SEM). Cocultured cells invaded stronger (1973 % $\pm$ 693 % SEM) with no significant difference between control conditions and treatment.
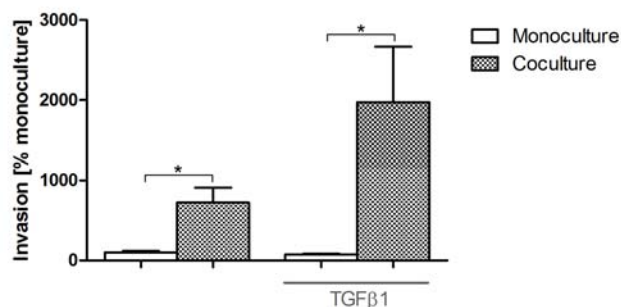
Figure 3.12: Invasion of MCF-7 cells treated with TGFβ_1

Invasion of the breast cancer cell line MCF-7 was studied by a modified Boyden chamber assay for cells treated with TGFβ_1 [2 µM] and controls without treatment in monoculture (white columns) and cocultivated with osteosarcoma cells (dotted columns). Invasion is graphed in relation to the invaded cells in monoculture without treatment after 48 h. Results were analyzed by paired t-test comparing data constant in culture conditions respectively treatment (mean $\pm$ SEM; *: p $<$ 0.05; n $=$ 6).

Summing up, the effect of TGFβ_1 treatment on invasion was marginal. Only HCC 1806 cells showed stronger invasion by TGFβ_1 in monoculture. No significant difference was observed for the other cell lines for treated and untreated cells within monoculture and respectively coculture.

3.2.4 Motility marker expression affected by cocultivation and TGFβ_1

Investigations on motility marker expression were done by mRNA analysis (see chapters 2.2.3.1-2.2.3.4). The cell lines MDA-MB-231, HCC 1806 and MCF-7 were studied under monoculture or coculture conditions and treatment with 2 µM TGFβ_1 after 24 h. The same marker were used as in chapter 3.2.4.

In figure 3.13, expression of the epithelial marker is graphed. The results for CDH1 are shown in figure 3.13(a). No difference was observed between monocultured and cocultured cells in all of the studied cell lines (MDA-MB-231: 100 % vs. 94 % $\pm$ 10 % SEM; HCC 1806: 100 % vs. 101 % $\pm$ 3 % SEM; MCF-7: 100 % vs. 94 % $\pm$ 3 % SEM). CDH1 expression was not changed significantly by TGFβ_1 treatment in cocultured MDA-MB-231 cells (134 % $\pm$ 35 % SEM) and HCC 1806 cells (95 % $\pm$ 6 % SEM). Significantly lower expression levels of CDH1 were found in cocultured MCF-7 cells exposed to TGFβ_1 (77 % $\pm$ 5 % SEM).

Further studies on TJP1 showed different results (see figure 3.13(b)). Little changes in expression levels of TJP1 were observed by comparison of monoculture and coculture conditions (MDA-MB-231: 100 % vs. 113 % $\pm$ 14 % SEM; HCC 1806: 100 % vs. 101 % $\pm$ 7 % SEM; MCF-7: 100 % vs. 96 % $\pm$ 2 % SEM) with no significance. Cocultured cells showed increased expression by TGFβ_1 treatment in MDA-MB-231 (145 % $\pm$ 13 % SEM) and in HCC 1806 (130 % $\pm$ 10 % SEM) with a significant difference. In treated MCF-7 cells, TJP1 expression was significantly decreased (85 % $\pm$ 3 % SEM).

(a) CDH1

(b) TJP1
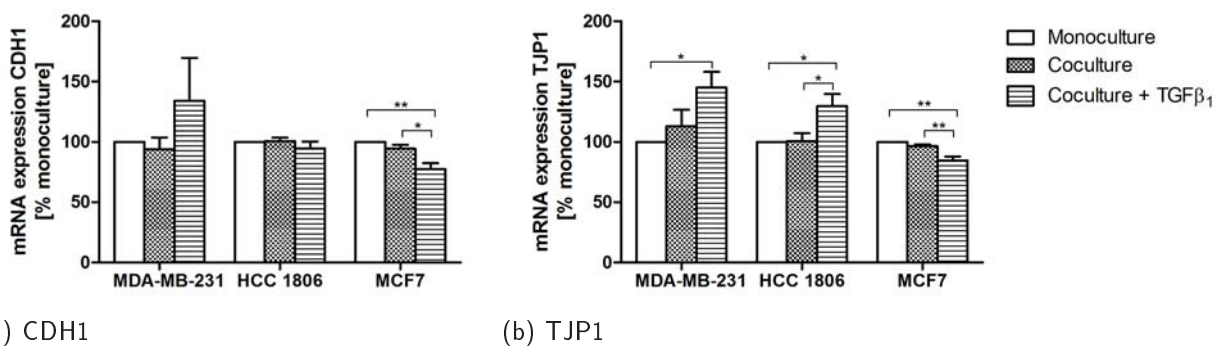
Figure 3.13: Expression of epithelial marker in breast cancer cells treated with TGFβ_1

Epithelial marker distribution was investigated in the breast cancer cell lines MDA-MB-231, HCC 1806 and MCF-7 by gene expression analysis via RT-PCR. Expression was standardized to the expression of the housekeeping gene L7 for each condition and normalized to the expression in monoculture. Levels of CDH1 (a) and TJP1 (b) expression are graphed for monocultured cells (white columns), cocultured cells (dotted columns) and cocultured cells treated with TGFβ_1 (lined columns). Results were analyzed by 1way ANOVA and Tukey's multiple comparison test within one cell line (mean $\pm$ SEM; *: p $<$ 0.05; **: p $<$ 0.01; n = 4).

Expression of the mesenchymal marker VIM and S100A4 is shown in figure 3.14(a) and (b). Comparing untreated monoculture and coculture gene expression for VIM, no significant changes in expression levels were observed in all of the cell lines (MDA-MB-231: 100 % vs. 94 % $\pm$ 5 % SEM; HCC 1806: 100 % vs. 151 % $\pm$ 32 % SEM; MCF-7: 100 % vs. 90 % $\pm$ 6 % SEM). Cocultured cells treated with TGFβ_1 had significantly increased expression levels in MDA-MB-231 (148 % $\pm$ 7 % SEM) and HCC 1806 cells (1059 % $\pm$ 56 % SEM). In MCF-7 cells, VIM expression was significantly decreased (69 % $\pm$ 4 % SEM).

Expression analysis for S100A4 showed different changes in cocultured cells compared to monoculture. In MDA-MB-231 cells, S100A4 expression was not altered (100 % vs. 109 % $\pm$ 7 % SEM). The cell line HCC 1806 had significantly decreased S100A4 expression (100 % vs. 94 % $\pm$ 2 % SEM). MCF-7 cells showed a significantly increased expression by cocultivation (100 % vs. 114 % $\pm$ 3 % SEM). Treatment with TGFβ_1 led to significantly decreased gene expression in all of the cell lines (MDA-MB-231: 87 % $\pm$ 4 % SEM; HCC 1806: 43 % $\pm$ 1 % SEM; MCF-7: 88 % $\pm$ 3 % SEM).

(a) VIM   (b) S100A4
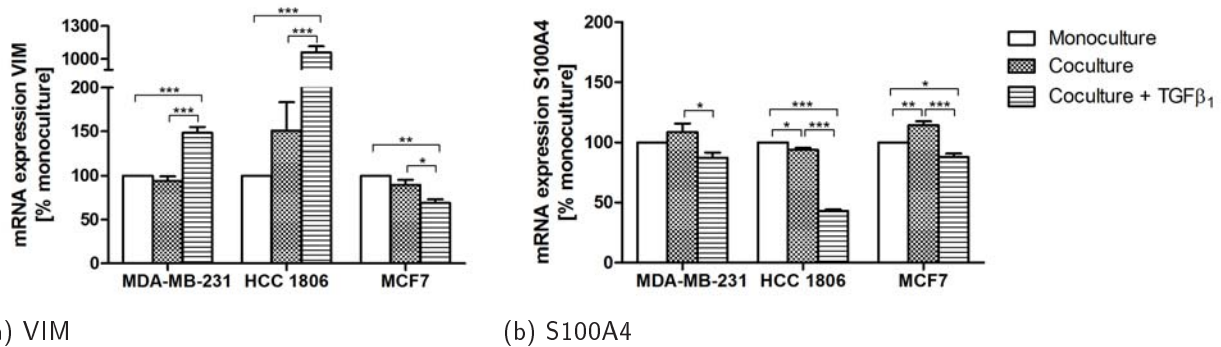
Figure 3.14: Expression of mesenchymal marker in breast cancer cells treated with TGFβ_1

Mesenchymal marker distribution was investigated in the breast cancer cell lines MDA-MB-231, HCC 1806 and MCF-7 by gene expression analysis via RT-PCR. Expression was standardized to the expression of the housekeeping gene L7 for each condition and normalized to the expression in monoculture. Levels of VIM (a) and S100A4 (b) expression are graphed for monocultured cells (white columns), cocultured cells (dotted columns) and cocultured cells treated with TGFβ_1 (lined columns). Results were analyzed by 1way ANOVA and Tukey's multiple comparison test within one cell line (mean $\pm$ SEM; *: $p < 0.05$; **: $p < 0.01$; ***: $p < 0.001$; VIM: n = 4 in MDA-MB-231, MCF-7; n = 3 in HCC 1806; S100A4: n = 4).

Taken together, no great changes in epithelial and mesenchymal marker expression was observed in MDA-MB-231, HCC 1806 and MCF-7 cells by cocultivation with osteosarcoma cells. Treatment with TGFβ_1 affected motility marker expression especially for TJP1, VIM and S100A4. A consistent gene regulation was only seen for S100A4 in all of the tested cell lines.

3.3 Gene expression in MCF-7 cells during cocultivation

MCF-7 cells showed a different invasive behavior during cocultivation with osteosarcoma cells (see chapter 3.2.2.3). Expression analysis of genes involved in EMT revealed no connection between increased invasion and EMT processes (see chapter 3.2.4). A microarray analysis was carried out to get information on the gene pattern regulated by cocultivation.

3.3.1 Microarray analysis

mRNA samples of monocultured and cocultured MCF-7 cells were analyzed by a microarray technique (see chapter 2.2.3.1.2 and 2.2.3.5). The data was clustered for the six samples (three independent samples for each condition; see Appendix A1) and showed a correlation within each condition.

The results show that the expression of 325 genes was changed comparing monocultured and cocultured samples (see Appendix A2). Data was log_2-transformed. Expression intensity was analyzed as fold change (FC). A change was considered as meaningful, if it was at least two-fold upregulated (logFC treatment-control > 1) respectively downregulated (logFC treatment-control $< $ -1). The heatmap in figure 3.15 shows the 50 genes which were regulated the most. The monocultured samples are represented as controls and the cocultured samples are named treatments. The expression of these genes was at least up to 2.14 logFC respectively not exceeding -2.17 logFC. A black area shows no difference, a blue area shows less expression and a yellow area shows upregulated expression of the treatment group compared to the control group. 44 genes (88 %) were upregulated and six genes (12 %) were downregulated.
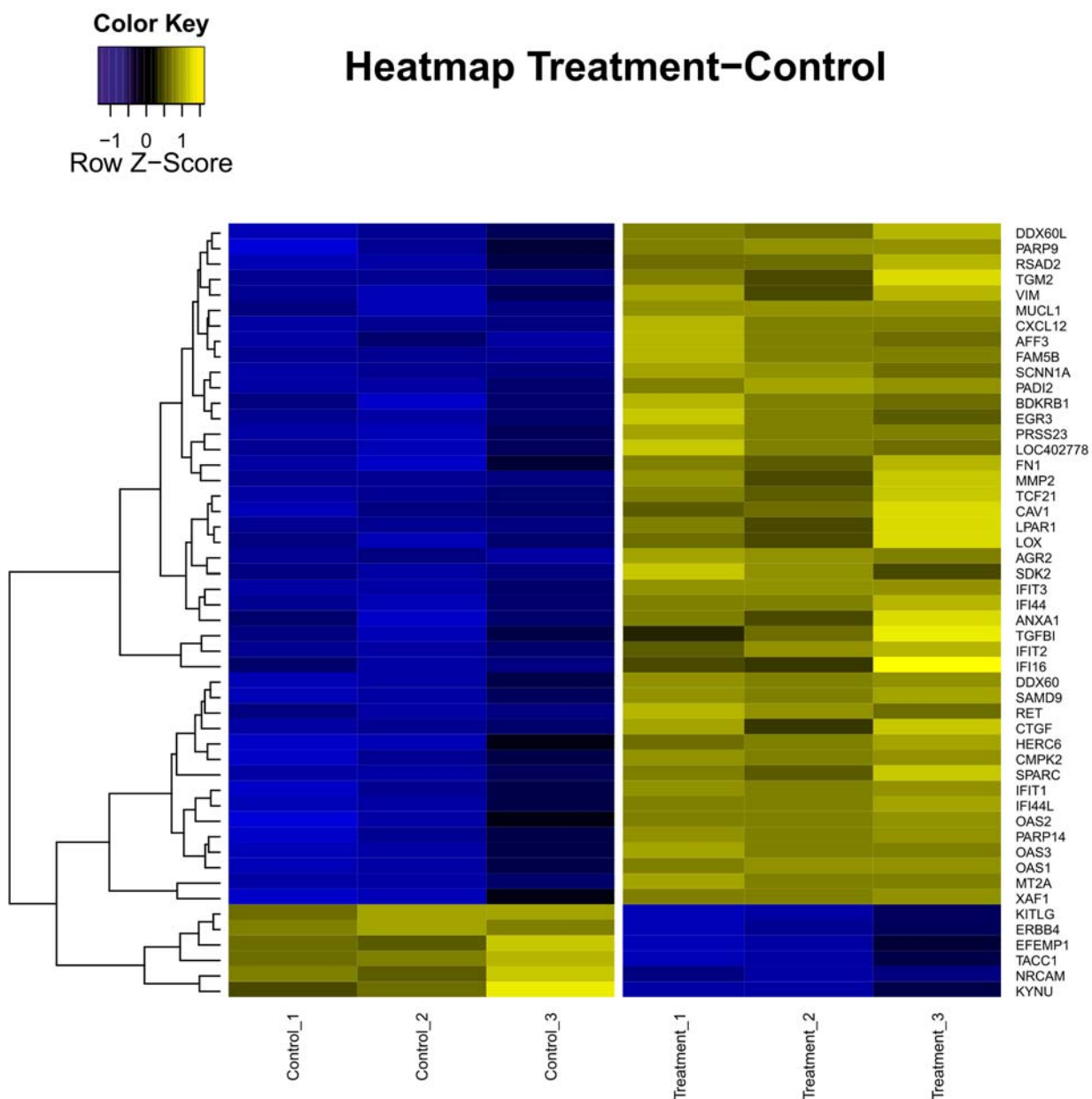
Figure 3.15: Heatmap of genes most affected by cocultivation

The breast cancer cell line MCF-7 was studied by microarray analysis for genes which were regulated during cocultivation with osteosarcoma cells. Three independent samples of monocultured cells (controls) and of cocultured cells (treatments) were investigated. The heatmap shows the 50 genes which were regulated the most (black area = no difference between control and treatment; blue area = downregulated expression; yellow area = upregulated expression). Data was log_2-transformed. Expression intensity is represented as fold change (FC).

The 50 genes were classified in five groups (see table 3.1). The first group represents genes involved in immune response activities including inflammation, viral infection and interferon dependent processes. The second group is characterized by mechanisms covering cell motility, adhesion, metastasis and cell morphology. Genes involved in cancer, oncogenes and genes affected by oncogenes are grouped in the third column. The fourth group of genes participate in proliferation

processes. Genes with no reference to the mentioned groups are taken together as others in the last column.

Immune response	Cell motility	Cancer	Proliferation	Others
IFIT2	TGFBI	CTGF	KITLG	CMPK2
BDKRB1	SDK2	ERBB4	ERBB4	PARP14
MMP2	MMP2	AFF3	MMP2	PRSS23
MT2A	SAMD9	MT2A	SAMD9	DDX60L
EGR3	EGR3	EGR3	EGR3	HERC6
IFI16	MUCL1	TGM2	IFI16	LOC402778
OAS1	CAV1	CAV1		PADI2
RSAD2	AGR2	XAF1		FAM5B
DDX60	LPAR1	LPAR1		SCNN1A
IFIT1	EFEMP1	EFEMP1		
ANXA1	RET	RET		
OAS3	LOX			
PARP9	PARP9			
VIM	VIM			
IFIT3	FN1			
CXCL12	CXCL12			
OAS2	TCF21			
IFI44	NRCAM			
IFI44L	TACC1			
SPARC	SPARC			
KYNU				

Table 3.1: Classification of genes most affected by cocultivation

The 50 genes were classified with respect to their known cellular functions. Some genes were allocated to more than one group. Each column is representative for processes and mechanisms involved in the function mentioned in the headline (immune response: inflammation, viral infection, interferon dependent processes; cell motility: adhesion, metastasis, cell morphology; cancer: oncogenes, genes affected by oncogenes; proliferation: cell growth).

The relative distribution of the 50 genes was as follows: 42 % of the genes are involved in immune response processes, 40 % of the genes are active in cell motility processes, 22 % of the genes participate in cancer processes, 12 % of the genes are involved in cell proliferation and 18 % of the genes show no relation to these four groups. Because of multiple entry of one gene to more than one group, the sum of the ratios exceeds 100 %.

3.3.2 Expression of genes involved in cell motility processes

The results of the microarray were validated by qPCR for selected genes (see chapter 2.2.3.7.1). Eight genes involved in cell motility processes were chosen. Transforming acidic coiled-coil containing protein 1 (TACC1) as one gene downregulated by coculture conditions and VIM, CXCL12,

fibronectin 1 (FN1), poly (ADP-ribose) polymerase 9 (PARP9), MMP2, secreted protein acidic and rich in cysteine (SPARC) and transcription factor 21 (TCF21) as genes, which were upregulated by the treatment, were analyzed.

In figure 3.16, the results of the qPCR analysis are graphed. The observed downregulation of TACC1 was approved by significant data ($0.14\% \pm 0.01\%$ SEM). FN1 showed a significant higher expression in cocultured cells ($6.43\% \pm 1.03\%$ SEM). A trend towards an upregulated expression of VIM ($55.14\% \pm 44.92\%$ SEM), CXCL12 ($7.37\% \pm 2.01\%$ SEM), PARP9 ($4.56\% \pm 1.00\%$ SEM), MMP2 ($62.65\% \pm 29.74\%$ SEM), SPARC ($61.59\% \pm 16.10\%$ SEM) and TCF21 ($11.01\% \pm 2.51\%$ SEM) was observed with no significant results.
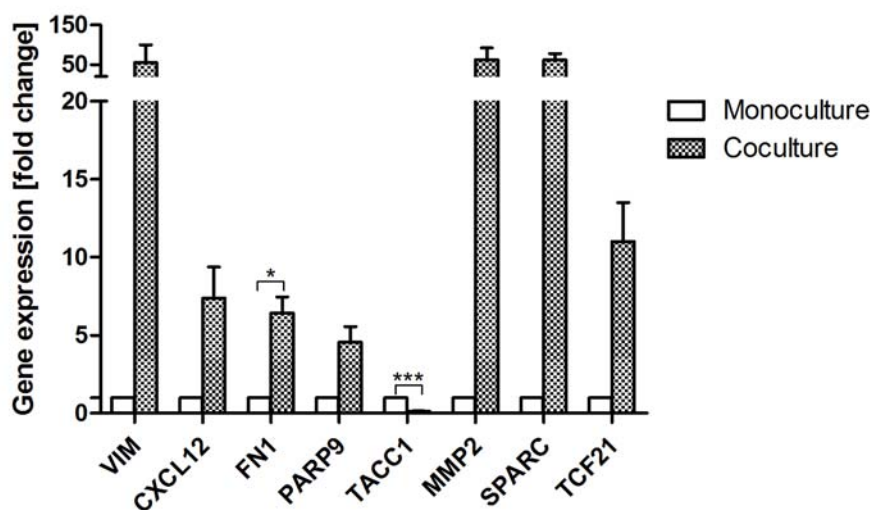
Figure 3.16: Gene expression in breast cancer cells affected by cocultivation

Gene expression of selected genes was investigated in the breast cancer cell line MCF-7 by qPCR. Expression was standardized to the expression of the housekeeping gene YWHAZ and normalized to the expression in monoculture. Levels of gene expression are graphed for monocultured cells (white columns) and cocultured cells (dotted columns). Results were analyzed by paired t-test comparing data of monoculture and coculture conditions for one gene (mean $\pm$ SEM; *: $p < 0.05$; ***: $p < 0.001$; n = 3).

In summary, microarray analysis of cocultivated MCF-7 cells showed changes in expression levels of genes involved mostly in immune response, cell motility, cancer and proliferation processes. Verification of the data by qPCR for selected genes validated the microarray data.

3.4 Effects of kisspeptin-10 and analogs on bone-directed invasion

The inhibitory effect of KP-10 was shown in the breast cancer cell lines MCF-7 and MDA-MB-231 [Olbrich, 2010a, Olbrich et al., 2010b]. KP-10 inhibited cell invasion within a concentration

window. MCF-7 cells were inhibited significantly by 10^{-9} M up to 10^{-11} M of KP-10, whereas MDA-MB-231 cells showed significantly less invasion by 10^{-10} M KP-10. The experiments were continued for the cell line HCC 1806 based on the experimental setting in chapter 2.2.2.1. Further invasion studies for the KP-10 analog DK6-kisspeptin-10 (DKP-10) were carried out. DKP-10 was revealed by substitution of Phe at position six with dLys.

3.4.1 Invasion of breast cancer cells treated with kisspeptin-10

Invasion of HCC 1806 cells was measured after 72 h and daily treatment with KP-10 in different concentrations.

Results of the coculture controls are represented in figure 3.17(a). Invasion of cells in coculture was significantly increased (100 % $\pm$ 8 % SEM vs. 2066 % $\pm$ 306 % SEM). Treatment with KP-10 in concentrations of 10^{-14} M to 10^{-8} M showed no effect on monocultured cells (data not shown). No significant inhibition was observed in coculture by KP-10 (coculture: 100 % $\pm$ 5 % SEM; 10^{-14} M: 58 % $\pm$ 7 % SEM; 10^{-13} M: 90 % $\pm$ 18 % SEM; 10^{-12} M: 72 % $\pm$ 9 % SEM; 10^{-11} M: 102 % $\pm$ 22 % SEM; 10^{-10} M: 88 % $\pm$ 13 % SEM; 10^{-9} M: 63 % $\pm$ 7 % SEM; 10^{-8} M: 98 % $\pm$ 7 % SEM; see figure 3.17(b)).
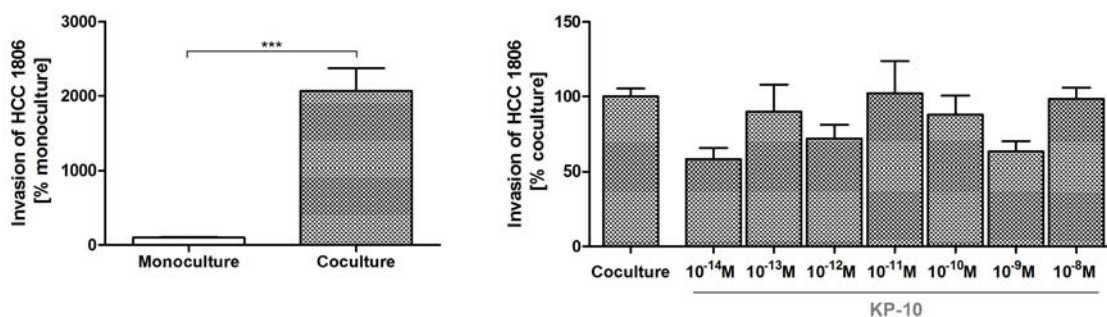
(a) Invasion of HCC 1806   (b) Invasion of cocultured cells treated with KP-10

Figure 3.17: Invasion of HCC 1806 cells treated with KP-10

Invasion was studied by a modified Boyden chamber assay for the breast cancer cell line HCC 1806 treated with KP-10. (a) Invasion of HCC 1806 cells was measured without treatment in monoculture (white columns) and cocultivated with osteosarcoma cells (dotted columns). Invasion is graphed in relation to the invaded cells in monoculture after 72 h. Results were analyzed by paired t-test (mean $\pm$ SEM; ***: p < 0.001; n = 20). (b) Invasion of cocultured HCC 1806 cells was analyzed under treatment with KP-10 daily in different concentrations. Invasion is graphed in relation to the invaded cells in coculture without treatment after 72 h. Results were analyzed by 1way ANOVA and Dunnett's multiple comparison test (mean $\pm$ SEM; n = 20 for coculture control; n = 8 for KP-10 [10^{-14} M, 10^{-13} M]; n = 12 for KP-10 [10^{-12} M to 10^{-8} M]).

3.4.2 Invasion of breast cancer cells treated with a kisspeptin-10 analog

Invasion of HCC 1806 cells was measured after 72 h and daily treatment with DKP-10 in different concentrations.

Invasion in coculture was significantly increased without treatment (100 % $\pm$ 8 % SEM vs. 2219 % $\pm$ 386 % SEM; see figure 3.18(a)). Treatment with DKP-10 in concentrations of 10^{-14} M to 10^{-8} M showed no effect on monocultured cells (data not shown). In figure 3.18(b), the effect on invasion by DKP-10 in coculture is graphed. In concentrations of 10^{-12} M (48 % $\pm$ 10 % SEM), 10^{-10} M (61 % $\pm$ 10 % SEM) and 10^{-9} M (56 % $\pm$ 6 % SEM), invasion was decreased significantly. Except the samples treated with 10^{-8} M DKP-10, other concentrations tended to inhibit invasion of cells (coculture: 100 % $\pm$ 5 % SEM; 10^{-14} M: 74 % $\pm$ 11 % SEM; 10^{-13} M: 69 % $\pm$ 10 % SEM; 10^{-11} M: 70 % $\pm$ 17 % SEM; 10^{-8} M: 101 % $\pm$ 18 % SEM).
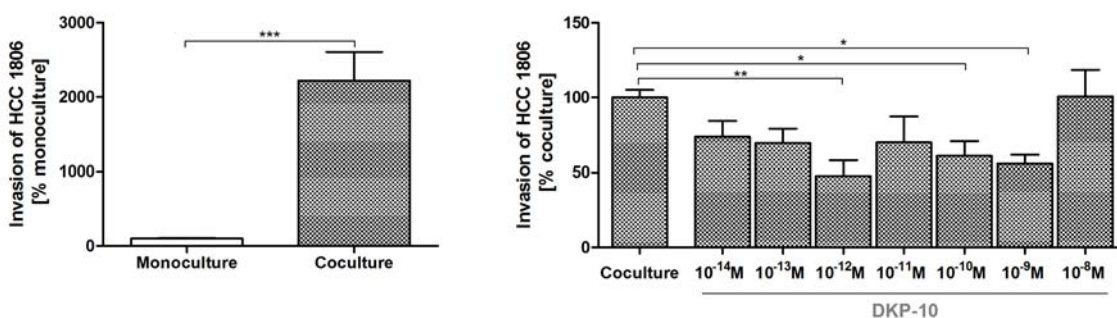
(a) Invasion of HCC 1806   (b) Invasion of cocultured cells treated with DKP-10

Figure 3.18: Invasion of HCC 1806 cells treated with DKP-10

Invasion was studied by a modified Boyden chamber assay for the breast cancer cell line HCC 1806 treated with DKP-10. (a) Invasion of HCC 1806 cells was measured without treatment in monoculture (white columns) and cocultivated with osteosarcoma cells (dotted columns). Invasion is graphed in relation to the invaded cells in monoculture after 72 h. Results were analyzed by paired t-test (mean $\pm$ SEM; ***: $p < 0.001$; n = 14). (b) Invasion of cocultured HCC 1806 cells was analyzed under treatment with DKP-10 daily in different concentrations. Invasion is graphed in relation to the invaded cells in coculture without treatment after 72 h. Results were analyzed by 1way ANOVA and Dunnett's multiple comparison test (mean $\pm$ SEM; *: $p < 0.05$; **: $p < 0.01$; n = 14 for coculture control; n = 8 for KP-10 [10^{-14} M, 10^{-13} M]; n = 6 for KP-10 [10^{-12} M to 10^{-8} M]).

Summing up, KP-10 did not affect HCC 1806 cells cocultivated with osteosarcoma cells significantly. In contrast, the KP-10 analog DKP-10 led to significantly reduced invasion. Both peptides showed no effect on monocultured cells.

3.5 Effects of kisspeptin-10 *in vivo*

According to the inhibited invasion of breast cancer cells by KP-10 *in vitro* [Olbrich, 2010a, Olbrich et al., 2010b], the results of the following chapter describe the effect of kisspeptin-10 on metastasis and tumor growth *in vivo*. Different breast cancer xenograft models in mice were used (see chapter 2.2.6). Metastasis was analyzed in murine organs, as lung, bone and liver. Circulating tumor cells were identified in blood. Tumor growth was measured.

3.5.1 MDA-MB-231 breast cancer xenograft

Tumor cell metastasis was studied by intracardiacally injection of MDA-MB-231 cells. Metastasis of CTCs was investigated. Three experimental groups were kept: the control group without tumor cell injection and without treatment, the tumor group with tumor cell injection and without treatment and the treatment group with tumor cell injection and treatment with KP-10 [50 µg/mouse] daily starting the day after injection. The study lasted up to 34 days.

3.5.1.1 Metastasis

Analysis of the results showed no significant amounts of hDNA in murine organs, lung, liver and bone, and in blood for treated and untreated mice (data not shown).

3.5.2 HCC 1806 breast cancer xenograft

Metastasis was studied by injecting HCC 1806 cells orthotopically at the mammary glands of mice. Two tumors were set per mouse. Three experimental groups were kept: the control group without tumor cell injection and without treatment, the tumor group with tumor cell injection and without treatment and the treatment group with tumor cell injection and treatment with KP-10 [50 µg/mouse] daily starting the day after injection. On day 28, the experiment was determined.

3.5.2.1 Tumor growth

All of the mice in the tumor group and in the treatment group developed tumors at the mammary glands.

The graph in figure 3.19 shows a constant tumor growth in both groups. The tumors in the treatment group grew significantly slower than in the tumor group (day 11: $47.2 \, \text{mm}^3 \pm 13.9 \, \text{mm}^3$ SEM vs. $105.3 \, \text{mm}^3 \pm 10.7 \, \text{mm}^3$ SEM; day 14: $79.2 \, \text{mm}^3 \pm 16.5 \, \text{mm}^3$ SEM vs. $133.2 \, \text{mm}^3 \pm 13.1 \, \text{mm}^3$ SEM; day 17: $134.7 \, \text{mm}^3 \pm 25.0 \, \text{mm}^3$ SEM vs. $239.4 \, \text{mm}^3 \pm 22.5 \, \text{mm}^3$ SEM; day 20:

209.1 mm^3 ± 40.9 mm^3 SEM vs. 415.3 mm^3 ± 34.8 mm^3 SEM; day 24: 296.8 mm^3 ± 45.4 mm^3 SEM vs. 545.9 mm^3 ± 45.3 mm^3 SEM; day 28: 446.2 mm^3 ± 58.6 mm^3 SEM vs. 674.9 mm^3 ± 71.3 mm^3 SEM).
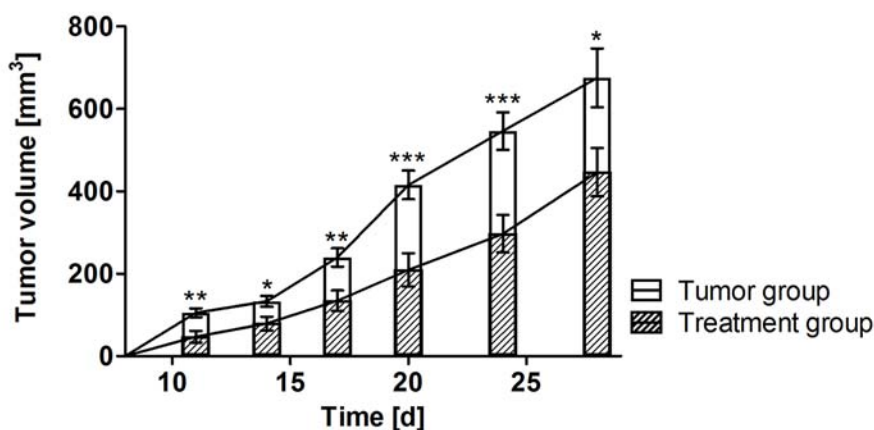
Figure 3.19: Tumor growth in xenografts with HCC 1806

Mice were injected orthotopically at the mammary glands with HCC 1806 breast cancer cells. Two tumors were set per mouse. In the tumor group (white columns), tumor growth was observed without treatment. In the treatment group (shaded columns), treatment with KP-10 [50 µg/mouse] daily started the day after injection. Tumor growth is represented as tumor volume. Results were analyzed by paired t-test comparing data of tumor and treatment group within one day of measurement (mean ± SEM; *: p < 0.05; **: p < 0.01; ***: p < 0.001; n = 20 (ten mice with two tumors/mouse)).

3.5.2.2 Metastasis

hDNA was detected in lung. CTCs were measured in blood. No hDNA was found in bone and liver (data not shown).

In figure 3.20, the amount of hDNA in lung is represented. The results of the tumor group show a significant pattern of hDNA related to the control group (control group: 1.35*10^{-7} % ± 1.35*10^{-7} % SEM; tumor group: 1.26*10^{-4} % ± 3.63*10^{-5} % SEM; see figure 3.20a). In the tumor group respectively in the treatment group, eight of ten mice developed metastasis in lung. Comparing the ratio of hDNA in the tumor group and the treatment group, no significant difference was measured (treatment group: 1.80*10^{-4} % ± 1.18*10^{-4} % SEM; see figure 3.20b).

(a) Lung metastasis in untreated mice

(b) Lung metastasis in mice treated with KP-10
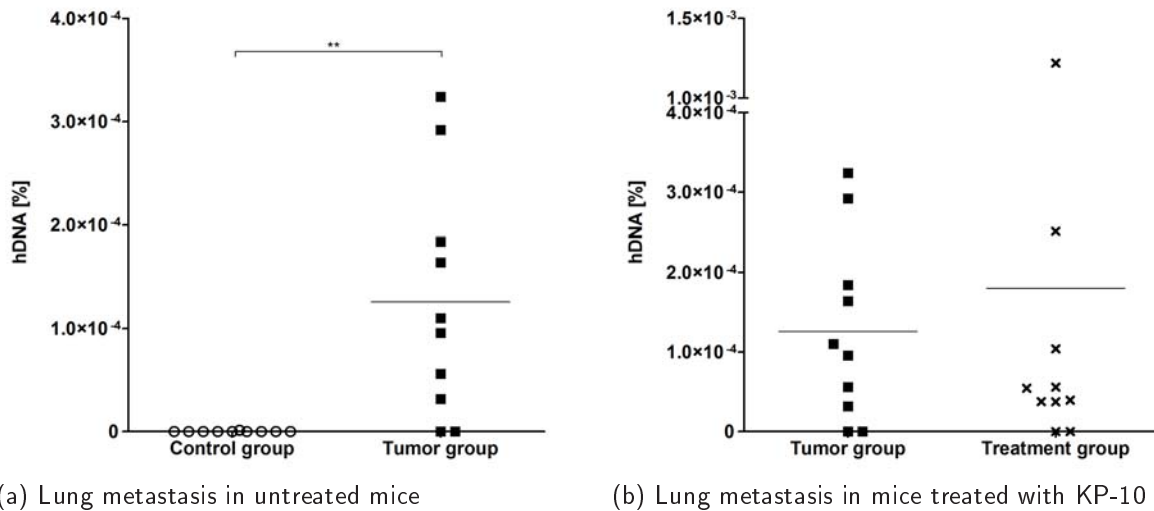
Figure 3.20: Lung metastasis in xenografts with HCC 1806

Mice were injected orthotopically at the mammary glands with HCC 1806 breast cancer cells and treated with KP-10 [50 µg/mouse] daily starting the day after injection. Lungs were collected at the end of the study and analyzed by DNA isolation and qPCR. Metastasis is represented as ratio of hDNA in mDNA. (a) For verification of the metastasis model, a control group was kept in parallel without tumors and treatment (white circles). In the tumor group (black rectangles), mice were untreated. Results were analyzed by Mann Whitney test (mean; **: $p < 0.01$; n = 10). (b) Metastasis in the tumor group (black rectangles) and in the treatment group (black crosses) was compared. Results were analyzed by paired t-test (mean; n = 10).

The amount of hDNA detected in blood is graphed in figure 3.21. In seven of ten mice of the tumor group, CTCs were found. Significant more hDNA was measured in contrast to the control group (control group: $1.36*10^{-6}$ % $\pm$ $1.36*10^{-6}$ % SEM; tumor group: $7.81*10^{-4}$ % $\pm$ $7.41*10^{-4}$ % SEM; see figure 3.21a). hDNA was detected in one of the mice of the control group. In the treatment group, in eight of ten mice, tumor cells were circulating in blood. The analysis of hDNA of the treatment group showed comparable results as detected in the tumor group (treatment group: $6.86*10^{-4}$ % $\pm$ $2.44*10^{-4}$ % SEM; see figure 3.21b).

(a) Circulating tumor cells in untreated mice

(b) Circulating tumor cells in mice treated with KP-10
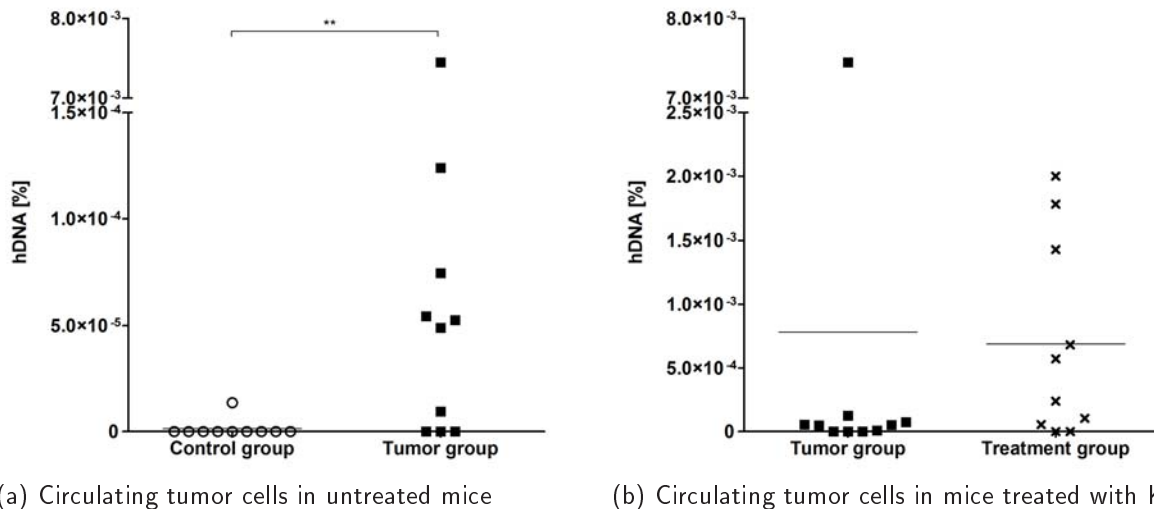
Figure 3.21: Circulating tumor cells in xenografts with HCC 1806

Mice were injected orthotopically at the mammary glands with HCC 1806 breast cancer cells and treated with KP-10 [50 µg/mouse] daily starting the day after injection. Blood was collected at the end of the study and analyzed by DNA isolation and qPCR. CTCs are represented as ratio of hDNA in mDNA. (a) For verification of the experimental model, a control group was kept in parallel without tumors and treatment (white circles). In the tumor group (black rectangles), mice were untreated. Results were analyzed by Mann Whitney test (mean; **: $p < 0.01$; n = 10). (b) CTCs in the tumor group (black rectangles) and in the treatment group (black crosses) were compared. Results were analyzed by paired t-test (mean; n = 10).

3.5.3 MDA-MB-435s breast cancer xenograft

MDA-MD-435s cells were injected orthotopically at the mammary glands of mice. Two tumors were set per mouse. Three experimental groups were kept: the control group without tumor cell injection and without treatment, the tumor group with tumor cell injection and without treatment and the treatment group with tumor cell injection and treatment with KP-10 [50 µg/mouse] daily starting the day after injection. Study was determined on day 41.

3.5.3.1 Tumor growth

In the tumor group and in the treatment group, 20 % of the injection sites in mice developed no tumors.

In figure 3.22, tumor growth of the tumor group and the treatment group is graphed. Tumors of mice treated with KP-10 showed a trend towards a slower growth rate than untreated mice. The difference was not significant (day 15: $8.8 \, \text{mm}^3 \pm 4.8 \, \text{mm}^3$ SEM vs. $17.2 \, \text{mm}^3 \pm 6.7 \, \text{mm}^3$ SEM; day 18: $22.7 \, \text{mm}^3 \pm 10.4 \, \text{mm}^3$ SEM vs. $36.9 \, \text{mm}^3 \pm 11.3 \, \text{mm}^3$ SEM; day 22: $42.2 \, \text{mm}^3 \pm 17.7 \, \text{mm}^3$ SEM vs. $88.4 \, \text{mm}^3 \pm 27.3 \, \text{mm}^3$ SEM; day 25: $76.1 \, \text{mm}^3 \pm 28.9 \, \text{mm}^3$ SEM vs.

129.6 mm^3 $\pm$ 34.9 mm^3 SEM; day 29: 112.2 mm^3 $\pm$ 41.7 mm^3 SEM vs. 198.8 mm^3 $\pm$ 51.2 mm^3 SEM; day 32: 197.3 mm^3 $\pm$ 69.0 mm^3 SEM vs. 289.6 mm^3 $\pm$ 71.3 mm^3 SEM; day 36: 281.6 mm^3 $\pm$ 88.7 mm^3 SEM vs. 407.6 mm^3 $\pm$ 93.3 mm^3 SEM; day 39: 394.8 mm^3 $\pm$ 116.4 mm^3 SEM vs. 507.0 mm^3 $\pm$ 120.2 mm^3 SEM; day 41: 459.0 mm^3 $\pm$ 135.7 mm^3 SEM vs. 574.5 mm^3 $\pm$ 134.6 mm^3 SEM).
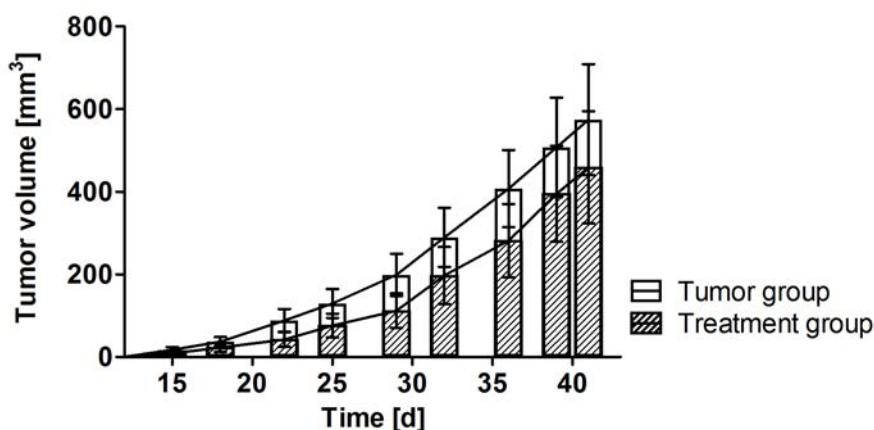
Figure 3.22: Tumor growth in xenografts with MDA-MB-435s

Mice were injected orthotopically at the mammary glands with MDA-MB-435s breast cancer cells. Two tumors were set per mouse. In the tumor group (white columns), tumor growth was observed without treatment. In the treatment group (shaded columns), treatment with KP-10 [50 µg/mouse] daily started the day after injection. Tumor growth is represented as tumor volume. Results were analyzed by paired t-test comparing data of tumor and treatment group within one day of measurement (mean $\pm$ SEM; n = 20 (ten mice with two tumors/mouse)).

3.5.3.2 Metastasis

hDNA was detected in lung, but not in bone (data not shown).

The graph in figure 3.23 represents the ratio of hDNA in lung. In figure 3.23a, the results are graphed for the control group and the tumor group. In the tumor group, in eight of ten mice, the cells metastasized to lung. hDNA was found in one of the mice of the control group. The amount of hDNA was significantly different (control group: 3.40*10^{-5} % $\pm$ 3.29*10^{-5} % SEM; tumor group: 1.08*10^{-3} % $\pm$ 9.08*10^{-4} % SEM). Figure 3.23b shows the ratio of hDNA for the tumor group and the treatment group, which showed metastasis in seven of ten mice. A trend towards lower hDNA amounts in the treated mice was observed with no significance (treatment group: 2.19*10^{-4} % $\pm$ 1.35*10^{-4} % SEM).

(a) Lung metastasis in untreated mice

(b) Lung metastasis in mice treated with KP-10
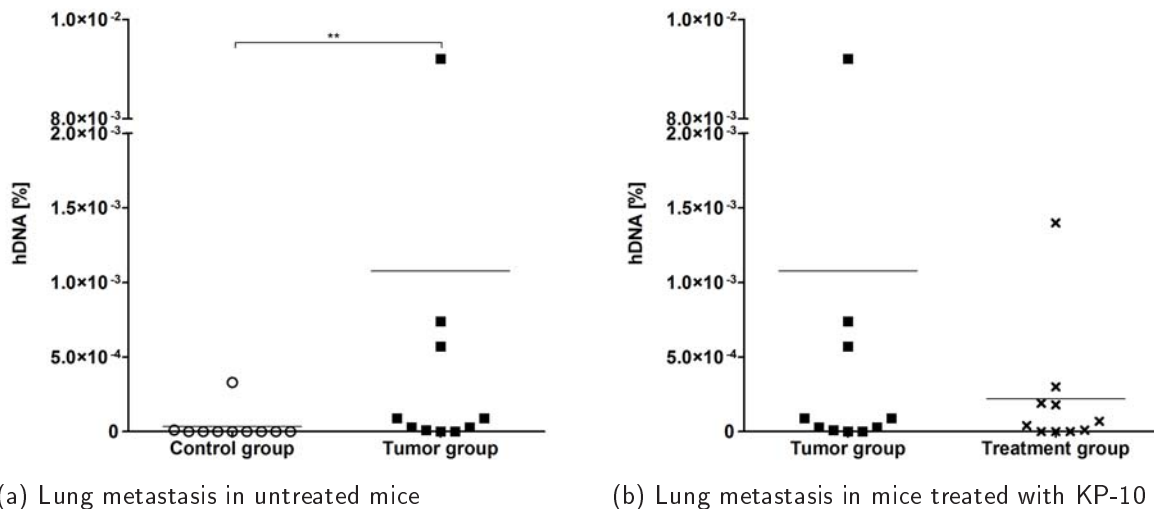
Figure 3.23: Lung metastasis in xenografts with MDA-MB-435s

Mice were injected orthotopically at the mammary glands with MDA-MB-435s breast cancer cells and treated with KP-10 [50 µg/mouse] daily starting the day after injection. Lungs were collected at the end of the study and analyzed by DNA isolation and qPCR. Metastasis is represented as ratio of hDNA in mDNA. (a) For verification of the metastasis model, a control group was kept in parallel without tumors and treatment (white circles). In the tumor group (black rectangles), mice were untreated. Results were analyzed by Mann Whitney test (mean; **: $p < 0.01$; n = 10). (b) Metastasis in the tumor group (black rectangles) and in the treatment group (black crosses) was compared. Results were analyzed by paired t-test (mean; n = 10).

In summary, two xenograft models were studied for metastasis. Intracardiac injection of MDA-MB-231 cells did not lead to detectable metastasis. After orthotopical injection of HCC 1806 and MDA-MB-435s cells, tumors developed. Sporadic metastasis was observed in lung and blood for some of the mice of the experimental groups. An effect of KP-10 treatment on metastasis *in vivo* could not be clarified by the used experimental setting.

3.6 Effects of kisspeptin-10 on proliferation

The results in chapter 3.5 showed a reduced tumor growth by kisspeptin-10 treatment *in vivo*. The experiments of the following chapter describe the effect of KP-10 on proliferation *in vitro*. Therefore, breast cancer cell lines were investigated for their endogenous GPR54 expression. Their proliferation was studied under KP-10 treatment. For reasons of comparison, further experiments were carried out with cells transfected to overexpress GPR54.

3.6.1 GPR54 expression in breast cancer cells and transfected cells

GPR54 receptor expression was studied by immune cytochemistry, mRNA and protein analysis (see chapter 2.2.4.1, 2.2.3.1-2.2.3.4 and 2.2.4.2).

3.6.1.1 Receptor detection in breast cancer cells

Figure 3.24 shows the results of the immune cytochemical staining. All cell lines expressed GPR54, visualized by the red staining with GPR54 antibody.
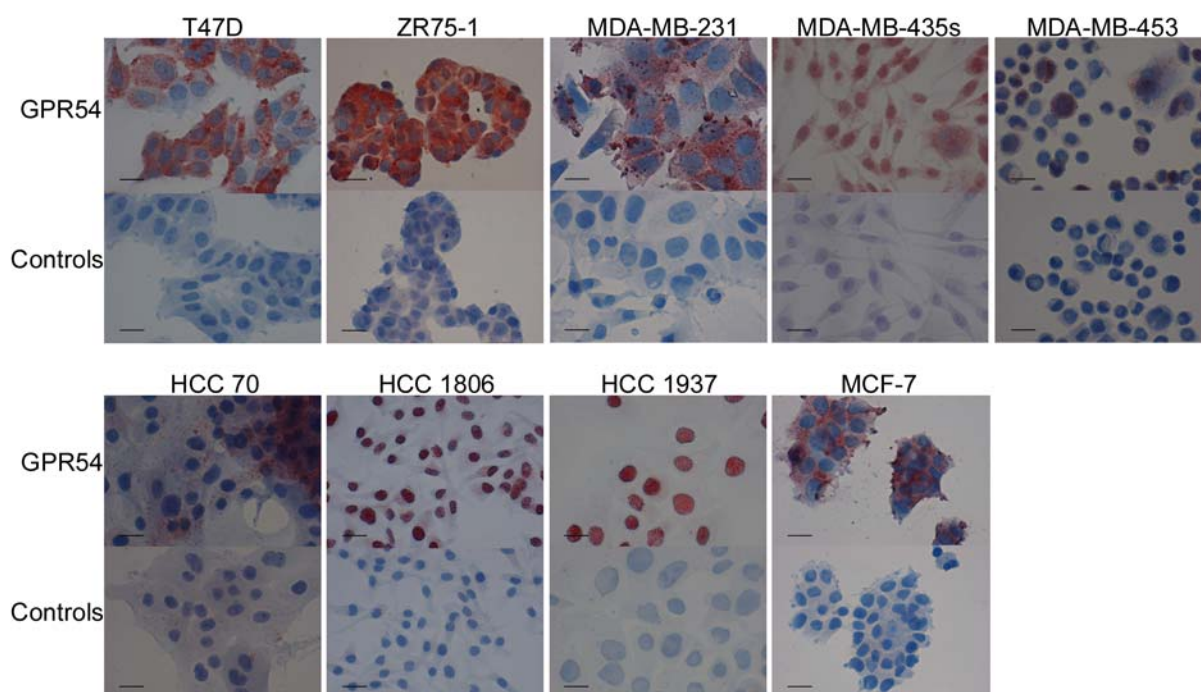
Figure 3.24: GPR54 expression in breast cancer cell lines

Breast cancer cell lines T47D, ZR75-1, MDA-MB-231, MDA-MB-435s, MDA-MB-453, HCC 70, HCC 1806, HCC 1937 and MCF-7 were grown on microscope chamber slides. GPR54 was detected immunocytochemically by red staining with the corresponding antibody (upper lines). Controls were performed by omission of the primary antibody (lower lines). Bright field images were taken (scale bar = 40 µm). Images represent the findings in at least three different passages of each cell line. This figure is published in Ziegler et al. 2013.

Further investigations on mRNA levels are represented in figure 3.25. T47D, ZR75-1 and MCF-7 showed receptor mRNA expression. In MDA-MB-231, MDA-MB-435s, MDA-MB-453, HCC 70, HCC 1806 and HCC 1937 no clear signal for GPR54 mRNA was found. In addition, figure 3.25 shows GPR54 expression of B35 clone 1 transfected to overexpress GPR54 (see chapter 3.6.1.2). The initial amount of cDNA of the clone used for mRNA analysis was 100 times smaller than the amount of cDNA used for the breast cancer cell lines. This was documented by the low signal

of the housekeeping gene L7 in the clone samples compared to the breast cancer cell samples whereas the signal for GPR54 was clearly detectable.
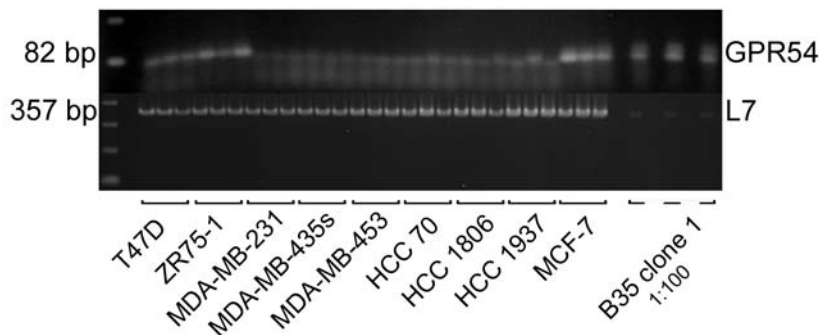
Figure 3.25: GPR54 mRNA expression

GPR54 mRNA expression was investigated by gene expression analysis via RT-PCR for breast cancer cell lines and B35 clone 1 transfected to overexpress GPR54 (cDNA dilution 1:100). For reasons of comparison, mRNA controls were performed by proof of the housekeeping gene L7. Images represent the findings in at least three different passages of each cell line. This figure is published in Ziegler et al. 2013.

Protein expression of GPR54 is imaged in figure 3.26. Protein levels were detected in every breast cancer cell line with different quantities. For reasons of comparison, GPR54 protein expression of B35 clone 1 was also detected.
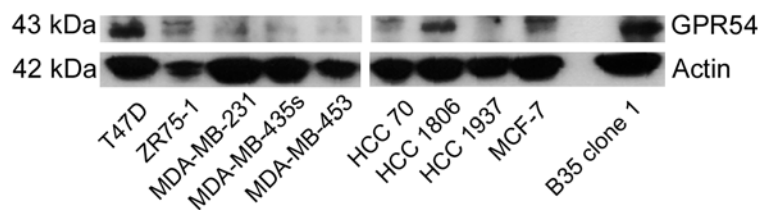
Figure 3.26: GPR54 protein expression

GPR54 protein expression was studied by Western blot analysis for breast cancer cell lines and B35 clone 1 (30 μg protein per sample). Controls were performed by proof of actin as protein standard. The image is representable for findings in at least three different passages of each cell line respectively clone. This figure is published in Ziegler et al. 2013.

3.6.1.2 Receptor detection in cells transfected with GPR54

B35 neuronal rat cells stable transfected with murine GPR54 were chosen as an artificial cell model overexpressing GPR54. Six clones of transfected B35 cells were tested for their GPR54 expression levels.

Results of the mRNA analysis are shown in figure 3.27. Clone 2 (0.72 ± 0.16 SEM), clone 4 (1.36 ± 0.61 SEM), clone 5 (1.32 ± 0.24 SEM) and clone 6 (0.75 ± 0.16 SEM) expressed GPR54 in

a similar quantity compared to clone 1. GPR54 expression level in clone 3 was significantly higher (2.74 ± 0.70 SEM) than in clone 1.
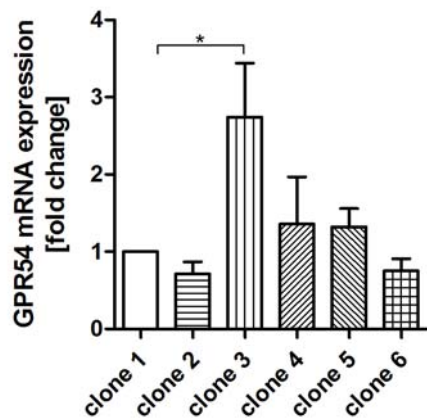
(a) Relative mRNA expression levels of GPR54
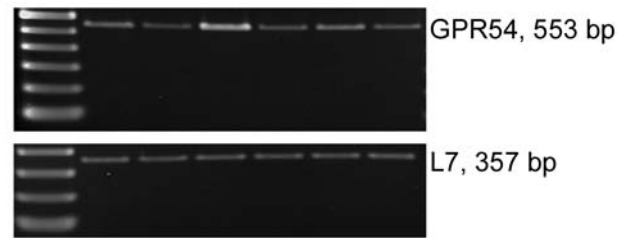
(b) Agarose gel of GPR54 expression

Figure 3.27: GPR54 mRNA expression in B35 mGPR54 clones

GPR54 distribution was investigated in six B35 mGPR54 clones by gene expression analysis via RT-PCR. (a) Expression was standardized to the expression of the housekeeping gene L7 and normalized to the expression of clone 1 (white column). Results were analyzed by 1way ANOVA and Dunnett's multiple comparison test (mean $\pm$ SEM; *: $p < 0.05$; n = 3). (b) Images of agarose gels showing the PCR products of GPR54 and the housekeeping gene L7. Images represent the findings in at least three different passages of each clone. These figures are published in Ziegler et al. 2013.

On protein levels, no significant differences of GPR54 expression were observed in clone 2 (0.70 ± 0.20 SEM), clone 3 (1.12 ± 0.22 SEM) clone 4 (1.47 ± 0.40 SEM), clone 5 (1.34 ± 0.20 SEM) and clone 6 (1.02 ± 0.24 SEM; see figure 3.28) compared to clone 1.
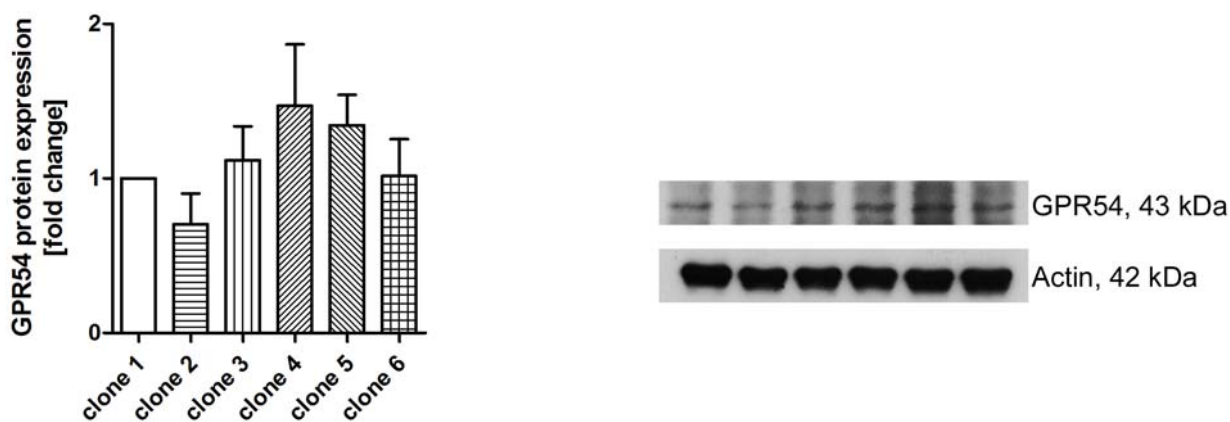
(a) Relative protein expression levels of GPR54

(b) Western blot of GPR54 expression

Figure 3.28: GPR54 protein expression in B35 mGPR54 clones

GPR54 protein expression was studied in six B35 mGPR54 clones by Western blot analysis. (a) Expression was standardized to the expression of actin and normalized to the expression of clone 1 (white column). Results were analyzed by 1way ANOVA and Dunnett's multiple comparison test (mean $\pm$ SEM; n = 3). (b) Images of Western blots showing GPR54 and actin proteins. Images represent the findings in at least three different passages of each clone. These figures are published in Ziegler et al. 2013.

3.6.2 Cell growth under kisspeptin-10 treatment

For proliferation studies, four breast cancer cell lines and three B35 cell clones transfected to overexpress GPR54 were chosen. Proliferation was measured after treatment with KP-10 in different concentrations. KP-10 solutions were added once daily. Proliferation assays were prepared as described in chapter 2.2.5 after 72 h.

3.6.2.1 Proliferation of breast cancer cells treated with kisspeptin-10

MDA-MB-231, MDA-MB-435s, HCC 1806 and MCF-7 showed different GPR54 expression levels according to the results on mRNA and protein levels (see chapter 3.6.1.1). Proliferation was measured in controls and treated samples. No significant differences were observed for each cell line (MDA-MB-231: 100.0 % $\pm$ 0.7 % SEM; 10^{-11} M: 100.1 % $\pm$ 0.8 % SEM; 10^{-9} M: 101.1 % $\pm$ 1.0 % SEM; 10^{-7} M: 100.3 % $\pm$ 1.9 % SEM; 10^{-5} M: 96.4 % $\pm$ 2.6 % SEM; MDA-MB-435s: 100.0 % $\pm$ 2.7 % SEM; 10^{-11} M: 99.3 % $\pm$ 3.2 % SEM; 10^{-9} M: 100.1 % $\pm$ 4.1 % SEM; 10^{-7} M: 100.2 % $\pm$ 4.6 % SEM; 10^{-5} M: 101.5 % $\pm$ 7.0 % SEM; HCC 1806: 100.0 % $\pm$ 1.2 % SEM; 10^{-11} M: 100.5 % $\pm$ 1.6 % SEM; 10^{-9} M: 96.6 % $\pm$ 2.6 % SEM; 10^{-7} M: 99.1 % $\pm$ 1.9 % SEM; 10^{-5} M: 99.0 % $\pm$ 3.9 % SEM; MCF-7: 100.0 % $\pm$ 0.7 % SEM; 10^{-11} M: 99.7 % $\pm$ 2.4 % SEM; 10^{-9} M: 95.5 % $\pm$ 2.1 % SEM; 10^{-7} M: 99.5 % $\pm$ 4.9 % SEM; 10^{-5} M: 105.8 % $\pm$ 3.9 % SEM; see figure 3.29).
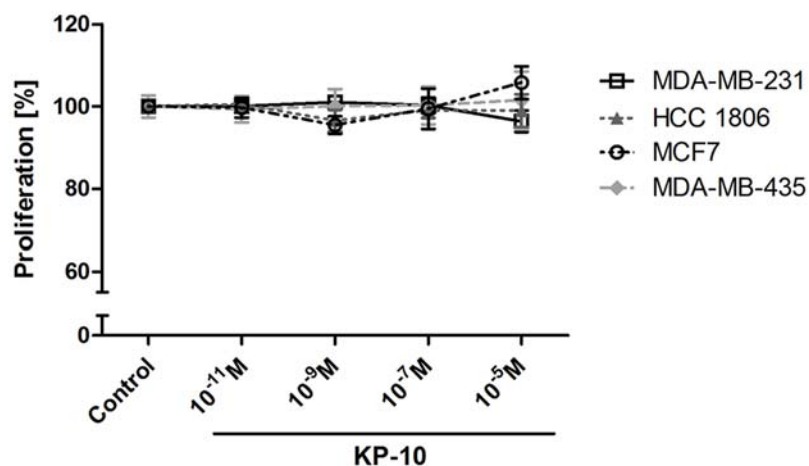
Figure 3.29: Proliferation of breast cancer cells treated with KP-10

The breast cancer cell lines MDA-MB-231, MDA-MB-435s, HCC 1806 and MCF-7 were grown in 96 well-plates and treated with KP-10 daily in different concentrations for 72 h. Proliferation was normalized to the growth rate of the untreated controls. Results were analyzed by 1way ANOVA and Dunnett's multiple comparison test within each cell line (mean $\pm$ SEM; n = 6/8). This figure is published in Ziegler et al. 2013.

3.6.2.2 Proliferation of cells overexpressing GPR54 treated with kisspeptin-10

Proliferation of cells transfected to overexpress GPR54 was measured in B35 clone 1, clone 3 and clone 4. Clone 3 showed the highest mRNA levels of GPR54 and the largest protein amount was detected in clone 4 (see chapter 3.6.1.2).

Proliferation is graphed in figure 3.30. Proliferation of clone 1 was marginal affected by treatment with high concentrations of KP-10 compared to controls (control: 100.0 % $\pm$ 1.2 % SEM; 10^{-11} M: 100.9 % $\pm$ 5.0 % SEM; 10^{-9} M: 101.7 % $\pm$ 4.0 % SEM; 10^{-7} M: 95.1 % $\pm$ 3.6 % SEM; 10^{-5} M: 91.3 % $\pm$ 1.8 % SEM). The proliferation of clone 3 and clone 4 was significantly inhibited by KP-10 concentrations of 10^{-7} M and 10^{-5} M (clone 3: control: 100.0 % $\pm$ 1.8 % SEM; 10^{-11} M: 101.3 % $\pm$ 1.4 % SEM; 10^{-9} M: 99.3 % $\pm$ 2.7 % SEM; 10^{-7} M: 83.5 % $\pm$ 1.6 % SEM; 10^{-5} M: 80.0 % $\pm$ 1.8 % SEM; clone 4: control: 100.0 % $\pm$ 1.5 % SEM; 10^{-11} M: 98.2 % $\pm$ 2.8 % SEM; 10^{-9} M: 96.9 % $\pm$ 2.1 % SEM; 10^{-7} M: 87.5 % $\pm$ 4.1 % SEM; 10^{-5} M: 86.4 % $\pm$ 2.1 % SEM).
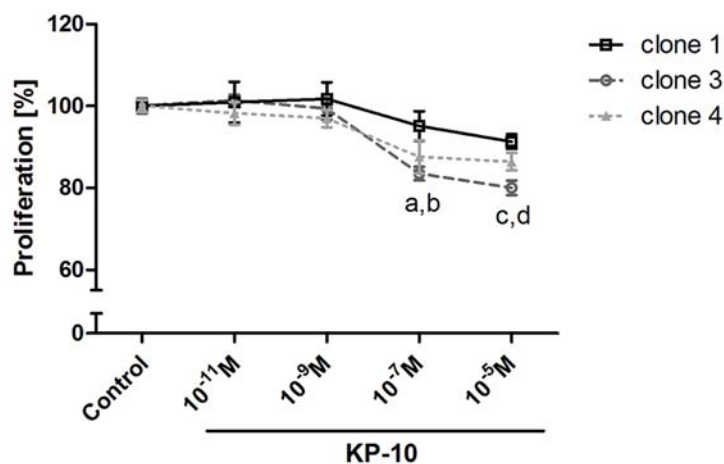
Figure 3.30: Proliferation of B35 mGPR54 clones treated with KP-10

The B35 clones 1, 3 and 4 were grown in 96 well-plates and treated with KP-10 daily in different concentrations for 72 h. Proliferation was normalized to the growth rate of the untreated controls. Results were analyzed by 1way ANOVA and Dunnett's multiple comparison test within each clone (mean $\pm$ SEM; a, c: $p < 0.001$ for clone 3 vs. control; b: $p < 0.01$ for clone 4 vs. control; d: $p < 0.001$ for clone 4 vs. control; n = 6/8). This figure is published in Ziegler et al. 2013.

Taken together, GPR54 was expressed in all of the studied breast cancer cell lines. Results of different analytical methods vary in the amount of cellular receptor expression and a direct comparison of GPR54 levels was not possible. It seemed that GPR54 expression in the breast cancer cell lines was lower than in the transfected clones. Proliferation studies showed inhibited cell growth by KP-10 in B35 clone 3 and clone 4, but not in MDA-MD-231, MDA-MB-435s, HCC 1806 and MCF-7 cells.

4 Discussion

4.1 Coculture effects on breast cancer cells

The interaction of breast cancer and osteoblast-like osteosarcoma cells led to increased invasion properties of non-invasive cells in an established coculture system. One important system, the CXCL12/CXCR4 system, was already identified for the interaction between CXCR4 expressing breast cancer cells and CXCL12 secreting osteosarcoma cells [von Alten et al., 2006]. Further work with CXCL12 antibodies reduced the invasion partially, but it was not able to abolish it [Olbrich, 2010a]. Thus, the altered invasive characteristics should be further investigated for a better understanding of other factors involved.

An increased cell motility is often accompanied by morphological alterations and a modified gene expression. One important process, the EMT, is often associated with cancer progression leading to loss of cell-cell adhesions and an enhanced invasiveness [Christiansen and Rajasekaran, 2006]. Thus, analysis of motility marker involved in EMT was carried out.

4.1.1 Classification of breast cancer cell lines

The primary attempt was to classify breast cancer cell lines in epithelial or mesenchymal phenotypes to estimate their invasive character. Cells can be differentiated by morphology, physical characteristics, intracellular junctions, molecular marker expression and cytoskeletal organization. Two aspects were chosen. Breast cancer cell lines were characterized for their morphological appearance and the expression of epithelial and mesenchymal marker. It was expected, that well-differentiated cells growing in clusters with strong cell-cell contacts would express more epithelial marker. On the contrary, cells with a more spindle-like morphology and less differentiation would express mainly mesenchymal marker. The marker were chosen based on gene expression analysis in literature correlating CDH1 and TJP1 with an epithelial phenotype and VIM and S100A4 with a mesenchymal phenotype [Wu and Zhou, 2008, Kalluri and Weinberg, 2009]. CDH1 is a transmembrane protein involved in cell-cell adhesions by adherents junctions. Loss of that protein is

highly associated with an invasive phenotype. TJP1 forms interconnections between single cells as permeability barriers for a restricted lateral diffusion. Its function is important for membrane polarity. The intermediate filament VIM facilitates cytoskeletal remodeling and is linked to an increased cell invasiveness. S100A4 belongs to the S100 family, which is responsible for motility, invasion and tubulin polymerization [Christiansen and Rajasekaran, 2006]. All of the studied marker vary in their cellular functions and were selected to check the expression from different starting points.

Seven of the nine tested breast cancer cell lines, T47D, ZR75-1, MDA-MB-453, HCC 70, HCC 1806, HCC 1937 and MCF-7, showed a more epithelial-like morphology, whereas MDA-MB-231 and MDA-MB-435s had a more mesenchymal-like appearance (see chapter 3.1.1). The presence of the two epithelial marker were analyzed in all of the cell lines. CDH1 expression correlated well with the morphological findings showing a strong expression in the first seven cell lines and very low respectively no amounts in MDA-MB-231 and MDA-MB-435s cells. The detection of TJP1 was not meaningful in this experimental setting. It was expressed in all of the cell lines without any observable difference. TJP1 was not a suitable marker in this context. Mesenchymal marker expression showed a correlation for VIM with the morphological appearance of the cells. Its strongest amount was detected in MDA-MB-231 and MDA-MB-435s cells. The other cell lines showed less or no expression. S100A4 showed different expression patterns in the cell lines. No direct link could be seen between its presence and the morphological phenotype of the cells (see chapter 3.1.2).

Based on these results, the breast cancer cell lines T47D, ZR75-1, MDA-MB-453, HCC 70, HCC 1806, HCC 1937 and MCF-7 were classified as epithelial-like cell lines. The results of MDA-MB-231 and MDA-MB-435s cells demonstrated these cell lines as mesenchymal-like. These findings are comparable with diverse studies in literature. Based on morphological analysis, T47D, ZR75-1 and MCF-7 cells showed a fused appearance in Matrigel^{TM}, whereas the cell lines MDA-MB-231 and MDA-MB-435s had a stellate morphology [Sommers et al., 1994, Zajchowski et al., 2001]. Gene expression profiling led to a clustering of breast cancer cells in luminal and basal cell lines. The luminal part was more differentiated and connected by tight cell-cell junctions identified for T47D, ZR75-1, MDA-MB-453 and MCF-7 cells. The basal phenotype was characterized by less differentiation and a mesenchymal-like appearance detected in MDA-MB-231 [Charafe-Jauffret et al., 2006, Neve et al., 2006]. In addition, gene analysis in T47D, ZR75-1 and MCF-7 cells showed expression of CDH1, but no expression of VIM. The expression pattern of these two genes was found in the cell lines MDA-MB-231 and MDA-MB-435s vice versa [Sommers et al., 1994, Zajchowski et al., 2001]. This is consistent with the observations in the present work. In MDA-MB-453 cells, no CDH1 and no VIM was expressed [Sommers et al., 1994, Zajchowski et al., 2001], whereas the present results showed low expression rates of these genes in MDA-MB-453 cells. One study characterized the cell line HCC 1937 as basal respectively mesenchymal-like based

on gene expression analysis. HCC 1937 cells expressed high amounts of VIM, MMP2, FN1 and S100A2, another member of the S100 protein family. All of the genes were related to the less differentiated phenotype [Charafe-Jauffret et al., 2006]. In the present work, HCC 1937 cells were classified as a more epithelial-like cell line adapted from the high expression rate of CDH1 and its morphology showing growth in clusters with direct cell-cell contacts. However, a clear expression of VIM was also observed and an absolute definition of this cell line can not be offered.

Although breast cancer cell lines were classified by several studies in literature, an analysis of the used cell lines was necessary due to possible changes caused by cultivation and growing. The media used in the different laboratories and the culture conditions varied. Furthermore, genetical changes over years of cultivation were possible and could have led to different behavior and phenotypes. Therefore, the cell lines were used for experiments in early passages (except for MDA-MB-453) to maintain their characteristics. Comparison with the results available in literature showed a good analogy for most of the cell lines used in the present work.

4.1.2 Invasive and migratory behavior

In addition to the morphological and gene expression analysis of the nine breast cancer cell lines, they were studied for their invasive properties. The morphological phenotype and the invasive behavior of cells were shown to be interdependent. A more mesenchymal-like respectively basal appearance was associated with high invasiveness and a more epithelial-like respectively luminal morphology was connected with low or no invasion [Sommers et al., 1994, Zajchowski et al., 2001, Neve et al., 2006, Cheng et al., 2007]. For the epithelial-like classified cell lines, T47D, ZR75-1, MDA-MB-453, HCC 70, HCC 1806, HCC 1937 and MCF-7, less invasion was estimated. Whereas the more mesenchymal-like cell lines MDA-MD-231 and MDA-MB-435s were expected to show strong invasion.

During the first experiments, the individual invasion was investigated of each cell line (see chapter 3.2.1). The strongest cell movement was identified for the cell lines MDA-MB-435s and MDA-MB-231. An intermediate invasion was detected in HCC 70, HCC 1806 and HCC 1937 and almost no invasion was observed in T47D, ZR75-1, MDA-MB-453 and MCF-7 cells. These findings correlated well with the observed phenotypical characteristics and EMT marker expression in the present study. Studies in literature showed consistent results classifying the cell lines T47D, ZR75-1, MDA-MB-453 and MCF-7 as less or poorly invasive and MDA-MB-231 and MDA-MB-435s as moderately respectively highly invasive [Neve et al., 2006, Kokkinos et al., 2007].

Further experiments of the present work focused on the invasion in coculture. Therefore, breast cancer cells were grown with an osteoblast-like osteosarcoma cell line without direct cell-cell contact. Invasion increased in all of the cell lines except for MDA-MB-231 and MDA-MB435s. In

comparison with their individual invasion, T47D and MCF-7 showed the largest increase in their invasive properties with an raise of more than 300 times. Based on these observations, invasion of four different behaving cell lines, MCF-7, HCC 1806, MDA-MB-231 and MDA-MB435s, was studied in detail (see chapter 3.2.2). The non-invasive cell line MCF-7 and the intermediate invasive cell line HCC 1806 showed an increased invasion already after 48 h under coculture conditions. MDA-MB-231 and MDA-MB435s were decreased in their invasion by cocultivation after 96 h. But the detailed analysis showed an increase in the invasive behavior for the first 48 h of coculture. After 72 h, no differences in invasion could be observed between both conditions and after 96 h, the invasion in monoculture was higher. In literature, related experimental settings were described focusing an interaction of breast cancer cell lines with other cells respectively tissues. Cancer-associated fibroblasts (CAFs) are cells arising from tumor stroma. They can interact with the tumor cells by release of soluble factors as TGFβ, hepatocyte growth factor (HGF) and insulin-like growth factors (IGFs). Thereby, CAFs were shown to promote cancer cell proliferation and invasion. Coculture studies with CAFs led to increased migration of PMC42-LA, MCF-7 and MDA-MB-231 breast cancer cells [Lebret et al., 2007, Angelucci et al., 2012]. Other experiments with conditioned media from NIH3T3 murine fibroblasts showed only low invasion and migration of T47D, ZR75-1, MDA-MB-453 and MCF-7 cells, whereas the invasion of MDA-MB-231 and MDA-MB435s was high respectively intermediate [Sommers et al., 1994, Zajchowski et al., 2001]. The influence on invasion seems to be dependent on the kind of interacting cells respectively tissues showing different changes. An explanation for the "switch" of the invasive behavior of MDA-MB-231 and MDA-MB-435s cells during cocultivation may be, that one of the factors released by the osteosarcoma cells leads to a receptor internalization caused by an enhanced stimulation over time. Further analysis of factors triggering invasion in coculture is discussed in chapter 4.1.3.

Migration analysis of MCF-7 and MDA-MB-231 cells cocultivated with CAFs showed a more directed cell movement [Angelucci et al., 2012]. According to this, experiments with MCF-7 cells showed no influence on migratory behavior by cocultivation with osteosarcoma cells in the present work (see chapter 3.2.2.3). Thus, the interaction of breast cancer cells with osteosarcoma cells seems to be important in three-dimensional cell movement leading to a "bone"-directed invasion in the studied coculture system. Studies on bone-directed invasion identified the CXCL12/CXCR4 system as a potent regulating system. Earlier works revealed an involvement of the CXCL12/CXCR4 system in the coculture system [von Alten et al., 2006]. In addition, CXCL12 was identified in bone marrow and its protein extract respectively CXCL12 treatment led to increased invasion and migration of CXCR4-expressing MDA-MB-231 cells [Müller et al., 2001]. CXCL12 treatment was also shown to change morphology of oral squamous carcinoma cells to a mesenchymal-like phenotype and to increase chemotaxis [Uchida et al., 2003, Onoue et al., 2006]. An increase in chemotactic migration by CXCL12 was observed in CXCR4-expressing

ovarian carcinoma cells as well [Scotton et al., 2001]. Further experiments of the present work on gene expression of cocultured breast cancer cells are discussed in chapter 4.1.3.

Another experimental setting of the present work was carried out according to evidence in literature on EMT triggered by TGFβ. TGFβ is known as tumor suppressor in early tumor development, but later on, it is promoting cancer progression. Invasion is increased by induction of EMT via TGFβ [Zavadil and Bottinger, 2005, Iwatsuki et al., 2010, Taylor et al., 2010, Drabsch and Dijke, 2011]. Rat hepatoma cells were treated permanently with TGFβ leading to a morphological conversion from epithelial-like cells to a more mesenchymal-like phenotype. Their invasion and migration was increased against conditioned media from fibroblasts and osteoclasts [Bertran et al., 2009]. Similar effects were observed in squamous carcinoma cells treated with TGFβ. Their cellular morphology was changed and their migratory properties were increased [Taki et al., 2008]. In the present work, breast cancer cells were treated with TGFβ_1 under monoculture and coculture conditions to test whether the invasion rate could be increased. This was important for further experiments on gene expression analysis upon an involvement of EMT in invasion processes during cocultivation (see chapter 4.1.3). TGFβ_1 affected invasion was studied in the cell lines MDA-MB-231, HCC 1806 and MCF-7. In monoculture, an increased invasion was shown for HCC 1806 cells, but no changes were observed for MDA-MB-231 and MCF-7. No significant effects on invasion in coculture were identified for all of the three cell lines. Thus, TGFβ_1 regulation was not able to enhance invasion in the used experimental setting.

4.1.3 Gene expression

Gene expression analysis was carried out for a better understanding of the mechanisms leading to increased invasion of breast cancer cells cocultivated with osteoblast-like osteosarcoma cells. The focus was put on EMT as an important process of cell motility. In literature, several studies indicated activators of EMT. TGFβ was shown to induce morphological changes from an epithelial-like to a mesenchymal-like phenotype. It increased invasive and migratory properties of cells and changed the expression of genes involved in EMT as downregulation of CDH1 and upregulation of VIM [Sommers et al., 1994, Bertran et al., 2009]. The CXCL12/CXCR4 system seems to be also involved in EMT. Treatment with CXCL12 resulted in conversion of cell morphology, increased invasion and CDH1 downregulation respectively VIM upregulation [Uchida et al., 2003, Onoue et al., 2006]. In addition, coculture interactions of CAFs with cancer cells caused increased migration, downregulated CDH1 and upregulated VIM [Angelucci et al., 2012]. In the present work, another interaction should be studied in relation to EMT: the cocultivation of breast cancer and osteosarcoma cells leading to increased invasive properties.

Epithelial marker CDH1 and TJP1 and mesenchymal marker VIM and S100A4 were analyzed in MDA-MB-231, HCC 1806 and MCF-7 cells in monoculture and coculture. An additional treat-

ment of cocultivated cells with $TGF\beta_1$ was performed to induce changes of marker expression according to altered expression patterns generated by EMT (see chapter 3.2.3). These experiments should serve as positive controls for EMT. It was expected, that increased invasion was correlated with downregulation of epithelial marker and upregulation of mesenchymal marker. In the present work, CDH1, TJP1, VIM and S100A4 expression were not affected by cocultivation in MDA-MB-231 cells. Treatment with $TGF\beta_1$ did not influence expression of CDH1 and S100A4, but it upregulated TJP1 and VIM expression in this cell line. In HCC 1806 cells, coculture conditions led to no differences in CDH1, TJP1 and VIM expression, but expression of S100A4 was decreased. Exposure to $TGF\beta_1$ did not changed CDH1 expression, but upregulated TJP1 and VIM expression and downregulated expression of S100A4. Cocultivation of MCF-7 cells showed no effect on CDH1, TJP1 and VIM expression levels. It increased expression of S100A4. $TGF\beta_1$ treatment decreased CDH1, TJP1, VIM and S100A4 expression. These results indicated no influence on gene expression of CDH1, TJP1 and VIM by cocultivation in all of the cell lines. Only S100A4 was changed differently in HCC 1806 and MCF-7. These findings lead to the assumption, that the increased invasion of breast cancer cells seems not to be induced by mechanisms involved in EMT in the used coculture system. But the gene expression analyzed under $TGF\beta_1$ treatment also showed no homogeneous expression pattern for epithelial marker respectively mesenchymal marker, neither for all of the cell lines nor within one cell line. Expression was changed, but in every possible direction. One explanation may be, that $TGF\beta_1$ is not a reliable inducer of EMT. In literature, there are studies on motility marker expression showing no correlation of expression changes by $TGF\beta$ for several cell lines. Invasion was not investigated [Brown et al., 2004, Chai et al., 2010]. But a lot of studies in literature support the opinion, that $TGF\beta$ increases invasion by induction of EMT [Zavadil and Bottinger, 2005, Bertran et al., 2009, Iwatsuki et al., 2010, Taylor et al., 2010, Drabsch and Dijke, 2011]. In agreement with the high evidence of $TGF\beta$ induced EMT, another factor may be responsible for the inconsistent results in the experimental setting of the present work. On the one hand, the choice of motility marker may be not suitable for the analysis. As discussed in chapter 4.1.1, TJP1 and S100A4 did not correlate with the morphological phenotype of the cells, but CDH1 and VIM were acceptable. CDH1 and VIM were also studied well in literature showing good associations with the epithelial respectively mesenchymal phenotype and invasive properties [Sommers et al., 1994, Zajchowski et al., 2001]. Thus, their detection is maintainable in this context. On the other hand, the sample preparation may be insufficient. The coculture system consisted of two chambers. The bottom well was used for osteosarcoma cell cultivation. As upper well, a cell culture insert was used with a Matrigel^{TM} coated filter membrane. This membrane allowed medium exchange and an invasion of the breast cancer cells towards the bottom well. For RNA isolation, all of the breast cancer cells of the upper well were collected. This included cells, which invaded through the gel and other subpopulations ontop of the gel, which were not influenced by these conditions. But cells were not included in the sample, which invaded through the filter. It is possible, that the results of the gene expression

analysis were overlaid by RNA of cell subpopulations which were not influenced by coculture conditions. This would explain, why the findings of the present work did not show an EMT induction by TGFβ_1. According to this, it may be possible, that invasion in the coculture system influences expression of the motility marker as well.

In further experiments, the setting and RNA collection was optimized. Therefore, only cells at the bottom of the filter were collected, which were invaded through Matrigel^{TM} and membrane. The cell line MCF-7 was used and the samples of monocultured and cocultured cells were investigated by microarray analysis (see chapter 3.3). 50 genes, which were regulated the most (88 % were upregulated and 12 % were downregulated), were classified into groups for their cellular functions. The main part of the genes belonged to immune response mechanisms as inflammation, viral infection and interferon dependent processes, and cell motility processes, adhesion and metastasis. The microarray data was validated for VIM, FN1, SPARC, MMP2, TCF21, CXCL12, PARP9 and TACC1 by qPCR. VIM and FN1 represented marker of EMT. FN1 belongs to the ECM proteins and its expression correlated with the mesenchymal-like phenotype [Wu and Zhou, 2008, Kalluri and Weinberg, 2009, Yilmaz and Christofori, 2010]. Another ECM protein is SPARC, also known as osteonectin (ON). It promoted EMT-like changes as decreased CDH1 and enhanced fibronectin and MMP expression together with an increased invasiveness and metastasis [Chen et al., 2012, Fenouille et al., 2012]. MMP2 degrades the ECM and is often secreted by invasive and mesenchymal-like cells [Kalluri and Weinberg, 2009, Yilmaz and Christofori, 2010, van Zijl et al., 2011]. TCF21 is a marker for mesenchymal cells. During tissue development, its expression was shown to be located at mesenchymal sites of EMT, but not in epithelial compartments [Quaggin et al., 1998]. The results of the microarray showed many regulated genes which were involved in immune response. According to this, PARP9 was selected. It is induced by inflammatory mediators like interferons. Expression of PARP9 led to upregulation of other interferon induced proteins as interferon induced protein with tetratricopeptide repeats (IFITs), 2'-5'-oligoadenylate synthetase (OASs) and signal transducer and activator of transcription 1 (STAT1) [Juszczynski et al., 2006]. PARP9 levels were enlarged in high-risk lymphomas and its overexpression enhanced migration of lymphoma cells independent of the CXCL12/CXCR4 system [Aguiar et al., 2000]. CXCL12 was chosen based on the high evidence in literature on an interaction of the CXCL12/CXCR4 system with invasion especially to bone tissue as protein extracts, cells or conditioned medium [Müller et al., 2001, Wang et al., 2006, Olbrich, 2010a]. TACC1, one of the genes which was downregulated by coculture conditions, represents a centrosomal protein. It interacts with microtubule organization [Gergely et al., 2000] and was less expressed in tumor tissue compared to normal tissue in breast, lung, ovarian and uterine cancer [Conte et al., 2002].

The present microarray data correlated well with the findings in literature for VIM, FN1, SPARC and MMP2. Thus, the cocultured cells showed a change to a more mesenchymal-like behavior. This may be one explanation for the increased invasive capabilities of the MCF-7 cells in the

coculture system. In case of EMT, the results of the present work offer no link to a downregulation of epithelial marker as CDH1. In contrast to the supported opinion in literature that CDH1 downregulation is a "hallmark" in EMT [Kalluri and Weinberg, 2009, Yilmaz and Christofori, 2010, van Zijl et al., 2011], different studies indicated that loss of CDH1 was not necessarily required for invasion and migratory processes [Christiansen and Rajasekaran, 2006, Chen et al., 2007, Chai et al., 2010]. A conditioning of MCF-7 cells by repeated invasion cycles showed an increase in invasive properties compared to the parental cells. This was accompanied by an unchanged expression of CDH1. Comparison of gene expression profiles of the selected invasive MCF-7 cells with MDA-MB-231 cells revealed genes associated with a more invasive phenotype as CXCL12 and CD44 [Uchino et al., 2010]. These genes were also upregulated by coculture conditions in the present work. Evidence for a phenotypical conversion of the MCF-7 cells by cocultivation is also given by other factors regulated in the microarray data. TCF21 was upregulated, which is mainly expressed in mesenchymal cells. TACC1 was downregulated offering hints for a different microtubule organization. Therefore, a change to a more mesenchymal character of the MCF-7 cells seems to be performed by cocultivation with osteosarcoma cells without an alteration of epithelial properties. Thus, hints for an EMT were partially observed. In literature, an "incomplete" EMT is discussed. Evidence for a well-differentiated epithelial morphology in invasive and metastatic cancers is given. Thus, loss of epithelial characteristics seems not to be necessary for invasiveness [Christiansen and Rajasekaran, 2006]. An incomplete EMT had possibly occurred in the present work.

Another system involved in invasion is the CXCL12/CXCR4 system. In literature, there is great evidence showing high expression of CXCR4 in tumor cells which were attracted by secreted CXCL12 of the microenvironmental tissues and cells [Mantovani et al., 2010]. At the site of primary tumor in breast cancer, studies showed that CXCR4 was expressed in great amounts [Wang et al., 2006]. Whereas CXCL12 expression was at high levels in tissue as lymph nodes, lung, liver and bone marrow representing the most common sites of breast cancer metastasis. Migration and invasion of CXCR4 expressing MDA-MB-231 cells was increased against CXCL12 respectively protein extracts of lymph nodes, lung, liver and bone marrow. *In vivo*, treatment with CXCR4 antibodies decreased metastasis rates of MDA-MB-231 in mice [Müller et al., 2001]. The present data showed an increase in CXCL12 expression in the cocultured MCF-7 cells, but CXCR4 expression was not changed. Thus, there is no link to the common assumption. Further studies in literature revealed an interaction of endogenous CXCL12 with invasiveness. In breast cancer, CXCL12 levels correlated with prognosis, disease-free survival and overall survival of patients [Kang et al., 2005b, Mirisola et al., 2009]. Poor prognosis was also connected with CXCL12 positive cases in oral squamous cell carcinoma [Uchida et al., 2007]. Transfection of cells with CXCL12, which showed endogenous CXCR4 expression, led to increased invasion and migration in breast cancer, oral squamous carcinoma and non-small cell lung carcinoma cells [Kang et al., 2005b,

Uchida et al., 2007, Dai et al., 2013]. Vice versa, knockdown of CXCL12 was accompanied by a reduced invasive and migratory behavior [Kang et al., 2005a]. CXCL12 expression was also shown to upregulate MMP expression [Singh et al., 2004, Shen et al., 2009, Dai et al., 2013]. In addition, an upregulation of MMP2 was observed in the cocultured MCF-7 cells in the present work. This represents an important mechanism of enhanced invasive properties by degradation of the ECM. The autocrine interaction of CXCL12 with its receptor leading to increased invasiveness was also detected *in vivo* and discussed as necessary for distant metastasis [Uchida et al., 2007]. The MCF-7 cells used in the present work expressed CXCR4 endogenously, which was shown in earlier works [von Alten et al., 2006, Olbrich et al., 2010b]. This leads to the assumption that an autocrine interaction of CXCL12 with CXCR4 is triggered by cocultivation of breast cancer cells with osteosarcoma cells. Thereby, the osteosarcoma cells affect the breast cancer cells to increase their CXCL12 expression. This seems to be one important aspect in the enhancement of invasiveness. The detailed mechanism and the involved factors are still not known.

A great part of the genes regulated by coculture conditions is involved in immune response processes as inflammation and infection. Evidence for a connection between these mechanisms and cancer is offered in literature. Chronic exposure to pathogens can lead to repeated injuries which facilitate acute and chronic inflammation. Hepatitis virus B and C infections were identified as risk factors for the development of hepatocellular carcinomas. Oncogenic papilloma virus was related to invasive cervical cancer. Factors interacting with interleukin receptors, toll-like receptors and the tumor necrosis factor (TNF) receptor family were associated with these processes [Karin et al., 2006]. Recruitment of bone marrow derived cells as tumor associated macrophages (TAMs) was also shown to enhance invasiveness and migration of tumor cells by secretion of epidermal growth factor (EGF). In a paracrine loop, the tumor cells responded by expressing colony stimulating factor 1 (CSF1), which attracted TAMs [Joyce and Pollard, 2009]. The microarray data of the present work revealed a slight upregulation of CSF1 in the cocultured breast cancer cells. According to this, EGF may represent one factor which triggers the enhanced invasiveness. Another gene involved in inflammatory processes, PARP9, was upregulated by cocultivation. It is one of the 50 genes showing the strongest regulations. Its expression led to upregulation of other interferon induced proteins as IFITs, OASs and STAT1 [Juszczynski et al., 2006]. These genes were also upregulated in the present microarray data. Interferon induced proteins were shown to increase migration *in vitro* together with enhanced MMPs activity by transfection of IFITM1 in colorectal cancer cells. *In vivo*, tumor volumes and weights were also enlarged [He et al., 2012]. In clinical samples of patients with metastatic carcinoma, the interferon regulated OAS were upregulated compared to healthy persons [Merritt et al., 1985]. STAT1 expression was induced by interferon leading to increased migration and invasion in breast cancer cells [Greenwood et al., 2012]. Interferon seems to be interacting in processes important for cellular invasion, migration and metastasis. Thus, it may be an interesting factor of investigation in the coculture studies of

the present work.

Further research in literature on culture effects on invasive properties showed similar effects as observed in the present work. In breast cancer cells, an increased migration concomitant with an upregulated VIM expression was induced by cocultivation with CAFs [Lebret et al., 2007]. Cocultivation of MCF-7 cells with macrophages led to increased invasion under treatment with endothelin 1 (ET1) and upregulated expression of MMP2 and MMP9. Expression of ETs was higher in tumor tissue at the invasive front [Grimshaw et al., 2004]. Enlarged ET1 and MMP2 expression were also detected in the present work. Gene expression analysis of cocultured mammary adenocarcinoma cells with pre-osteoblastic cells resulted in upregulation of genes involved in wound healing processes, cell migration and adhesion processes [Glait-Santar et al., 2012]. The genes VIM, serpin peptidase inhibitor, clade E, member 2 (SerpinE2) and CD44 were also affected in the coculture system of the present work. SerpinE2 was shown to be involved in MMP expression and metastasis in breast cancer [Fayard et al., 2009]. CD44 expression as cell-surface glycoprotein was correlated with high invasiveness and accompanied by enhanced expression rates of CXCR4, MMP1 and connective tissue growth factor (CTGF) in breast cancer cells [Sheridan et al., 2006]. CD44 transfected cells showed increased migration and invasion *in vitro* and higher mortality rates and metastasis *in vivo*. Upregulation of CD44 is associated with increased production of FN1 and collagens [Rutnam and Yang, 2012]. Additionally, the present microarray demonstrated an upregulation of CD44 and CTGF by cocultivation. CTGF, MMP1, CXCR4 and others were also shown to be responsible for increased bone metastasis of breast cancer cells [Kang et al., 2003]. Thus, cellular mechanisms including CD44 and CTGF seem to play a role in the coculture system used in the present work.

4.2 Kisspeptin-10 and breast cancer

Kisspeptin-10, a peptide derived from the metastasis suppressor gene KISS1, was shown to inhibit invasion in the coculture system of breast cancer cells and osteoblast-like osteosarcoma cells [Olbrich et al., 2010b, Olbrich, 2010a]. Further studies on KP-10 *in vivo* were carried out to investigate an antimetastatic effect on breast cancer xenografts by peripheral administration.

4.2.1 *In vitro* effects on invasion

Several studies in literature reported decreasing effects of KP-10 on invasion in different cell lines and different invasion respectively migration assays. In trophoblasts, inhibited invasion was observed in a transwell invasion assay [Bilban et al., 2004]. Invasion of renal cell carcinoma cells was reduced by KP-10 in an invasion assay against FCS [Chen et al., 2011]. In Chinese

hamster ovary CHO cells transfected with hGPR54, KP-10 inhibited migration via interaction with its receptor [Hori et al., 2001]. In addition, in cells expressing GPR54 endogenously invasion respectively migration was decreased by KP-10 [Shoji et al., 2009, Kang et al., 2011, Roseweir et al., 2012]. An *in vitro* effect of KP-10 on invasion of the breast cancer cell lines MCF-7 and MDA-MB-231 was shown in earlier works [Olbrich et al., 2010b, Olbrich, 2010a]. Another breast cancer cell line, HCC 1806, should be also used *in vivo*. Therefore, an effect of KP-10 in cocultivated HCC 1806 cells was investigated in preliminary works. The results did not show a significant inhibition of invasion in this breast cancer cell line by KP-10 (see chapter 3.4.1).

In parallel works, an analog of KP-10 was studied in the coculture system. The Phe at position six of the peptide was substituted by dLys in order to create an effective analog with a possible longer half life. The half life of KP-10 was shown to be very short especially in serum. This is mainly caused by degradation by MMPs [Tomita et al., 2008]. Studies in literature demonstrated a more potent KP-10 analog by the exchange of enantiomers from L-amino to D-amino. The replacement of Tyr against dTyr at position one resulted in an extended effect compared to the original peptide *in vivo* [Curtis et al., 2009]. During the development of analogs, it was important to keep the C-terminal end of the peptide, because especially Arg and Phe at positions nine respectively ten were shown to be critical for receptor activity [Clements et al., 2001, Kotani et al., 2001, Orsini et al., 2007]. The KP-10 analog DKP-10 inhibited invasion of HCC 1806 cells significantly in the coculture system (see chapter 3.4.2). The effect was related to the observed concentration window in the cell line MCF-7 [Olbrich et al., 2010b]. Thus, effectiveness of DKP-10 was proved *in vitro*. The effect was even stronger compared to KP-10 in HCC 1806 cells. The original peptide did not show a significant inhibition of invasion, only a trend was observed in that cell line.

4.2.2 *In vivo* effects on tumor growth and metastasis

In literature, an antimetastatic effect of KP-10 respectively KISS1 *in vivo* was shown by transfection of the gene in melanoma [Lee et al., 1996, Lee and Welch, 1997a] and breast [Lee and Welch, 1997b], ovarian [Jiang et al., 2005] and pancreatic cancer cells [McNally et al., 2010]. Reduced metastasis by peripherally administered KP-10 was studied in xenografts with melanoma [Ohtaki et al., 2001], prostate [Cho et al., 2009b] and endometrial cancer cells [Kang et al., 2011]. In the present work, the effect of a peripheral treatment with KP-10 should be investigated in breast cancer xenografts. Evidence for a possible role of KP-10 as therapeutic option in the treatment of metastatic breast cancer should be studied. As breast cancer is not a homogeneous disease, the experimental setting covered different breast cancer xenografts with varying cell lines and two kinds of tumor cell injections. Metastasis should be studied in bone, lung and liver representing the most common sites of tumor cell settlement in breast cancer patients [Disibio and French, 2008]. The metastatic lesions in murine organs were analyzed by quantitative real-time PCR after DNA

isolation. Target sequence was the ALU element, which is specific for primate genomes [Batzer and Deininger, 2002]. Thus, only human DNA of the breast cancer cells, which were injected in mice, was detected by this method. Metastasis was determined as ratio of human DNA in murine DNA. In contrast to histological analysis of metastasis, this sensitive assay enables detection of micrometastases by differentiation of species specific DNA and is not limited to a minimum extent of the metastases [McKenzie et al., 1991, Shoemaker et al., 1992, Schneider et al., 2002].

One of the xenograft models was performed by intracardiac injection. This assay was chosen as metastasis model for the later steps during the metastasis cascade. The tumor cells were injected directly into the bloodstream to study organ specific metastasis without primary tumor development. The breast cancer cell line MDA-MB-231 was used, which was shown to metastasize preferentially to bone and liver in nude mice by intracardiac injection [Sasaki et al., 1995, Yoneda, 2000, Richert et al., 2009]. This cell line was also affected by KP-10 in vitro [Olbrich, 2010a]. In the present work, no metastasis were detected in lung, liver and bone and no CTCs were found. As animal models and cellular systems are very sensible experimental settings, it is possible, that this kind of assay do not work anytime and anywhere. The mice would have reacted unlikely with the tumor cell injections. The cells of the used passage would have been unable to settle down at distant organ sites. And, maybe, the cell preparations respectively the injection technique were not sufficient. The analytical assay worked based on detection of positive control samples. According to this, the intracardiac injection of MDA-MB-231 cells in mice did not worked for studying metastasis and the effect of KP-10 in the present work.

Another xenograft model was carried out by orthotopic tumor cell injection into the mammary glands of the mice. According to this, the whole metastasis cascade could be passed through from primary tumor growth until metastatic colonization at distant sites. Two breast cancer cell lines were used, MDA-MB-435s and HCC 1806. MDA-MB-435s cells were shown to develop tumors and metastasis to bone, lung and liver after orthotopic injection [Price and Zhang, 1990, Castillo-Pichardo et al., 2009, Schubert et al., 2011]. This cell line was discussed controversially in literature for being not a breast cancer but a melanoma cell line by contamination or mistake. Gene expression analysis revealed an expression pattern more likely for a melanoma origin [Ellison et al., 2002, Rae et al., 2004]. But others reported, that the melanoma cell line, which should have been responsible for the contamination, was of male origin. Analysis of the MDA-MB-435 cell line revealed a female origin. Thus, the melanoma cell line seemed to be contaminated by the breast cancer cell line [Chambers, 2009]. According to this, MDA-MB-435s cells were used as breast cancer cells within this work.

The cell line HCC 1806 was also proved for tumor growth and metastasis to lung and liver [Föst et al., 2011, Volk-Draper et al., 2012]. An influence of KP-10 on HCC 1806 cells was investigated showing a trend towards lower invasion (see chapter 3.4.1). Because of the different invasive behavior of cocultured MDA-MB-435s (see chapter 3.2.1), these cells were not studied for an

effect of KP-10 *in vitro*. The results of the present work demonstrated a significantly inhibited tumor growth of HCC 1806 cells in mice by KP-10 treatment. Metastases were detected in lung and CTCs were found in blood. No difference in treated and untreated mice were determined for both sites. In bone and liver, no hDNA was found (see chapter 3.5.2). In xenografts with MDA-MB-435s cells, tumor growth in the treatment group was slightly, but not significantly reduced. Metastasis was only detected in lung showing no effect by treatment with KP-10 (see chapter 3.5.3). Analysis was also carried out for mice without tumor cell injections and without treatment. Data of these control groups revealed low hDNA in CTCs respectively lung in one of the mice. This may be due to contaminations during the multi-step sample preparations including organ collection at study end, purification of each organ, shredding, DNA isolation and PCR analysis. Contaminations should be avoided by sterile working, but they still occurred. The potentially contaminated samples were not excluded from analysis to keep the analytical fault the same for all of the study groups.

Based on the results on tumor growth, KP-10 seems to be involved in antitumorigenic processes *in vivo*. This effect is discussed controversially in literature. In xenografts with prostate cancer cells, treatment with KP-10 led to reduced tumor volume [Cho et al., 2009b]. Whereas KP-10 decreased metastasis, but not tumor size in mouse models with melanoma [Ohtaki et al., 2001] or endometrial cancer cells [Kang et al., 2011]. In the present work, the reduced tumor growth was not expected. According to this, further investigations were carried out on antiproliferative properties of KP-10 *in vitr*o. Results are discussed in chapter 4.2.3. An antimetastatic effect by KP-10 treatment was not observed for both breast cancer xenografts in the present work. Due to the results, this effect can not be excluded either. The metastatic spread was very inhomogeneous within the animal groups. Metastasis did not occur in any mouse and the extent of hDNA was diverse. To investigate the effect of a treatment with KP-10 on breast cancer metastasis, the used xenograft models are not valid enough. Enlargement of the study population or development of a more reproducible animal model may be two options to optimize the experimental setting. But the use of larger groups of animals is not arguable based on ethical reasons. The present results do not offer considerations on a possible use of KP-10 in therapy of the breast cancer disease.

4.2.3 *In vitro* effects on proliferation

The effect of KP-10 on tumor growth *in vivo* revealed lower proliferation rates in treated mice in the present work (see chapters 3.5.2 and 3.5.3). Research in literature demonstrated controversial results. A decreased effect on tumor proliferation was shown in xenografts with prostate cancer cells by treatment with KP-10 [Cho et al., 2009b]. Whereas KP-10 treatment in mouse models with melanoma [Ohtaki et al., 2001] respectively endometrial cancer cells led to decreased metastasis, but tumor growth was unaffected [Kang et al., 2011]. *In vitro* studies revealed no

consistent data as well. In Chinese hamster ovary CHO cells transfected to overexpress GPR54, an antiproliferative effect was detected by treatment with kisspeptins [Hori et al., 2001, Kotani et al., 2001]. In addition, the same result was observed in murine fibroblasts NIH3T3 cells [Stafford et al., 2002] and MDA-MB-435s cells [Becker et al., 2005], which were overexpressing GPR54. No effect on cell proliferation was shown in carcinoma cell lines of pancreatic cancer [Masui et al., 2004] and renal cell cancer [Shoji et al., 2009], and in trophoblasts [Bilban et al., 2004]. All of these cells expressed GPR54 endogenously. In human umbilical vein endothelial cells HUVECs, a reduced proliferation was detected by KP-10 on the one hand [Ramaesh et al., 2010] and, on the other hand, no influence on proliferation was stated as well in these cells [Cho et al., 2009b]. Experiments with breast cancer cell lines revealed no influence on proliferation by treatment with KP-10, but expression of GPR54 was not studied [Cho et al., 2009a]. Taken together, cells were not affected in proliferation by KP-10, which showed endogenous GPR54 expression. Whereas an antiproliferative action of KP-10 was observed in cell models with artificial GPR54 expression. The aim of this part of the present work was to study the relationship of an antiproliferative effect of KP-10 in dependence of the nature of GPR54 expression. Conclusions for the inhibited tumor growth observed *in vivo* could be offered possibly by this analysis. Therefore, breast cancer cell lines were investigated in their GPR54 expression and proliferation under treatment with KP-10. Cells showing GPR54 overexpression were analyzed as well.

GPR54 expression levels were detected by immunocytochemistry, on mRNA and on protein levels. Based on controversial results in literature, three independent analytical assays were carried out. Immunocytochemical staining showed receptor expression in all of the nine breast cancer cell lines. GPR54 mRNA was found in T47D, ZR75-1 and MCF-7 cells. In MDA-MB-231, MDA-MB-435s, MDA-MB-453, HCC 70, HCC 1806 and HCC 1937 cells, no definite signal was received. All of the cell lines showed GPR54 protein expression in different amounts (see chapter 3.6.1.1). In literature, the cell lines T47D, ZR75-1 and MCF-7 were detected as GPR54-positive by mRNA analysis, whereas no receptor expression was found in MDA-MB-231 and MDA-MB-435 [Marot et al., 2007]. In contrast, GPR54 expression was shown in MDA-MB-231 cells by mRNA analysis [Martin et al., 2005, Pampillo et al., 2009]. In addition, mRNA analysis revealed no GPR54 in MDA-MB-435 cells [Becker et al., 2005, Nash et al., 2007]. According to the results of the present work showing GPR54 expression in all of the tested cell lines by immunocytochemical and protein expression analysis, the cell lines were regarded as receptor positive.

Proliferation was investigated in MDA-MB-231, MDA-MB-435s, HCC 1806 and MCF-7. These cell lines were chosen based on different GPR54 protein amounts. The results of the present work indicated no effect on proliferation in cells endogenously expressing GPR54 by KP-10 treatment. For proliferation studies in cells transfected to overexpress GPR54, B35 neuronal rat cells with stable mGPR54 expression were used. The amino acid structure of human GPR54 and murine GPR54 was shown to be homologous up to 82 % [Kirby et al., 2010]. In addition, the gene

products of human KISS1 and murine KISS1 were analyzed as related structures with a strong conservation within the active short forms [Stafford et al., 2002]. Human respectively murine receptor and peptides were used interchangeable in literature showing similar effects [Kotani et al., 2001, Mikkelsen et al., 2009]. Thus, it is acceptable to compare the results of breast cancer cells with endogenous hGPR54 expression with a mGPR54 transfected cell system.

Different B35 mGPR54 clones were used. They showed variable GPR54 expression levels by mRNA and protein analysis (see chapter 3.6.1.2). Proliferation was significantly inhibited by KP-10 in two of the clones. These results support the assumption, that KP-10 affects proliferation only in cells with artificial GPR54 expression. This may be due to the cellular GPR54 amount. On mRNA levels, comparison of receptor expression in the breast cancer and B35 cells revealed more mRNA within the transfected cells. Further experiments on protein levels could not confirm this observation. An explanation may be, that the antigen structure recognized by the used antibody was not represented comparably in hGPR54 respectively mGPR54. When experiments were run, an antibody was not available for a parallel detection of human and murine receptor. Nevertheless, the results of the present work match well with data in literature, that the breast cancer cell line MDA-MB-435s was not affected on proliferation by KP-10, but its GPR54 transfected clone was inhibited [Becker et al., 2005]. Evidence is given, that an antiproliferative effect of KP-10 is GPR54 mediated and only detectable in GPR54 overexpressing cell systems and not in cells with endogenous receptor expression.

Comparing the *in vitro* results of KP-10 on cell proliferation with the *in vivo* results on tumor growth, KP-10 seemed to reduce tumor size not directly on the cellular level. Another possible role of KP-10 in decreasing *in vivo* tumor growth may be by inhibition of angiogenetic mechanisms. In literature, studies with HUVECs demonstrated reduced tumor angiogenesis by KP-10 mediated suppression of VEGF expression [Cho et al., 2009b]. KP-10 was shown to decrease new vessel sprouting as important process in angiogenesis [Ramaesh et al., 2010]. Thus, further experiments are necessary, which investigate an interaction of KP-10 within angiogenesis in breast cancer xenografts.

5 Summary and conclusions

The aim of the present work was to study cocultivated human breast cancer cells on invasive behavior and expression of genes involved in cell motility processes. Kisspeptin-10, a peptide derived from the metastasis suppressor gene KISS1, was shown to interfere within this cell system by inhibition of invasion. An influence of KP-10 *in vivo* should be further investigated to evaluate KP-10 as a possible therapeutic option in the metastatic breast cancer disease.

Breast cancer cell lines were classified phenotypically for their epithelial respectively mesenchymal properties by morphology and gene expression of motility markers. The individual invasion rates correlated well with the phenotypic characteristics demonstrating low cell movement for epithelial-like cells and high invasion for mesenchymal-like cells. Cocultivation with osteoblast-like osteosarcoma cells led to increased invasiveness in epithelial-like cells. The "bone"-directed cell movement was proved for invasion processes in three-dimensional settings. For migration, no influence of the cocultivation was observed. Microarray gene expression analysis indicated an involvement of EMT processes in the increased cellular invasiveness. This was based on enhanced mesenchymal properties, but without a change in the epithelial phenotype. Thus, a kind of "incomplete" EMT could have happened. In addition, the microarray data documented another important factor, CXCL12. Its upregulation could have triggered the coculture effect by an autocrine CXCL12/CXCR4 loop. Detection of inflammatory processes during coculture invasion revealed factors as EGF and interferons, which could have mediated the interaction of osteosarcoma cells and breast cancer cells. The present analysis indicated several starting points for further studies on the processes happening in the coculture system.

KP-10 was shown to decrease invasion *in vitro* by interaction with its receptor GPR54 and it reduced metastasis *in vivo* in different cancer cell systems. In a breast cancer xenograft, treatment with the peptide inhibited tumor growth. Further studies on cell proliferation revealed no antiproliferative effect in cells expressing GPR54 endogenously. Thus, KP-10 may be involved in angiogenetic processes *in vivo*, which represent an interesting assumption for future investigations. A conclusion could not be offered on an antimetastatic effect of KP-10 as possible therapeutic option in breast cancer based on the poor metastasis model in mice.

Bibliography

R. C. Aguiar, Y. Yakushijin, S. Kharbanda, R. Salgia, J. A. Fletcher, and M. A. Shipp. Bal is a novel risk-related gene in diffuse large b-cell lymphomas that enhances cellular migration. *Blood*, 96(13): 4328–4334, Dec 2000.

C. Angelucci, G. Maulucci, G. Lama, G. Proietti, A. Colabianchi, M. Papi, A. Maiorana, M. D. Spirito, A. Micera, O. B. Balzamino, A. D. Leone, R. Masetti, and G. Sica. Epithelial-stromal interactions in human breast cancer: effects on adhesion, plasma membrane fluidity and migration speed and directness. *PLoS One*, 7(12):e50804, 2012.

M. A. Batzer and P. L. Deininger. Alu repeats and human genomic diversity. *Nat Rev Genet*, 3(5):370–9, 2002.

J. A. Becker, J. F. Mirjolet, J. Bernard, E. Burgeon, M. J. Simons, G. Vassart, M. Parmentier, and F. Libert. Activation of gpr54 promotes cell cycle arrest and apoptosis of human tumor cells through a specific transcriptional program not shared by other gq-coupled receptors. *Biochem Biophys Res Commun*, 326(3):677–86, 2005.

E. Bertran, L. Caja, E. Navarro, P. Sancho, J. Mainez, M. M. Murillo, A. Vinyals, A. Fabra, and l. Fabregat. Role of cxcr4/sdf-1 alpha in the migratory phenotype of hepatoma cells that have undergone epithelial-mesenchymal transition in response to the transforming growth factor-beta. *Cell Signal*, 21(11):1595–1606, Nov 2009.

F.-C. Bidard, J.-Y. Pierga, A. Vincent-Salomon, and M.-F. Poupon. A "class action" against the microenvironment: do cancer cells cooperate in metastasis? *Cancer Metastasis Rev*, 27(1):5–10, Mar 2008.

M. Bilban, N. Ghaffari-Tabrizi, E. Hintermann, S. Bauer, S. Molzer, C. Zoratti, R. Malli, A. Sharabi, U. Hiden, W. Graier, M. Knofler, F. Andreae, O. Wagner, V. Quaranta, and G. Desoye. Kisspeptin-10, a kiss-1/metastin-derived decapeptide, is a physiological invasion inhibitor of primary human trophoblasts. *J Cell Sci*, 117(Pt 8):1319–28, 2004.

A. Billiau, V. G. Edy, H. Heremans, J. V. Damme, J. Desmyter, J. A. Georgiades, and P. D. Somer. Human interferon: mass production in a newly established cell line, mg-63. *Antimicrob Agents Chemother*, 12 (1):11–15, Jul 1977.

M. M. Bradford. A rapid and sensitive method for the quantitation of microgram quantities of protein utilizing the principle of protein-dye binding. *Anal Biochem*, 72:248–254, May 1976.

K. A. Brown, M. E. Aakre, A. E. Gorska, J. O. Price, S. E. Eltom, J. A. Pietenpol, and H. L. Moses. Induction by transforming growth factor-beta1 of epithelial to mesenchymal transition is a rare event in vitro. *Breast Cancer Res*, 6(3):R215–R231, 2004.

R. Cailleau, R. Young, M. Olivé, and W. J. Reeves. Breast tumor cell lines from pleural effusions. *J Natl Cancer Inst*, 53(3):661–674, Sep 1974.

R. Cailleau, M. Olivé, and Q. V. Cruciger. Long-term human breast carcinoma cell lines of metastatic origin: preliminary characterization. *In Vitro*, 14(11):911–915, Nov 1978.

L. Castillo-Pichardo, M. M. Martínez-Montemayor, J. E. Martínez, K. M. Wall, L. A. Cubano, and S. Dharmawardhane. Inhibition of mammary tumor growth and metastases to bone and liver by dietary grape polyphenols. *Clin Exp Metastasis*, 26(6):505–516, 2009.

J. Y. Chai, C. Modak, W. Mouazzen, R. Narvaez, and J. Pham. Epithelial or mesenchymal: Where to draw the line? *Biosci Trends*, 4(3):130–142, Jun 2010.

A. F. Chambers. Mda-mb-435 and m14 cell lines: identical but not m14 melanoma? *Cancer Res*, 69 (13):5292–5293, Jul 2009.

E. Charafe-Jauffret, C. Ginestier, F. Monville, P. Finetti, J. Adélaïde, N. Cervera, S. Fekairi, L. Xerri, J. Jacquemier, D. Birnbaum, and F. Bertucci. Gene expression profiling of breast cell lines identifies potential new basal markers. *Oncogene*, 25(15):2273–2284, Apr 2006.

J. Chen, D. Shi, X. Liu, S. Fang, J. Zhang, and Y. Zhao. Targeting sparc by lentivirus-mediated rna interference inhibits cervical cancer cell growth and metastasis. *BMC Cancer*, 12:464, 2012.

P.-S. Chen, M.-Y. Wang, S.-N. Wu, J.-L. Su, C.-C. Hong, S.-E. Chuang, M.-W. Chen, K.-T. Hua, Y.-L. Wu, S.-T. Cha, M. S. Babu, C.-N. Chen, P.-H. Lee, K.-J. Chang, and M.-L. Kuo. Ctgf enhances the motility of breast cancer cells via an integrin-alphavbeta3-erk1/2-dependent s100a4-upregulated pathway. *J Cell Sci*, 120(Pt 12):2053–2065, Jun 2007.

Y. Chen, M. V. Yusenko, and G. Kovacs. Lack of kiss1r expression is associated with rapid progression of conventional renal cell carcinomas. *J Pathol*, 223(1):46–53, 2011.

G. Z. Cheng, J. Chan, Q. Wang, W. Zhang, C. D. Sun, and L.-H. Wang. Twist transcriptionally up-regulates akt2 in breast cancer cells leading to increased migration, invasion, and resistance to pacli-taxel. *Cancer Res*, 67(5):1979–1987, Mar 2007.

S. G. Cho, D. Li, L. J. Stafford, J. Luo, M. Rodriguez-Villanueva, Y. Wang, and M. Liu. Kiss1 suppresses tnfalpha-induced breast cancer cell invasion via an inhibition of rhoa-mediated nf-kappab activation. *J Cell Biochem*, 107(6):1139–1149, 2009a.

S. G. Cho, Z. Yi, X. Pang, T. Yi, Y. Wang, J. Luo, Z. Wu, D. Li, and M. Liu. Kisspeptin-10, a kiss1-derived decapeptide, inhibits tumor angiogenesis by suppressing sp1-mediated vegf expression and fak/rho gtpase activation. *Cancer Res*, 69(17):7062–70, 2009b.

P. Chomczynski and N. Sacchi. Single-step method of rna isolation by acid guanidinium thiocyanate-phenol-chloroform extraction. *Anal Biochem*, 162(1):156–159, Apr 1987.

J. J. Christiansen and A. K. Rajasekaran. Reassessing epithelial to mesenchymal transition as a prerequisite for carcinoma invasion and metastasis. *Cancer Res*, 66(17):8319–8326, Sep 2006.

S. L. Chua, W. C. S. Too, B. Y. Khoo, and L. L. Few. Ubc and ywhaz as suitable reference genes for accurate normalisation of gene expression using mcf7, hct116 and hepg2 cell lines. *Cytotechnology*, 63 (6):645–654, Dec 2011.

M. K. Clements, T. P. McDonald, R. Wang, G. Xie, B. F. O'Dowd, S. R. George, C. P. Austin, and Q. Liu. Fmrfamide-related neuropeptides are agonists of the orphan g-protein-coupled receptor gpr54. *Biochem Biophys Res Commun*, 284(5):1189–93, 2001.

N. Conte, E. Charafe-Jauffret, B. Delaval, J. Adélaïde, C. Ginestier, J. Geneix, D. Isnardon, J. Jacquemier, and D. Birnbaum. Carcinogenesis and translational controls: Tacc1 is down-regulated in human cancers and associates with mrna regulators. *Oncogene*, 21(36):5619–5630, Aug 2002.

A. E. Curtis, J. H. Cooke, J. E. Baxter, J. R. Parkinson, A. S. Bataveljic, M. A. Ghatei, S. R. Bloom, and K. G. Murphy. A kisspeptin-10 analogue with greater in vivo bioactivity than kisspeptin-10. *Am J Physiol Endocrinol Metab*, 2009.

K. M. Curtis, L. A. Gomez, C. Rios, E. Garbayo, A. P. Raval, M. A. Perez-Pinzon, and P. C. Schiller. Ef1alpha and rpl13a represent normalization genes suitable for rt-qpcr analysis of bone marrow derived mesenchymal stem cells. *BMC Mol Biol*, 11:61, 2010.

X. Dai, Z. Mao, J. Huang, S. Xie, and H. Zhang. The cxcl12/cxcr4 autocrine loop increases the metastatic potential of non-small cell lung cancer in vitro. *Oncol Lett*, 5(1):277–282, Jan 2013.

G. Disibio and S. W. French. Metastatic patterns of cancers: results from a large autopsy study. *Arch Pathol Lab Med*, 132(6):931–939, Jun 2008.

DKG. Deutsche Krebsgesellschaft. DGGG. Deutsche Gesellschaft für Gynäkologische und Geburtshilfe. *Leitlinienprogramm Onkologie. Interdisziplinäre S3-Leitlinie für die Diagnostik, Therpaie und Nachsorge des Mammakarzinoms*. Berlin, 2012.

Y. Drabsch and P. T. Dijke. Tgf-beta signaling in breast cancer cell invasion and bone metastasis. *J Mammary Gland Biol Neoplasia*, 16(2):97–108, Jun 2011.

G. Ellison, T. Klinowska, R. F. Westwood, E. Docter, T. French, and J. C. Fox. Further evidence to support the melanocytic origin of mda-mb-435. *Mol Pathol*, 55(5):294–9, 2002.

L. W. Engel, N. A. Young, T. S. Tralka, M. E. Lippman, S. J. O'Brien, and M. J. Joyce. Establishment and characterization of three new continuous cell lines derived from human breast carcinomas. *Cancer Res*, 38(10):3352–3364, Oct 1978.

B. Fayard, F. Bianchi, J. Dey, E. Moreno, S. Djaffer, N. E. Hynes, and D. Monard. The serine protease inhibitor protease nexin-1 controls mammary cancer metastasis through lrp-1-mediated mmp-9 expression. *Cancer Res*, 69(14):5690–5698, Jul 2009.

N. Fenouille, M. Tichet, M. Dufies, A. Pottier, A. Mogha, J. K. Soo, S. Rocchi, A. Mallavialle, M.-D. Galibert, A. Khammari, J.-P. Lacour, R. Ballotti, M. Deckert, and S. Tartare-Deckert. The epithelial-mesenchymal transition (emt) regulatory factor slug (snai2) is a downstream target of sparc and akt in promoting melanoma cell invasion. *PLoS One*, 7(7):e40378, 2012.

J. Ferlay, H.-R. Shin, F. Bray, D. Forman, C. Mathers, and D. M. Parkin. Estimates of worldwide burden of cancer in 2008: Globocan 2008. *Int J Cancer*, 127(12):2893–2917, Dec 2010.

E. Ferreira and M. J. Cronjé. Selection of suitable reference genes for quantitative real-time pcr in apoptosis-induced mcf-7 breast cancer cells. *Mol Biotechnol*, 50(2):121–128, Feb 2012.

I. J. Fidler. The pathogenesis of cancer metastasis: the 'seed and soil' hypothesis revisited. *Nat Rev Cancer*, 3(6):453–8, 2003.

P. Friedl and K. Wolf. Plasticity of cell migration: a multiscale tuning model. *J Cell Biol*, 188(1):11–19, Jan 2010.

C. Föst, F. Duwe, M. Hellriegel, S. Schweyer, G. Emons, and C. Gründker. Targeted chemotherapy for triple-negative breast cancers via lhrh receptor. *Oncol Rep*, 25(5):1481–1487, May 2011.

A. F. Gazdar, V. Kurvari, A. Virmani, L. Gollahon, M. Sakaguchi, M. Westerfield, D. Kodagoda, V. Stasny, H. T. Cunningham, I. I. Wistuba, G. Tomlinson, V. Tonk, R. Ashfaq, A. M. Leitch, J. D. Minna, and J. W. Shay. Characterization of paired tumor and non-tumor cell lines established from patients with breast cancer. *Int J Cancer*, 78(6):766–774, Dec 1998.

F. Gergely, C. Karlsson, I. Still, J. Cowell, J. Kilmartin, and J. W. Raff. The tacc domain identifies a family of centrosomal proteins that can interact with microtubules. *Proc Natl Acad Sci U S A*, 97(26): 14352–14357, Dec 2000.

C. Glait-Santar, M. Pasmanik-Chor, V. Oron-Karni, and D. Benayahu. Molecular profiling of functional interactions between pre-osteoblastic and breast carcinoma cells. *Genes Cells*, 17(4):302–315, Apr 2012.

A. Goldhirsch, W. C. Wood, A. S. Coates, R. D. Gelber, B. Thürlimann, H.-J. Senn, and P. members. Strategies for subtypes–dealing with the diversity of breast cancer: highlights of the st. gallen international expert consensus on the primary therapy of early breast cancer 2011. *Ann Oncol*, 22(8): 1736–1747, Aug 2011.

C. Greenwood, G. Metodieva, K. Al-Janabi, B. Lausen, L. Alldridge, L. Leng, R. Bucala, N. Fernandez, and M. V. Metodiev. Stat1 and cd74 overexpression is co-dependent and linked to increased invasion and lymph node metastasis in triple-negative breast cancer. *J Proteomics*, 75(10):3031–3040, Jun 2012.

M. J. Grimshaw, T. Hagemann, A. Ayhan, C. E. Gillett, C. Binder, and F. R. Balkwill. A role for endothelin-2 and its receptors in breast tumor cell invasion. *Cancer Res*, 64(7):2461–2468, Apr 2004.

E. Gutierrez-Pascual, J. Leprince, A. J. Martinez-Fuentes, I. Segalas-Milazzo, R. Pineda, J. Roa, M. Duran-Prado, L. Guilhaudis, E. Desperrois, A. Lebreton, L. Pinilla, M. C. Tonon, M. M. Malagon, H. Vaudry, M. Tena-Sempere, and J. P. Castano. In vivo and in vitro structure-activity relationships and structural conformation of kisspeptin-10-related peptides. *Mol Pharmacol*, 76(1):58–67, 2009.

J.-D. He, H.-L. Luo, J. Li, W.-T. Feng, and L.-B. Chen. Influences of the interferon induced transmembrane protein 1 on the proliferation, invasion, and metastasis of the colorectal cancer sw480 cell lines. *Chin Med J (Engl)*, 125(3):517–522, Feb 2012.

R. Higuchi, C. Fockler, G. Dollinger, and R. Watson. Kinetic pcr analysis: real-time monitoring of dna amplification reactions. *Biotechnology (N Y)*, 11(9):1026–1030, Sep 1993.

A. Hori, S. Honda, M. Asada, T. Ohtaki, K. Oda, T. Watanabe, Y. Shintani, T. Yamada, M. Suenaga, C. Kitada, H. Onda, T. Kurokawa, O. Nishimura, and M. Fujino. Metastin suppresses the motility and growth of cho cells transfected with its receptor. *Biochem Biophys Res Commun*, 286(5):958–63, 2001.

K. W. Hunter, N. P. S. Crawford, and J. Alsarraj. Mechanisms of metastasis. *Breast Cancer Res*, 10 Suppl 1:S2, 2008.

M. Ikeguchi, Y. Hirooka, and N. Kaibara. Quantitative reverse transcriptase polymerase chain reaction analysis for kiss-1 and orphan g-protein-coupled receptor (hot7t175) gene expression in hepatocellular carcinoma. *J Cancer Res Clin Oncol*, 129(9):531–5, 2003.

M. Ikeguchi, K. Yamaguchi, and N. Kaibara. Clinical significance of the loss of kiss-1 and orphan g-protein-coupled receptor (hot7t175) gene expression in esophageal squamous cell carcinoma. *Clin Cancer Res*, 10(4):1379–83, 2004.

M. Iwatsuki, K. Mimori, T. Yokobori, H. Ishi, T. Beppu, S. Nakamori, H. Baba, and M. Mori. Epithelial-mesenchymal transition in cancer development and its clinical significance. *Cancer Sci*, 101(2):293–299, Feb 2010.

Y. Jiang, M. Berk, L. S. Singh, H. Tan, L. Yin, C. T. Powell, and Y. Xu. Kiss1 suppresses metastasis in human ovarian cancer via inhibition of protein kinase c alpha. *Clin Exp Metastasis*, 22(5):369–76, 2005.

J. A. Joyce and J. W. Pollard. Microenvironmental regulation of metastasis. *Nat Rev Cancer*, 9(4): 239–252, Apr 2009.

P. Juszczynski, J. L. Kutok, C. Li, J. Mitra, R. C. T. Aguiar, and M. A. Shipp. Bal1 and bbap are regulated by a gamma interferon-responsive bidirectional promoter and are overexpressed in diffuse large b-cell lymphomas with a prominent inflammatory infiltrate. *Mol Cell Biol*, 26(14):5348–5359, Jul 2006.

R. Kalluri and R. A. Weinberg. The basics of epithelial-mesenchymal transition. *J Clin Invest*, 119(6): 1420–8, 2009.

H. Kang, R. E. Mansel, and W. G. Jiang. Genetic manipulation of stromal cell-derived factor-1 attests the pivotal role of the autocrine sdf-1-cxcr4 pathway in the aggressiveness of breast cancer cells. *Int J Oncol*, 26(5):1429–1434, May 2005a.

H. Kang, G. Watkins, C. Parr, A. Douglas-Jones, R. E. Mansel, and W. G. Jiang. Stromal cell derived factor-1: its influence on invasiveness and migration of breast cancer cells in vitro, and its association with prognosis and survival in human breast cancer. *Breast Cancer Res*, 7(4):R402–R410, 2005b.

H. S. Kang, T. Baba, M. Mandai, N. Matsumura, J. Hamanishi, B. Kharma, E. Kondoh, Y. Yoshioka, S. Oishi, N. Fujii, S. K. Murphy, and I. Konishi. Gpr54 is a target for suppression of metastasis in endometrial cancer. *Mol Cancer Ther*, 10(4):580–590, Apr 2011.

Y. Kang, P. M. Siegel, W. Shu, M. Drobnjak, S. M. Kakonen, C. Cordón-Cardo, T. A. Guise, and J. Massagué. A multigenic program mediating breast cancer metastasis to bone. *Cancer Cell*, 3(6): 537–549, Jun 2003.

M. Karin, T. Lawrence, and V. Nizet. Innate immunity gone awry: linking microbial infections to chronic inflammation and cancer. *Cell*, 124(4):823–835, Feb 2006.

I. Keydar, L. Chen, S. Karby, F. R. Weiss, J. Delarea, M. Radu, S. Chaitcik, and H. J. Brenner. Establishment and characterization of a cell line of human breast carcinoma origin. *Eur J Cancer*, 15(5): 659–670, May 1979.

H. R. Kirby, J. J. Maguire, W. H. Colledge, and A. P. Davenport. International union of basic and clinical pharmacology. lxxvii. kisspeptin receptor nomenclature, distribution, and function. *Pharmacol Rev*, 62 (4):565–78, 2010.

C. A. Klein. Parallel progression of primary tumours and metastases. *Nat Rev Cancer*, 9(4):302–312, Apr 2009.

T. Kobayashi, S. Sasaki, N. Tomita, S. Fukui, N. Kuroda, M. Nakayama, A. Kiba, Y. Takatsu, T. Ohtaki, F. Itoh, and A. Baba. Synthesis and structure-activity relationships of 2-acylamino-4,6-diphenylpyridine derivatives as novel antagonists of gpr54. *Bioorg Med Chem*, 18(11):3841–3859, Jun 2010.

M. I. Kokkinos, R. Wafai, M. K. Wong, D. F. Newgreen, E. W. Thompson, and M. Waltham. Vimentin and epithelial-mesenchymal transition in human breast cancer–observations in vitro and in vivo. *Cells Tissues Organs*, 185(1-3):191–203, 2007.

M. Kotani, M. Detheux, A. Vandenbogaerde, D. Communi, J. M. Vanderwinden, E. Le Poul, S. Brezillon, R. Tyldesley, N. Suarez-Huerta, F. Vandeput, C. Blanpain, S. N. Schiffmann, G. Vassart, and M. Parmentier. The metastasis suppressor gene kiss-1 encodes kisspeptins, the natural ligands of the orphan g protein-coupled receptor gpr54. *J Biol Chem*, 276(37):34631–6, 2001.

W. Kuohung, M. Burnett, D. Mukhtyar, E. Schuman, J. Ni, W. F. Crowley, M. A. Glicksman, and U. B. Kaiser. A high-throughput small-molecule ligand screen targeted to agonists and antagonists of the g-protein-coupled receptor gpr54. *J Biomol Screen*, 15(5):508–517, Jun 2010.

U. K. Laemmli. Cleavage of structural proteins during the assembly of the head of bacteriophage t4. *Nature*, 227(5259):680–5, 1970.

S. C. Lebret, D. F. Newgreen, E. W. Thompson, and M. L. Ackland. Induction of epithelial to mesenchymal transition in pmc42-la human breast carcinoma cells by carcinoma-associated fibroblast secreted factors. *Breast Cancer Res*, 9(1):R19, 2007.

J. H. Lee and D. R. Welch. Identification of highly expressed genes in metastasis-suppressed chromosome 6/human malignant melanoma hybrid cells using subtractive hybridization and differential display. *Int J Cancer*, 71(6):1035–44, 1997a.

J. H. Lee and D. R. Welch. Suppression of metastasis in human breast carcinoma mda-mb-435 cells after transfection with the metastasis suppressor gene, kiss-1. *Cancer Res*, 57(12):2384–7, 1997b.

J. H. Lee, M. E. Miele, D. J. Hicks, K. K. Phillips, J. M. Trent, B. E. Weissman, and D. R. Welch. Kiss-1, a novel human malignant melanoma metastasis-suppressor gene. *J Natl Cancer Inst*, 88(23):1731–7, 1996.

J. Y. Lee, J. S. Moon, Y. J. Eu, C. W. Lee, S. T. Yang, S. K. Lee, H. H. Jung, H. H. Kim, H. Rhim, J. Y. Seong, and J. I. Kim. Molecular interaction between kisspeptin decapeptide analogs and a lipid membrane. *Arch Biochem Biophys*, 485(2):109–14, 2009.

N. Li, H.-X. Wang, J. Zhang, Y.-P. Ye, and G.-Y. He. Kiss-1 inhibits the proliferation and invasion of gastric carcinoma cells. *World J Gastroenterol*, 18(15):1827–1833, Apr 2012.

K. J. Livak, S. J. Flood, J. Marmaro, W. Giusti, and K. Deetz. Oligonucleotides with fluorescent dyes at opposite ends provide a quenched probe system useful for detecting pcr product and nucleic acid hybridization. *PCR Methods Appl*, 4(6):357–362, Jun 1995.

A. Mantovani, B. Savino, M. Locati, L. Zammataro, P. Allavena, and R. Bonecchi. The chemokine system in cancer biology and therapy. *Cytokine Growth Factor Rev*, 21(1):27–39, Feb 2010.

D. Marot, I. Bieche, C. Aumas, S. Esselin, C. Bouquet, S. Vacher, G. Lazennec, M. Perricaudet, F. Kuttenn, R. Lidereau, and N. de Roux. High tumoral levels of kiss1 and g-protein-coupled receptor 54 expression are correlated with poor prognosis of estrogen receptor-positive breast tumors. *Endocr Relat Cancer*, 14(3):691–702, 2007.

T. A. Martin, G. Watkins, and W. G. Jiang. Kiss-1 expression in human breast cancer. *Clin Exp Metastasis*, 22(6):503–11, 2005.

T. Masui, R. Doi, T. Mori, E. Toyoda, M. Koizumi, K. Kami, D. Ito, S. C. Peiper, J. R. Broach, S. Oishi, A. Niida, N. Fujii, and M. Imamura. Metastin and its variant forms suppress migration of pancreatic cancer cells. *Biochem Biophys Res Commun*, 315(1):85–92, 2004.

L. Mathot and J. Stenninger. Behavior of seeds and soil in the mechanism of metastasis: a deeper understanding. *Cancer Sci*, 103(4):626–631, Apr 2012.

B. A. McKenzie, A. Barrieux, and N. M. Varki. A novel detection system for submicroscopic human metastases in athymic mice. *Cancer Commun*, 3(1):15–19, Jan 1991.

L. R. McNally, D. R. Welch, B. H. Beck, L. J. Stafford, J. W. Long, J. C. Sellers, Z. Q. Huang, W. E. Grizzle, C. R. Stockard, K. T. Nash, and D. J. Buchsbaum. Kiss1 over-expression suppresses metastasis of pancreatic adenocarcinoma in a xenograft mouse model. *Clin Exp Metastasis*, 27(8):591–600, Dec 2010.

J. A. Merritt, D. M. Meltzer, L. A. Ball, and E. C. Borden. 2-5a synthetase activity in patients with metastatic carcinoma and its response to interferon treatment. *Prog Clin Biol Res*, 202:423–430, 1985.

M. E. Miele, G. Robertson, J. H. Lee, A. Coleman, C. T. McGary, P. B. Fisher, T. G. Lugo, and D. R. Welch. Metastasis suppressed, but tumorigenicity and local invasiveness unaffected, in the human melanoma cell line meljuso after introduction of human chromosomes 1 or 6. *Mol Carcinog*, 15(4): 284–99, 1996.

J. D. Mikkelsen, A. H. Bentsen, L. Ansel, V. Simonneaux, and A. Juul. Comparison of the effects of peripherally administered kisspeptins. *Regul Pept*, 152(1-3):95–100, 2009.

V. Mirisola, A. Zuccarino, B. E. Bachmeier, M. P. Sormani, J. Falter, A. Nerlich, and U. Pfeffer. Cxcl12/sdf1 expression by breast cancers is an independent prognostic marker of disease-free and overall survival. *Eur J Cancer*, 45(14):2579–2587, Sep 2009.

A. Müller, B. Homey, H. Soto, N. Ge, D. Catron, M. E. Buchanan, T. McClanahan, E. Murphy, W. Yuan, S. N. Wagner, J. L. Barrera, A. Mohar, E. Verástegui, and A. Zlotnik. Involvement of chemokine receptors in breast cancer metastasis. *Nature*, 410(6824):50–56, Mar 2001.

S. Mooez, F. A. Malik, M. A. Kayani, R. Rashid, A. Zahid, and A. Khan. Expressional alterations and transcript isoforms of metastasis suppressor genes (kai1 and kiss1) in breast cancer patients. *Asian Pac J Cancer Prev*, 12(10):2785–2791, 2011.

A. I. Muir, L. Chamberlain, N. A. Elshourbagy, D. Michalovich, D. J. Moore, A. Calamari, P. G. Szekeres, H. M. Sarau, J. K. Chambers, P. Murdock, K. Steplewski, U. Shabon, J. E. Miller, S. E. Middleton, J. G. Darker, C. G. Larminie, S. Wilson, D. J. Bergsma, P. Emson, R. Faull, K. L. Philpott, and D. C. Harrison. Axor12, a novel human g protein-coupled receptor, activated by the peptide kiss-1. *J Biol Chem*, 276(31):28969–75, 2001.

K. Mullis, F. Faloona, S. Scharf, R. Saiki, G. Horn, and H. Erlich. Specific enzymatic amplification of dna in vitro: the polymerase chain reaction. *Cold Spring Harb Symp Quant Biol*, 51 Pt 1:263–273, 1986.

J. R. Munoz, B. R. Stoutenger, A. P. Robinson, J. L. Spees, and D. J. Prockop. Human stem/progenitor cells from bone marrow promote neurogenesis of endogenous neural stem cells in the hippocampus of mice. *Proc Natl Acad Sci U S A*, 102(50):18171–18176, Dec 2005.

K. Nagai, R. Doi, F. Katagiri, T. Ito, A. Kida, M. Koizumi, T. Masui, Y. Kawaguchi, K. Tomita, S. Oishi, N. Fujii, and S. Uemoto. Prognostic value of metastin expression in human pancreatic cancer. *J Exp Clin Cancer Res*, 28:9, 2009.

K. T. Nash, P. A. Phadke, J. M. Navenot, D. R. Hurst, M. A. Accavitti-Loper, E. Sztul, K. S. Vaidya, A. R. Frost, J. C. Kappes, S. C. Peiper, and D. R. Welch. Requirement of kiss1 secretion for multiple organ metastasis suppression and maintenance of tumor dormancy. *J Natl Cancer Inst*, 99(4):309–21, 2007.

J. M. Navenot, Z. Wang, M. Chopin, N. Fujii, and S. C. Peiper. Kisspeptin-10-induced signaling of gpr54 negatively regulates chemotactic responses mediated by cxcr4: a potential mechanism for the metastasis suppressor activity of kisspeptins. *Cancer Res*, 65(22):10450–6, 2005.

J. M. Navenot, N. Fujii, and S. C. Peiper. Activation of rho and rho-associated kinase by gpr54 and kiss1 metastasis suppressor gene product induces changes of cell morphology and contributes to apoptosis. *Mol Pharmacol*, 75(6):1300–6, 2009.

R. M. Neve, K. Chin, J. Fridlyand, J. Yeh, F. L. Baehner, T. Fevr, L. Clark, N. Bayani, J. P. Coppe, F. Tong, T. Speed, P. T. Spellman, S. DeVries, A. Lapuk, N. J. Wang, W. L. Kuo, J. L. Stilwell, D. Pinkel, D. G. Albertson, F. M. Waldman, F. McCormick, R. B. Dickson, M. D. Johnson, M. Lippman, S. Ethier, A. Gazdar, and J. W. Gray. A collection of breast cancer cell lines for the study of functionally distinct cancer subtypes. *Cancer Cell*, 10(6):515–27, 2006.

A. Niida, Z. Wang, K. Tomita, S. Oishi, H. Tamamura, A. Otaka, J. M. Navenot, J. R. Broach, S. C. Peiper, and N. Fujii. Design and synthesis of downsized metastin (45-54) analogs with maintenance of high gpr54 agonistic activity. *Bioorg Med Chem Lett*, 16(1):134–7, 2006.

T. Ohtaki, Y. Shintani, S. Honda, H. Matsumoto, A. Hori, K. Kanehashi, Y. Terao, S. Kumano, Y. Takatsu, Y. Masuda, Y. Ishibashi, T. Watanabe, M. Asada, T. Yamada, M. Suenaga, C. Kitada, S. Usuki, T. Kurokawa, H. Onda, O. Nishimura, and M. Fujino. Metastasis suppressor gene kiss-1 encodes peptide ligand of a g-protein-coupled receptor. *Nature*, 411(6837):613–7, 2001.

T. Olbrich. *Einfluss von Kisspeptin-10 auf die knochengerichtete Migration und Invasion von Mammakarzinomzellen*. Dissertation, 2010a.

T. Olbrich, E. Ziegler, G. Türk, A. Schubert, G. Emons, and C. Gründker. Kisspeptin-10 inhibits bone-directed migration of gpr54-positive breast cancer cells: Evidence for a dose-window effect. *Gynecol Oncol*, 119(3):571–578, Dec 2010b.

T. Onoue, D. Uchida, N. M. Begum, Y. Tomizuka, H. Yoshida, and M. Sato. Epithelial-mesenchymal transition induced by the stromal cell-derived factor-1/cxcr4 system in oral squamous cell carcinoma cells. *Int J Oncol*, 29(5):1133–8, 2006.

M. J. Orsini, M. A. Klein, M. P. Beavers, P. J. Connolly, S. A. Middleton, and K. H. Mayo. Metastin (kiss-1) mimetics identified from peptide structure-activity relationship-derived pharmacophores and directed small molecule database screening. *J Med Chem*, 50(3):462–71, 2007.

S. Paget. The distribution of secondary growths in cancer of the breast. 1889. *Cancer Metastasis Rev*, 8 (2):98–101, Aug 1889.

M. Pampillo, N. Camuso, J. E. Taylor, J. M. Szereszewski, M. R. Ahow, M. Zajac, R. P. Millar, M. Bhattacharya, and A. V. Babwah. Regulation of gpr54 signaling by grk2 and beta-arrestin. *Mol Endocrinol*, 23(12):2060–74, 2009.

K. Pantel and R. H. Brakenhoff. Dissecting the metastatic cascade. *Nat Rev Cancer*, 4(6):448–456, Jun 2004.

M. Parri and P. Chiarugi. Rac and rho gtpases in cancer cell motility control. *Cell Commun Signal*, 8:23, 2010.

L. M. Prentice, C. Klausen, S. Kalloger, M. Köbel, S. McKinney, J. L. Santos, C. Kenney, E. Mehl, C. B. Gilks, P. Leung, K. Swenerton, D. G. Huntsman, and S. A. J. Aparicio. Kisspeptin and gpr54 immunoreactivity in a cohort of 518 patients defines favourable prognosis and clear cell subtype in ovarian carcinoma. *BMC Med*, 5:33, 2007.

J. E. Price and R. D. Zhang. Studies of human breast cancer metastasis using nude mice. *Cancer Metastasis Rev*, 8(4):285–297, Feb 1990.

S. E. Quaggin, G. B. V. Heuvel, and P. Igarashi. Pod-1, a mesoderm-specific basic-helix-loop-helix protein expressed in mesenchymal and glomerular epithelial cells in the developing kidney. *Mech Dev*, 71(1-2): 37–48, Feb 1998.

J. M. Rae, S. J. Ramus, M. Waltham, J. E. Armes, I. G. Campbell, R. Clarke, R. J. Barndt, M. D. Johnson, and E. W. Thompson. Common origins of mda-mb-435 cells from various sources with those shown to have melanoma properties. *Clin Exp Metastasis*, 21(6):543–552, 2004.

T. Ramaesh, J. J. Logie, A. K. Roseweir, R. P. Millar, B. R. Walker, P. W. F. Hadoke, and R. M. Reynolds. Kisspeptin-10 inhibits angiogenesis in human placental vessels ex vivo and endothelial cells in vitro. *Endocrinology*, 151(12):5927–5934, Dec 2010.

M. M. Richert, K. S. Vaidya, C. N. Mills, D. Wong, W. Korz, D. R. Hurst, and D. R. Welch. Inhibition of cxcr4 by ctce-9908 inhibits breast cancer metastasis to lung and bone. *Oncol Rep*, 21(3):761–767, Mar 2009.

E. Richtig, G. Langmann, K. Mullner, G. Richtig, and J. Smolle. Calculated tumour volume as a prognostic parameter for survival in choroidal melanomas. *Eye (Lond)*, 18(6):619–23, 2004.

RKI. Robert Koch-Institut. *Krebs in Deutschland 2007/2008*. Berlin, 8th edition, 2012.

A. K. Roseweir, A. S. Kauffman, J. T. Smith, K. A. Guerriero, K. Morgan, J. Pielecka-Fortuna, R. Pineda, M. L. Gottsch, M. Tena-Sempere, S. M. Moenter, E. Terasawa, I. J. Clarke, R. A. Steiner, and R. P. Millar. Discovery of potent kisspeptin antagonists delineate physiological mechanisms of gonadotropin regulation. *J Neurosci*, 29(12):3920–9, 2009.

A. K. Roseweir, A. A. Katz, and R. P. Millar. Kisspeptin-10 inhibits cell migration in vitro via a receptor-gsk3 beta-fak feedback loop in htr8svneo cells. *Placenta*, 33(5):408–415, May 2012.

D. D. Ross, J. E. Karp, T. T. Chen, and L. A. Doyle. Expression of breast cancer resistance protein in blast cells from patients with acute leukemia. *Blood*, 96(1):365–368, Jul 2000.

Z. J. Rutnam and B. B. Yang. The non-coding 3' utr of cd44 induces metastasis by regulating extracellular matrix functions. *J Cell Sci*, 125(Pt 8):2075–2085, Apr 2012.

A. Sasaki, B. F. Boyce, B. Story, K. R. Wright, M. Chapman, R. Boyce, G. R. Mundy, and T. Yoneda. Bisphosphonate risedronate reduces metastatic human breast cancer burden in bone in nude mice. *Cancer Res*, 55(16):3551–3557, Aug 1995.

T. Schneider, F. Osl, T. Friess, H. Stockinger, and W. V. Scheuer. Quantification of human alu sequences by real-time pcr–an improved method to measure therapeutic efficacy of anti-metastatic drugs in human xenotransplants. *Clin Exp Metastasis*, 19(7):571–582, 2002.

A. Schubert, T. Hawighorst, G. Emons, and C. Gründker. Agonists and antagonists of gnrh-i and -ii reduce metastasis formation by triple-negative human breast cancer cells in vivo. *Breast Cancer Res Treat*, 130(3):783–790, Dec 2011.

D. Schubert, S. Heinemann, W. Carlisle, H. Tarikas, B. Kimes, J. Patrick, J. H. Steinbach, W. Culp, and B. L. Brandt. Clonal cell lines from the rat central nervous system. *Nature*, 249(454):224–227, May 1974.

C. J. Scotton, J. L. Wilson, D. Milliken, G. Stamp, and F. R. Balkwill. Epithelial cancer cell migration: a role for chemokine receptors? *Cancer Res*, 61(13):4961–4965, Jul 2001.

S. Sellappan, R. Grijalva, X. Zhou, W. Yang, M. B. Eli, G. B. Mills, and D. Yu. Lineage infidelity of mda-mb-435 cells: expression of melanocyte proteins in a breast cancer cell line. *Cancer Res*, 64(10): 3479–3485, May 2004.

X. Shen, S. Wang, H. Wang, M. Liang, L. Xiao, and Z. Wang. The role of sdf-1/cxcr4 axis in ovarian cancer metastasis. *J Huazhong Univ Sci Technolog Med Sci*, 29(3):363–367, Jun 2009.

C. Sheridan, H. Kishimoto, R. K. Fuchs, S. Mehrotra, P. Bhat-Nakshatri, C. H. Turner, J. Goulet, R., S. Badve, and H. Nakshatri. Cd44+/cd24- breast cancer cells exhibit enhanced invasive properties: an early step necessary for metastasis. *Breast Cancer Res*, 8(5):R59, 2006.

R. H. Shoemaker, A. M. Smythe, L. Wu, M. S. Balaschak, and M. R. Boyd. Evaluation of metastatic human tumor burden and response to therapy in a nude mouse xenograft model using a molecular probe for repetitive human dna sequences. *Cancer Res*, 52(10):2791–2796, May 1992.

S. Shoji, X. Y. Tang, S. Umemura, J. Itoh, S. Takekoshi, M. Shima, Y. Usui, Y. Nagata, T. Uchida, R. Y. Osamura, and T. Terachi. Metastin inhibits migration and invasion of renal cell carcinoma with overexpression of metastin receptor. *Eur Urol*, 55(2):441–9, 2009.

S. Singh, U. P. Singh, W. E. Grizzle, and J. W. Lillard. Cxcl12-cxcr4 interactions modulate prostate cancer cell migration, metalloproteinase expression and invasion. *Lab Invest*, 84(12):1666–1676, Dec 2004.

C. L. Sommers, S. W. Byers, E. W. Thompson, J. A. Torri, and E. P. Gelmann. Differentiation state and invasiveness of human breast cancer cell lines. *Breast Cancer Res Treat*, 31(2-3):325–35, 1994.

H. D. Soule, J. Vazquez, A. Long, S. Albert, and M. Brennan. A human cell line from a pleural effusion derived from a breast carcinoma. *J Natl Cancer Inst*, 51(5):1409–1416, Nov 1973.

L. J. Stafford, C. Xia, W. Ma, Y. Cai, and M. Liu. Identification and characterization of mouse metastasis-suppressor kiss1 and its g-protein-coupled receptor. *Cancer Res*, 62(19):5399–404, 2002.

J. M. Szereszewski, M. Pampillo, M. R. Ahow, S. Offermanns, M. Bhattacharya, and A. V. Babwah. Gpr54 regulates erk1/2 activity and hypothalamic gene expression in a g?(q/11) and ?-arrestin-dependent manner. *PLoS One*, 5(9):e12964, 2010.

M. Taki, K. Higashikawa, S. Yoneda, S. Ono, H. Shigeishi, M. Nagayama, and N. Kamata. Up-regulation of stromal cell-derived factor-1alpha and its receptor cxcr4 expression accompanied with epithelial-mesenchymal transition in human oral squamous cell carcinoma. *Oncol Rep*, 19(4):993–8, 2008.

T. Takino, N. Koshikawa, H. Miyamori, M. Tanaka, T. Sasaki, Y. Okada, M. Seiki, and H. Sato. Cleavage of metastasis suppressor gene product kiss-1 protein/metastin by matrix metalloproteinases. *Oncogene*, 22(30):4617–26, 2003.

M. A. Taylor, J. G. Parvani, and W. P. Schiemann. The pathophysiology of epithelial-mesenchymal transition induced by transforming growth factor-beta in normal and malignant mammary epithelial cells. *J Mammary Gland Biol Neoplasia*, 15(2):169–190, Jun 2010.

K. Tomita, A. Niida, S. Oishi, H. Ohno, J. Cluzeau, J. M. Navenot, Z. X. Wang, S. C. Peiper, and N. Fujii. Structure-activity relationship study on small peptidic gpr54 agonists. *Bioorg Med Chem*, 14 (22):7595–603, 2006.

K. Tomita, T. Narumi, A. Niida, S. Oishi, H. Ohno, and N. Fujii. Fmoc-based solid-phase synthesis of gpr54-agonistic pentapeptide derivatives containing alkene- and fluoroalkene-dipeptide isosteres. *Biopolymers*, 88(2):272–8, 2007.

K. Tomita, S. Oishi, H. Ohno, S. C. Peiper, and N. Fujii. Development of novel g-protein-coupled receptor 54 agonists with resistance to degradation by matrix metalloproteinase. *J Med Chem*, 51(23):7645–9, 2008.

S. Tyagi and F. R. Kramer. Molecular beacons: probes that fluoresce upon hybridization. *Nat Biotechnol*, 14(3):303–308, Mar 1996.

D. Uchida, N. M. Begum, A. Almofti, K. ichi Nakashiro, H. Kawamata, Y. Tateishi, H. Hamakawa, H. Yoshida, and M. Sato. Possible role of stromal-cell-derived factor-1/cxcr4 signaling on lymph node metastasis of oral squamous cell carcinoma. *Exp Cell Res*, 290(2):289–302, Nov 2003.

D. Uchida, T. Onoue, Y. Tomizuka, N. M. Begum, Y. Miwa, H. Yoshida, and M. Sato. Involvement of an autocrine stromal cell derived factor-1/cxcr4 system on the distant metastasis of human oral squamous cell carcinoma. *Mol Cancer Res*, 5(7):685–694, Jul 2007.

M. Uchino, H. Kojima, K. Wada, M. Imada, F. Onoda, H. Satofuka, T. Utsugi, and Y. Murakami. Nuclear beta-catenin and cd44 upregulation characterize invasive cell populations in non-aggressive mcf-7 breast cancer cells. *BMC Cancer*, 10:414, 2010.

S. Valastyan and R. A. Weinberg. Tumor metastasis: molecular insights and evolving paradigms. *Cell*, 147(2):275–292, Oct 2011.

F. van Zijl, G. Krupitza, and W. Mikulits. Initial steps of metastasis: cell invasion and endothelial transmigration. *Mutat Res*, 728(1-2):23–34, 2011.

I. M. Verma, R. A. Firtel, H. F. Lodish, and D. Baltimore. Synthesis of dna complementary to cellular slime mold messenger rna by reverse transcriptase. *Biochemistry*, 13(19):3917–3922, Sep 1974.

U. Veronesi, P. Boyle, A. Goldhirsch, R. Orecchia, and G. Viale. Breast cancer. *Lancet*, 365(9472): 1727–1741, 2005.

L. D. Volk-Draper, S. Rajput, K. L. Hall, A. Wilber, and S. Ran. Novel model for basaloid triple-negative breast cancer: behavior in vivo and response to therapy. *Neoplasia*, 14(10):926–942, Oct 2012.

J. von Alten, S. Fister, H. Schulz, V. Viereck, K.-H. Frosch, G. Emons, and C. Gründker. Gnrh analogs reduce invasiveness of human breast cancer cells. *Breast Cancer Res Treat*, 100(1):13–21, Nov 2006.

S. L. Voytik-Harbin, A. O. Brightman, B. Waisner, C. H. Lamar, and S. F. Badylak. Application and evaluation of the alamarblue assay for cell growth and survival of fibroblasts. *In Vitro Cell Dev Biol Anim*, 34(3):239–46, 1998.

J. Wang, R. Loberg, and R. S. Taichman. The pivotal role of cxcl12 (sdf-1)/cxcr4 axis in bone metastasis. *Cancer Metastasis Rev*, 25(4):573–587, Dec 2006.

D. R. Welch, P. Chen, M. E. Miele, C. T. McGary, J. M. Bower, E. J. Stanbridge, and B. E. Weissman. Microcell-mediated transfer of chromosome 6 into metastatic human c8161 melanoma cells suppresses metastasis but does not inhibit tumorigenicity. *Oncogene*, 9(1):255–62, 1994.

WHO. World Health Organization. *IARC Handbooks of Cancer Prevention. Breast Cancer Screening.*, volume 7. IARC Press, Lyon, 2002.

WHO. World Health Organization. *Classification of Tumours. Pathology and Genetics of Tumours of the Breast and Female Genital Organs*. IARC Press, Lyon, 2003.

Y. Wu and B. P. Zhou. New insights of epithelial-mesenchymal transition in cancer metastasis. *Acta Biochim Biophys Sin (Shanghai)*, 40(7):643–50, 2008.

C. Yan, H. Wang, and D. D. Boyd. Kiss-1 represses 92-kda type iv collagenase expression by down-regulating nf-kappa b binding to the promoter as a consequence of ikappa balpha -induced block of p65/p50 nuclear translocation. *J Biol Chem*, 276(2):1164–72, 2001.

M. Yilmaz and G. Christofori. Mechanisms of motility in metastasizing cells. *Mol Cancer Res*, 8(5): 629–642, May 2010.

T. Yoneda. Cellular and molecular basis of preferential metastasis of breast cancer to bone. *J Orthop Sci*, 5(1):75–81, 2000.

K. Yoshioka, Y. Ohno, Y. Horiguchi, C. Ozu, K. Namiki, and M. Tachibana. Effects of a kiss-1 peptide, a metastasis suppressor gene, on the invasive ability of renal cell carcinoma cells through a modulation of a matrix metalloproteinase 2 expression. *Life Sci*, 83(9-10):332–338, Aug 2008.

D. A. Zajchowski, M. F. Bartholdi, Y. Gong, L. Webster, H. L. Liu, A. Munishkin, C. Beauheim, S. Harvey, S. P. Ethier, and P. H. Johnson. Identification of gene expression profiles that predict the aggressive behavior of breast cancer cells. *Cancer Res*, 61(13):5168–5178, Jul 2001.

J. Zavadil and E. P. Bottinger. Tgf-beta and epithelial-to-mesenchymal transitions. *Oncogene*, 24(37): 5764–74, 2005.

E. Ziegler, T. Olbrich, G. Emons, and C. Gründker. Antiproliferative effects of kisspeptin-10 depend on artificial gpr54 (kiss1r) expression levels. *Oncol Rep*, 29(2):549–554, Feb 2013.

Appendix

A1 Sample heatmap of the microarray data
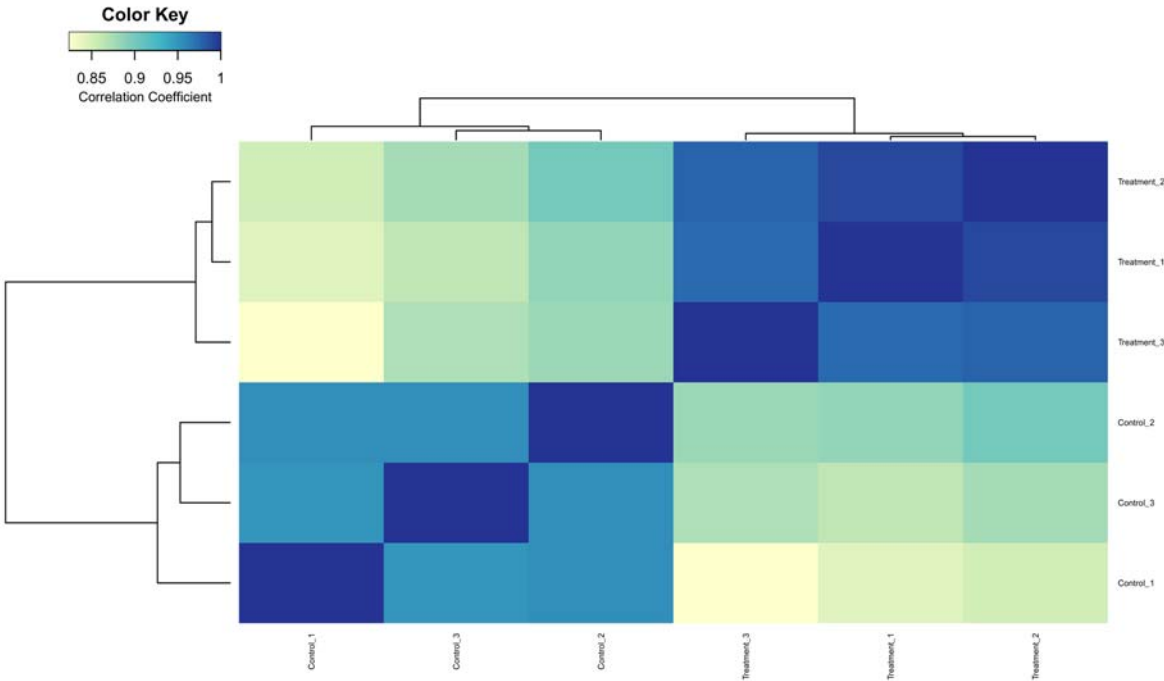
A2 Candidates list of the microarray data

Symbol	Description	Probe	Gene	logFC Treatment-Control	AveExpr Treatment-Control	P.Value Treatment-Control	FDR Treatment-Control
KYNU	kynureninase	8942_at	8942	-2,85	7,406266074	1,16E-04	0,68%
KITLG	KIT ligand	4254_at	4254	-2,72	8,475037516	2,88E-06	0,10%
ERBB4	v-erb-a erythroblastic leukemia viral oncogene homolog 4 (avian)	2066_at	2066	-2,56	8,447631597	1,36E-06	0,08%
NRCAM	neuronal cell adhesion molecule	4897_at	4897	-2,48	7,828567861	4,50E-06	0,12%
EFEMP1	EGF containing fibulin-like extracellular matrix protein 1	2202_at	2202	-2,38	8,919480102	5,98E-05	0,47%
TACC1	transforming, acidic coiled-coil containing protein 1	6867_at	6867	-2,17	9,548784414	1,68E-05	0,22%
NPNT	nephronectin	255743_at	255743	-2,13	10,44608789	9,73E-07	0,07%
LIN7A	lin-7 homolog A (C. elegans)	8825_at	8825	-2,10	7,696356695	8,90E-06	0,16%
UPK1A	uroplakin 1A	11045_at	11045	-2,04	7,583522905	1,33E-03	2,71%
SALL4	sal-like 4 (Drosophila)	57167_at	57167	-2,02	8,174255164	1,25E-04	0,71%
TRAV13-2	T cell receptor alpha variable 13-2	28670_at	28670	-1,98	6,28037951	2,35E-03	3,63%
ST8SIA4	ST8 alpha-N-acetyl-neuraminide alpha-2,8-sialyltransferase 4	7903_at	7903	-1,89	7,204850359	1,40E-06	0,08%
PMP22	peripheral myelin protein 22	5376_at	5376	-1,88	8,679818574	1,70E-04	0,86%
OR4K2	olfactory receptor, family 4, subfamily K, member 2	390431_at	390431	-1,87	7,144559138	1,91E-03	3,20%
IGFBP5	insulin-like growth factor binding protein 5	3488_at	3488	-1,83	7,380510353	2,60E-03	3,82%
GDPD3	glycerophosphodiester phosphodiesterase domain containing 3	79153_at	79153	-1,81	9,116905382	8,95E-04	2,16%
FAM83B	family with sequence similarity 83, member B	222584_at	222584	-1,78	10,07170838	4,60E-07	0,04%
MIR181B1	microRNA 181b-1	406955_at	406955	-1,77	8,874114332	6,18E-07	0,05%
CMYA5	cardiomyopathy associated 5	202333_at	202333	-1,74	6,911259143	4,65E-04	1,49%
TRAV14DV4	T cell receptor alpha variable 14/delta variable 4	28669_at	28669	-1,72	4,545292137	3,93E-06	0,11%
NELL2	NEL-like 2 (chicken)	4753_at	4753	-1,70	5,592997192	3,73E-05	0,36%
PGM5	phosphoglucomutase 5	5239_at	5239	-1,67	6,092060241	5,91E-05	0,47%
SLC26A2	solute carrier family 26 (sulfate transporter), member 2	1836_at	1836	-1,64	8,090917908	2,16E-06	0,09%
GSTM3	glutathione S-transferase mu 3 (brain)	2947_at	2947	-1,61	8,180511204	1,02E-05	0,17%
LIFR	leukemia inhibitory factor receptor alpha	3977_at	3977	-1,59	6,879524731	1,29E-05	0,20%
MATN2	matrilin 2	4147_at	4147	-1,54	8,065115075	6,60E-05	0,50%
MKRN9P	makorin ring finger protein 9, pseudogene	400058_at	400058	-1,51	6,777580298	2,22E-03	3,49%
ABCG2	ATP-binding cassette, sub-family G (WHITE), member 2	9429_at	9429	-1,49	5,943967309	2,76E-04	1,14%
NEDD4L	neural precursor cell expressed, developmentally down-regulated 4-like	23327_at	23327	-1,48	8,679391458	1,67E-05	0,22%
OR51A4	olfactory receptor, family 51, subfamily A, member 4	401666_at	401666	-1,48	5,622793421	2,15E-03	3,44%
SLC6A14	solute carrier family 6 (amino acid transporter), member 14	11254_at	11254	-1,48	7,454409733	1,21E-04	0,70%

Symbol	Description	Probe	Gene	logFC Treatment-Control	AveExpr Treatment-Control	P.Value Treatment-Control	FDR Treatment-Control
C18orf1	chromosome 18 open reading frame 1	753_at	753	-1,47	7,543478928	2,77E-06	0,10%
OR2M5	olfactory receptor, family 2, subfamily M, member 5	127059_at	127059	-1,46	6,199568116	3,94E-03	4,80%
ANXA3	annexin A3	306_at	306	-1,42	9,192114952	2,97E-04	1,19%
EFNA1	ephrin-A1	1942_at	1942	-1,39	8,554657267	6,01E-06	0,13%
IL1R1	interleukin 1 receptor, type I	3554_at	3554	-1,39	5,553848659	5,46E-05	0,44%
FAM190A	family with sequence similarity 190, member A	401145_at	401145	-1,38	6,560566784	3,46E-06	0,10%
MMP16	matrix metallopeptidase 16 (membrane-inserted)	4325_at	4325	-1,37	8,496755098	1,05E-06	0,07%
GPR115	G protein-coupled receptor 115	221393_at	221393	-1,37	5,070890942	1,68E-03	2,98%
ODZ3	odz, odd Oz/ten-m homolog 3 (Drosophila)	55714_at	55714	-1,36	7,544591964	2,38E-04	1,04%
YPEL3	yippee-like 3 (Drosophila)	83719_at	83719	-1,35	7,598959105	2,62E-05	0,30%
PMEPA1	prostate transmembrane protein, androgen induced 1	56937_at	56937	-1,34	7,604917876	5,89E-04	1,73%
DCDC2	doublecortin domain containing 2	51473_at	51473	-1,34	8,290499171	1,87E-03	3,17%
OR2M3	olfactory receptor, family 2, subfamily M, member 3	127062_at	127062	-1,33	5,071130007	5,83E-04	1,73%
BMF	Bcl2 modifying factor	90427_at	90427	-1,32	7,006350766	2,00E-05	0,25%
HEBP1	heme binding protein 1	50865_at	50865	-1,32	9,182310955	2,68E-04	1,12%
CRIM1	cysteine rich transmembrane BMP regulator 1 (chordin-like)	51232_at	51232	-1,32	8,467742946	2,13E-03	3,43%
OR2M2	olfactory receptor, family 2, subfamily M, member 2	391194_at	391194	-1,31	4,761045367	1,92E-03	3,21%
OR4K5	olfactory receptor, family 4, subfamily K, member 5	79317_at	79317	-1,31	5,914293006	4,25E-03	4,99%
UTRN	utrophin	7402_at	7402	-1,30	7,433529373	1,10E-04	0,67%
YPEL2	yippee-like 2 (Drosophila)	388403_at	388403	-1,30	7,918533368	1,61E-04	0,84%
SMYD2	SET and MYND domain containing 2	56950_at	56950	-1,29	8,162206929	7,30E-04	1,96%
KLHL24	kelch-like 24 (Drosophila)	54800_at	54800	-1,29	7,967952863	1,24E-03	2,59%
MIR181A1	microRNA 181a-1	406995_at	406995	-1,28	5,032751235	6,19E-06	0,13%
SLC25A30	solute carrier family 25, member 30	253512_at	253512	-1,27	7,698576039	1,11E-04	0,67%
WWC2	WW and C2 domain containing 2	80014_at	80014	-1,26	7,690531912	5,53E-05	0,44%
IRF6	interferon regulatory factor 6	3664_at	3664	-1,26	8,214889991	7,49E-04	1,99%
OR4M1	olfactory receptor, family 4, subfamily M, member 1	441670_at	441670	-1,25	5,249881964	1,95E-03	3,24%
OR14J1	olfactory receptor, family 14, subfamily J, member 1	442191_at	442191	-1,24	5,535000971	2,76E-03	3,94%
PLXDC2	plexin domain containing 2	84898_at	84898	-1,24	7,894429179	4,89E-05	0,42%
STON1-GTF2A1L	STON1-GTF2A1L readthrough	286749_at	286749	-1,23	4,40048753	4,50E-04	1,46%
RAB31	RAB31, member RAS oncogene family	11031_at	11031	-1,22	8,94421261	3,16E-05	0,33%
MIR27B	microRNA 27b	407019_at	407019	-1,22	5,640110131	3,37E-04	1,27%
TM4SF18	transmembrane 4 L six family member 18	116441_at	116441	-1,21	6,112117913	3,45E-03	4,46%
BLNK	B-cell linker	29760_at	29760	-1,20	6,937868872	3,36E-04	1,27%
MIR15A	microRNA 15a	406948_at	406948	-1,18	7,240130056	6,59E-05	0,50%
C3orf79	chromosome 3 open reading frame 79	152118_at	152118	-1,18	5,177150289	2,16E-04	0,99%
PMEL	premelanosome protein	6490_at	6490	-1,17	6,273951385	9,37E-05	0,60%
SECTM1	secreted and transmembrane 1	6398_at	6398	-1,17	7,756533126	8,27E-04	2,11%

Symbol	Description	Probe	Gene	logFC Treatment-Control	AveExpr Treatment-Control	P.Value Treatment-Control	FDR Treatment-Control
EPB41L5	erythrocyte membrane protein band 4.1 like 5	57669_at	57669	-1,17	9,742491922	1,23E-05	0,19%
DCAF4	DDB1 and CUL4 associated factor 4	26094_at	26094	-1,17	9,413860834	5,16E-04	1,61%
CCNG2	cyclin G2	901_at	901	-1,17	10,37886412	1,27E-03	2,63%
MXRA5	matrix-remodelling associated 5	25878_at	25878	-1,17	8,265112689	2,36E-04	1,04%
MIR30C2	microRNA 30c-2	407032_at	407032	-1,15	6,130575775	2,35E-03	3,63%
ATP7B	ATPase, Cu++ transporting, beta polypeptide	540_at	540	-1,14	7,25354421	8,56E-05	0,57%
MAGI1	membrane associated guanylate kinase, WW and PDZ domain containing 1	9223_at	9223	-1,14	9,028643182	9,12E-05	0,59%
C7orf41	chromosome 7 open reading frame 41	222166_at	222166	-1,13	6,596552875	2,70E-06	0,10%
CYP4B1	cytochrome P450, family 4, subfamily B, polypeptide 1	1580_at	1580	-1,13	7,096721096	1,59E-03	2,91%
DIO1	deiodinase, iodothyronine, type I	1733_at	1733	-1,13	6,012958646	1,18E-04	0,69%
ZNF217	zinc finger protein 217	7764_at	7764	-1,13	11,18543811	3,80E-05	0,36%
IL20	interleukin 20	50604_at	50604	-1,13	7,996277607	1,52E-04	0,82%
SPRR2A	small proline-rich protein 2A	6700_at	6700	-1,09	5,619491707	1,57E-03	2,91%
ARHGEF37	Rho guanine nucleotide exchange factor (GEF) 37	389337_at	389337	-1,09	6,560581069	1,45E-05	0,21%
PLLP	plasmolipin	51090_at	51090	-1,09	8,209628928	1,71E-05	0,23%
EDIL3	EGF-like repeats and discoidin I-like domains 3	10085_at	10085	-1,07	4,995220205	1,23E-03	2,59%
TPK1	thiamin pyrophosphokinase 1	27010_at	27010	-1,07	6,051792774	2,15E-06	0,09%
SMPDL3A	sphingomyelin phosphodiesterase, acid-like 3A	10924_at	10924	-1,07	7,943882155	7,21E-05	0,52%
ATP8A1	ATPase, aminophospholipid transporter (APLT), class I, type 8A, member 1	10396_at	10396	-1,07	6,310351626	4,35E-05	0,39%
CTNND2	catenin (cadherin-associated protein), delta 2 (neural plakophilin-related arm-repeat protein)	1501_at	1501	-1,06	7,867247363	5,43E-04	1,66%
C6orf155	chromosome 6 open reading frame 155	79940_at	79940	-1,05	8,183079237	2,19E-05	0,27%
OR52N5	olfactory receptor, family 52, subfamily N, member 5	390075_at	390075	-1,05	5,538167564	3,04E-03	4,16%
PVALB	parvalbumin	5816_at	5816	-1,04	7,644177408	3,78E-03	4,67%
HDGFRP3	hepatoma-derived growth factor, related protein 3	50810_at	50810	-1,04	9,414705288	5,51E-05	0,44%
INHBB	inhibin, beta B	3625_at	3625	-1,03	8,947079417	1,50E-03	2,84%
AMIGO2	adhesion molecule with Ig-like domain 2	347902_at	347902	-1,03	6,704993012	1,72E-04	0,86%
OR6N2	olfactory receptor, family 6, subfamily N, member 2	81442_at	81442	-1,02	6,824105065	2,55E-03	3,79%
TACSTD2	tumor-associated calcium signal transducer 2	4070_at	4070	-1,01	10,51765811	9,73E-04	2,28%
C3orf52	chromosome 3 open reading frame 52	79669_at	79669	-1,01	6,850900692	1,34E-04	0,75%
FBP1	fructose-1,6-bisphosphatase 1	2203_at	2203	-1,01	11,42804045	1,90E-06	0,09%
OR52N4	olfactory receptor, family 52, subfamily N, member 4	390072_at	390072	-1,01	4,328490978	2,43E-03	3,67%
OR8K5	olfactory receptor, family 8, subfamily K, member 5	219453_at	219453	-1,00	4,630598018	1,70E-03	3,00%
CNBD1	cyclic nucleotide binding domain containing 1	168975_at	168975	-1,00	5,312125451	1,63E-03	2,94%

Symbol	Description	Probe	Gene	logFC Treatment-Control	AveExpr Treatment-Control	P.Value Treatment-Control	FDR Treatment-Control
SNTB1	syntrophin, beta 1 (dystrophin-associated protein A1, 59kDa, basic component 1)	6641_at	6641	1,00	7,187488838	1,63E-03	2,94%
PTGS1	prostaglandin-endoperoxide synthase 1 (prostaglandin G/H synthase and cyclooxygenase)	5742_at	5742	1,00	6,369589517	1,99E-06	0,09%
FBXO39	F-box protein 39	162517_at	162517	1,00	7,054042868	8,14E-06	0,15%
EPAS1	endothelial PAS domain protein 1	2034_at	2034	1,00	6,389630304	4,87E-05	0,42%
EIF2AK2	eukaryotic translation initiation factor 2-alpha kinase 2	5610_at	5610	1,01	11,20446581	7,30E-06	0,14%
AFF1	AF4/FMR2 family, member 1	4299_at	4299	1,02	9,062796128	8,43E-06	0,15%
DOCK8	dedicator of cytokinesis 8	81704_at	81704	1,02	7,299326429	6,06E-06	0,13%
HSH2D	hematopoietic SH2 domain containing	84941_at	84941	1,02	7,014823175	3,44E-05	0,34%
ME1	malic enzyme 1, NADP(+)-dependent, cytosolic	4199_at	4199	1,02	9,108477168	1,32E-05	0,20%
PRPS1	phosphoribosyl pyrophosphate synthetase 1	5631_at	5631	1,02	8,017260516	4,02E-06	0,11%
OASL	2'-5'-oligoadenylate synthetase-like	8638_at	8638	1,02	7,322763345	1,14E-04	0,68%
ELOVL6	ELOVL family member 6, elongation of long chain fatty acids (FEN1/Elo2, SUR4/Elo3-like, yeast)	79071_at	79071	1,03	8,69090685	3,48E-04	1,28%
IRS1	insulin receptor substrate 1	3667_at	3667	1,03	7,027577498	6,56E-06	0,13%
PDCD4	programmed cell death 4 (neoplastic transformation inhibitor)	27250_at	27250	1,03	9,715621762	7,00E-05	0,51%
ETS2	v-ets erythroblastosis virus E26 oncogene homolog 2 (avian)	2114_at	2114	1,03	8,139213327	1,70E-04	0,86%
FMN1	formin 1	342184_at	342184	1,03	7,097489435	2,41E-03	3,66%
IER3	immediate early response 3	8870_at	8870	1,03	11,27718155	1,23E-04	0,71%
SERPINE2	serpin peptidase inhibitor, clade E (nexin, plasminogen activator inhibitor type 1), member 2	5270_at	5270	1,06	6,341013515	4,05E-03	4,88%
LOC100288637	hypothetical LOC100288637	100288637_at	100288637	1,06	6,249132666	1,18E-03	2,55%
GSTP1	glutathione S-transferase pi 1	2950_at	2950	1,06	7,120146409	7,18E-04	1,95%
ACSL4	acyl-CoA synthetase long-chain family member 4	2182_at	2182	1,07	6,12492246	5,34E-05	0,44%
ZMIZ1	zinc finger, MIZ-type containing 1	57178_at	57178	1,08	8,953868014	2,45E-04	1,06%
SLC10A5	solute carrier family 10 (sodium/bile acid cotransporter family), member 5	347051_at	347051	1,08	6,224612778	9,23E-06	0,16%
CREB3L1	cAMP responsive element binding protein 3-like 1	90993_at	90993	1,08	7,108265808	2,69E-06	0,10%
SYT11	synaptotagmin XI	23208_at	23208	1,09	5,341932141	3,37E-04	1,27%
PCDHB13	protocadherin beta 13	56123_at	56123	1,09	6,382831539	3,27E-04	1,25%
TMBIM1	transmembrane BAX inhibitor motif containing 1	64114_at	64114	1,09	6,899232446	1,73E-03	3,04%
TRIM21	tripartite motif containing 21	6737_at	6737	1,10	8,320874252	1,26E-05	0,19%
PCDHB14	protocadherin beta 14	56122_at	56122	1,10	7,605161509	5,13E-05	0,43%

Symbol	Description	Probe	Gene	logFC Treatment-Control	AveExpr Treatment-Control	P.Value Treatment-Control	FDR Treatment-Control
RBMS2	RNA binding motif, single stranded interacting protein 2	5939_at	5939	1,10	7,532805283	2,22E-05	0,27%
CSF1	colony stimulating factor 1 (macrophage)	1435_at	1435	1,10	7,232557251	6,01E-05	0,47%
HLA-C	major histocompatibility complex, class I, C	3107_at	3107	1,11	9,400715757	2,78E-05	0,31%
NFIA	nuclear factor I/A	4774_at	4774	1,11	8,244579714	4,49E-04	1,46%
MYO10	myosin X	4651_at	4651	1,12	7,362417639	8,09E-06	0,15%
MAP3K8	mitogen-activated protein kinase kinase kinase 8	1326_at	1326	1,12	6,921510496	2,40E-05	0,28%
ZFP36L1	zinc finger protein 36, C3H type-like 1	677_at	677	1,13	10,11393638	1,23E-04	0,71%
PCDHB4	protocadherin beta 4	56131_at	56131	1,13	5,279374502	2,38E-04	1,04%
IGF2BP3	insulin-like growth factor 2 mRNA binding protein 3	10643_at	10643	1,13	5,989384071	3,53E-03	4,50%
KRT15	keratin 15	3866_at	3866	1,14	6,439305018	3,30E-04	1,25%
PRSS12	protease, serine, 12 (neurotrypsin, motopsin)	8492_at	8492	1,15	6,950500375	1,01E-03	2,32%
SEC24D	SEC24 family, member D (S. cerevisiae)	9871_at	9871	1,15	8,22444607	2,73E-05	0,30%
MICAL2	microtubule associated monoxygenase, calponin and LIM domain containing 2	9645_at	9645	1,15	6,141711945	3,24E-05	0,33%
BTN3A1	butyrophilin, subfamily 3, member A1	11119_at	11119	1,16	5,190296349	1,22E-05	0,19%
RERG	RAS-like, estrogen-regulated, growth inhibitor	85004_at	85004	1,17	9,365657718	2,17E-03	3,46%
RECK	reversion-inducing-cysteine-rich protein with kazal motifs	8434_at	8434	1,18	6,895746662	1,19E-03	2,55%
CPNE4	copine IV	131034_at	131034	1,18	7,21890412	8,60E-06	0,15%
PKIB	protein kinase (cAMP-dependent, catalytic) inhibitor beta	5570_at	5570	1,19	7,804843382	1,38E-03	2,75%
MUC1	mucin 1, cell surface associated	4582_at	4582	1,19	10,08713053	4,41E-04	1,45%
C14orf132	chromosome 14 open reading frame 132	56967_at	56967	1,20	7,746849978	1,23E-03	2,59%
SYTL5	synaptotagmin-like 5	94122_at	94122	1,20	8,141087654	2,00E-03	3,29%
EDN1	endothelin 1	1906_at	1906	1,21	6,815974591	4,25E-06	0,11%
LRP1	low density lipoprotein receptor-related protein 1	4035_at	4035	1,22	7,428282893	4,94E-06	0,12%
GBP3	guanylate binding protein 3	2635_at	2635	1,22	5,602847219	3,75E-06	0,11%
FAM46C	family with sequence similarity 46, member C	54855_at	54855	1,22	7,666389632	4,60E-05	0,40%
SLC4A8	solute carrier family 4, sodium bicarbonate cotransporter, member 8	9498_at	9498	1,22	7,508882342	1,20E-04	0,70%
TNS1	tensin 1	7145_at	7145	1,22	8,050285528	8,54E-06	0,15%
ABCD3	ATP-binding cassette, sub-family D (ALD), member 3	5825_at	5825	1,23	8,335110877	3,81E-06	0,11%
DKK3	dickkopf homolog 3 (Xenopus laevis)	27122_at	27122	1,24	7,431843058	9,10E-04	2,18%
FASN	fatty acid synthase	2194_at	2194	1,27	10,69221411	2,50E-04	1,07%
FRK	fyn-related kinase	2444_at	2444	1,28	7,295885411	4,19E-04	1,40%
SEPT9	septin 9	10801_at	10801	1,28	8,86983729	6,12E-05	0,47%
COL3A1	collagen, type III, alpha 1	1281_at	1281	1,30	7,573377467	4,91E-04	1,55%
RUNX2	runt-related transcription factor 2	860_at	860	1,30	7,431456704	2,23E-05	0,27%

Symbol	Description	Probe	Gene	logFC Treatment-Control	AveExpr Treatment-Control	P.Value Treatment-Control	FDR Treatment-Control
B2M	beta-2-microglobulin	567_at	567	1,30	9,556534906	9,60E-07	0,07%
LGALS3BP	lectin, galactoside-binding, soluble, 3 binding protein	3959_at	3959	1,31	9,949297705	3,19E-05	0,33%
PDE4D	phosphodiesterase 4D, cAMP-specific	5144_at	5144	1,31	6,718386857	2,04E-06	0,09%
NEURL	neuralized homolog (Drosophila)	9148_at	9148	1,31	8,241856985	2,07E-04	0,96%
SEMA3B	sema domain, immunoglobulin domain (Ig), short basic domain, secreted, (semaphorin) 3B	7869_at	7869	1,31	6,255981287	5,30E-06	0,12%
STAT1	signal transducer and activator of transcription 1, 91kDa	6772_at	6772	1,31	10,86613724	2,01E-05	0,25%
SLC9A7	solute carrier family 9 (sodium/hydrogen exchanger), member 7	84679_at	84679	1,31	7,883368851	2,28E-04	1,02%
CELSR2	cadherin, EGF LAG seven-pass G-type receptor 2 (flamingo homolog, Drosophila)	1952_at	1952	1,33	9,838710785	2,33E-04	1,04%
IFITM3	interferon induced transmembrane protein 3 (1-8U)	10410_at	10410	1,33	12,44956283	6,47E-06	0,13%
SPRED1	sprouty-related, EVH1 domain containing 1	161742_at	161742	1,34	7,346541722	2,79E-05	0,31%
RPS4Y1	ribosomal protein S4, Y-linked 1	6192_at	6192	1,35	5,552372194	2,44E-04	1,06%
C5orf4	chromosome 5 open reading frame 4	10826_at	10826	1,37	6,702335325	4,59E-06	0,12%
UBE2L6	ubiquitin-conjugating enzyme E2L 6	9246_at	9246	1,37	9,119108197	9,02E-06	0,16%
MGP	matrix Gla protein	4256_at	4256	1,38	9,541935291	6,31E-04	1,81%
C19orf66	chromosome 19 open reading frame 66	55337_at	55337	1,38	8,086477939	3,30E-06	0,10%
GMPR	guanosine monophosphate reductase	2766_at	2766	1,39	7,875015767	3,16E-05	0,33%
ARHGAP29	Rho GTPase activating protein 29	9411_at	9411	1,39	7,421044507	6,63E-04	1,86%
MX2	myxovirus (influenza virus) resistance 2 (mouse)	4600_at	4600	1,39	6,438006749	3,06E-04	1,20%
FAM38B	family with sequence similarity 38, member B	63895_at	63895	1,39	5,928980827	2,15E-04	0,98%
PARP12	poly (ADP-ribose) polymerase family, member 12	64761_at	64761	1,40	9,611994527	4,31E-05	0,39%
TMC5	transmembrane channel-like 5	79838_at	79838	1,40	7,313439219	3,79E-07	0,04%
DTX3L	deltex 3-like (Drosophila)	151636_at	151636	1,40	9,61943333	2,44E-05	0,28%
TAP1	transporter 1, ATP-binding cassette, sub-family B (MDR/TAP)	6890_at	6890	1,41	9,007700765	7,38E-07	0,06%
TPM2	tropomyosin 2 (beta)	7169_at	7169	1,41	6,315382133	3,17E-05	0,33%
HOXC13	homeobox C13	3229_at	3229	1,41	8,643856601	4,07E-05	0,38%
IFITM1	interferon induced transmembrane protein 1 (9-27)	8519_at	8519	1,41	11,72118703	2,46E-05	0,28%
MYO18A	myosin XVIIIA	399687_at	399687	1,42	7,825208346	1,18E-06	0,07%
PDGFRA	platelet-derived growth factor receptor, alpha polypeptide	5156_at	5156	1,44	5,90701297	1,19E-03	2,55%

Symbol	Description	Probe	Gene	logFC Treatment-Control	AveExpr Treatment-Control	P.Value Treatment-Control	FDR Treatment-Control
MSI2	musashi homolog 2 (Drosophila)	124540_at	124540	1,44	8,991082904	1,08E-06	0,07%
TRIM14	tripartite motif containing 14	9830_at	9830	1,45	8,627528615	5,59E-06	0,13%
COL6A3	collagen, type VI, alpha 3	1293_at	1293	1,45	6,62163837	6,57E-04	1,85%
ETV5	ets variant 5	2119_at	2119	1,45	5,559421664	7,28E-06	0,14%
TMPRSS4	transmembrane protease, serine 4	56649_at	56649	1,46	6,98786033	1,14E-04	0,68%
ARHGEF6	Rac/Cdc42 guanine nucleotide exchange factor (GEF) 6	9459_at	9459	1,46	7,140665186	5,97E-06	0,13%
C6orf192	chromosome 6 open reading frame 192	116843_at	116843	1,46	6,517304181	2,64E-05	0,30%
SAMHD1	SAM domain and HD domain 1	25939_at	25939	1,47	8,866562844	3,51E-06	0,10%
LOH3CR2A	loss of heterozygosity, 3, chromosomal region 2, gene A	29931_at	29931	1,47	6,54651044	8,13E-05	0,55%
BGN	biglycan	633_at	633	1,49	7,775465713	5,12E-05	0,43%
GOLM1	golgi membrane protein 1	51280_at	51280	1,49	8,826160737	3,64E-07	0,04%
BNC2	basonuclin 2	54796_at	54796	1,51	5,806704432	2,95E-04	1,19%
CYP1B1	cytochrome P450, family 1, subfamily B, polypeptide 1	1545_at	1545	1,53	8,681359645	3,30E-06	0,10%
C10orf81	chromosome 10 open reading frame 81	79949_at	79949	1,53	7,898296449	3,23E-08	0,02%
MUC5B	mucin 5B, oligomeric mucus/gel-forming	727897_at	727897	1,54	8,626094708	3,92E-05	0,37%
SLC7A5	solute carrier family 7 (cationic amino acid transporter, y+ system), member 5	8140_at	8140	1,54	11,50081234	1,13E-05	0,18%
MSN	moesin	4478_at	4478	1,54	6,403989318	7,51E-04	2,00%
FRMD3	FERM domain containing 3	257019_at	257019	1,54	7,540879962	1,48E-06	0,08%
SPRY4	sprouty homolog 4 (Drosophila)	81848_at	81848	1,54	6,33955723	4,57E-05	0,40%
BST2	bone marrow stromal cell antigen 2	684_at	684	1,54	8,157384428	2,49E-03	3,73%
NMI	N-myc (and STAT) interactor	9111_at	9111	1,56	6,479639869	1,03E-05	0,17%
GSTM1	glutathione S-transferase mu 1	2944_at	2944	1,56	6,009259918	4,05E-04	1,38%
MIR21	microRNA 21	406991_at	406991	1,56	9,592869762	1,54E-04	0,82%
CRAT	carnitine O-acetyltransferase	1384_at	1384	1,57	7,614550187	1,33E-07	0,03%
PEG10	paternally expressed 10	23089_at	23089	1,58	6,878569508	3,06E-07	0,04%
CCKAR	cholecystokinin A receptor	886_at	886	1,58	6,062904045	6,69E-04	1,87%
TFF1	trefoil factor 1	7031_at	7031	1,58	11,82069475	2,27E-05	0,27%
CNN3	calponin 3, acidic	1266_at	1266	1,59	5,533918747	2,55E-03	3,79%
HEG1	HEG homolog 1 (zebrafish)	57493_at	57493	1,59	6,262465196	8,46E-06	0,15%
MT1E	metallothionein 1E	4493_at	4493	1,60	7,826020391	2,32E-05	0,28%
RARRES3	retinoic acid receptor responder (tazarotene induced) 3	5920_at	5920	1,60	7,050441904	8,21E-06	0,15%
LXN	latexin	56925_at	56925	1,61	7,197593556	1,25E-05	0,19%
CADPS2	Ca++-dependent secretion activator 2	93664_at	93664	1,61	8,038317549	1,53E-05	0,21%
TAP2	transporter 2, ATP-binding cassette, sub-family B (MDR/TAP)	6891_at	6891	1,62	7,759885972	4,56E-07	0,04%
USP18	ubiquitin specific peptidase 18	11274_at	11274	1,62	9,230878782	1,42E-05	0,21%
NRIP1	nuclear receptor interacting protein 1	8204_at	8204	1,62	9,3695053	1,31E-05	0,20%

Symbol	Description	Probe	Gene	logFC Treatment-Control	AveExpr Treatment-Control	P.Value Treatment-Control	FDR Treatment-Control
ABCC3	ATP-binding cassette, sub-family C (CFTR/MRP), member 3	8714_at	8714	1,63	7,961604802	2,22E-03	3,49%
IFIH1	interferon induced with helicase C domain 1	64135_at	64135	1,63	8,092288478	1,74E-05	0,23%
DDR2	discoidin domain receptor tyrosine kinase 2	4921_at	4921	1,64	6,752625408	9,34E-04	2,22%
IFI35	interferon-induced protein 35	3430_at	3430	1,64	9,125504844	1,23E-05	0,19%
TLR3	toll-like receptor 3	7098_at	7098	1,65	6,344474864	2,95E-06	0,10%
CD44	CD44 molecule (Indian blood group)	960_at	960	1,65	8,94898628	1,71E-04	0,86%
UCA1	urothelial cancer associated 1 (non-protein coding)	652995_at	652995	1,65	5,628423175	8,56E-06	0,15%
PCDHB8	protocadherin beta 8	56128_at	56128	1,66	5,446032138	3,67E-04	1,31%
NT5E	5'-nucleotidase, ecto (CD73)	4907_at	4907	1,66	5,832109506	4,23E-03	4,98%
SVEP1	sushi, von Willebrand factor type A, EGF and pentraxin domain containing 1	79987_at	79987	1,66	6,251339017	3,49E-04	1,28%
NCRNA00052	non-protein coding RNA 52	145978_at	145978	1,67	5,929461106	1,08E-05	0,18%
TIAM1	T-cell lymphoma invasion and metastasis 1	7074_at	7074	1,68	8,773042075	2,49E-06	0,10%
HLA-B	major histocompatibility complex, class I, B	3106_at	3106	1,69	9,07722762	4,94E-05	0,42%
BDKRB2	bradykinin receptor B2	624_at	624	1,71	7,174015988	2,90E-06	0,10%
LDHB	lactate dehydrogenase B	3945_at	3945	1,71	6,733305254	6,21E-04	1,79%
EGR1	early growth response 1	1958_at	1958	1,71	9,564396843	3,65E-03	4,58%
SYT12	synaptotagmin XII	91683_at	91683	1,71	8,072182319	4,98E-05	0,42%
GPX8	glutathione peroxidase 8 (putative)	493869_at	493869	1,73	5,984429246	1,28E-03	2,63%
FSTL1	follistatin-like 1	11167_at	11167	1,74	6,881321453	1,63E-04	0,84%
TGFB3	transforming growth factor, beta 3	7043_at	7043	1,74	8,461791881	5,04E-06	0,12%
SP110	SP110 nuclear body protein	3431_at	3431	1,76	7,796298243	1,42E-05	0,21%
NAV1	neuron navigator 1	89796_at	89796	1,76	7,05274052	7,19E-08	0,02%
ALDOC	aldolase C, fructose-bisphosphate	230_at	230	1,76	8,483623162	1,17E-03	2,53%
RGS16	regulator of G-protein signaling 16	6004_at	6004	1,76	8,417586262	5,31E-07	0,05%
MX1	myxovirus (influenza virus) resistance 1, interferon-inducible protein p78 (mouse)	4599_at	4599	1,77	6,449030253	8,44E-05	0,56%
SPATS2L	spermatogenesis associated, serine-rich 2-like	26010_at	26010	1,78	7,178799967	3,46E-04	1,28%
TSKU	tsukushi small leucine rich proteoglycan homolog (Xenopus laevis)	25987_at	25987	1,78	10,32739865	2,64E-07	0,04%
USP41	ubiquitin specific peptidase 41	373856_at	373856	1,79	8,310724967	3,01E-06	0,10%
DDX58	DEAD (Asp-Glu-Ala-Asp) box polypeptide 58	23586_at	23586	1,81	9,447755245	1,66E-05	0,22%
LHFP	lipoma HMGIC fusion partner	10186_at	10186	1,82	8,218518602	1,34E-03	2,72%
PLSCR1	phospholipid scramblase 1	5359_at	5359	1,83	9,442454124	4,88E-06	0,12%
FBN1	fibrillin 1	2200_at	2200	1,83	6,081068838	3,26E-04	1,25%
MBOAT1	membrane bound O-acyltransferase domain containing 1	154141_at	154141	1,85	9,042516241	1,50E-06	0,08%
CYBRD1	cytochrome b reductase 1	79901_at	79901	1,86	7,480524932	8,74E-04	2,13%
CTSD	cathepsin D	1509_at	1509	1,86	10,95111405	4,22E-05	0,39%
SP100	SP100 nuclear antigen	6672_at	6672	1,86	8,253230328	3,07E-05	0,33%
NRXN3	neurexin 3	9369_at	9369	1,89	7,018792506	2,73E-07	0,04%

Symbol	Description	Probe	Gene	logFC Treatment-Control	AveExpr Treatment-Control	P.Value Treatment-Control	FDR Treatment-Control
PLK2	polo-like kinase 2	10769_at	10769	1,89	10,80404779	5,49E-06	0,13%
ANPEP	alanyl (membrane) aminopeptidase	290_at	290	1,90	6,488611603	2,47E-06	0,10%
GBP1	guanylate binding protein 1, interferon-inducible	2633_at	2633	1,90	5,20424888	8,55E-04	2,12%
EHF	ets homologous factor	26298_at	26298	1,91	9,02228668	1,76E-06	0,09%
IFIT5	interferon-induced protein with tetratricopeptide repeats 5	24138_at	24138	1,91	8,682144239	9,93E-06	0,17%
SAMD9L	sterile alpha motif domain containing 9-like	219285_at	219285	1,92	6,009456877	6,70E-05	0,50%
PSMB9	proteasome (prosome, macropain) subunit, beta type, 9 (large multifunctional peptidase 2)	5698_at	5698	1,93	7,776233841	4,02E-07	0,04%
SUSD3	sushi domain containing 3	203328_at	203328	1,93	7,909122887	3,00E-05	0,32%
H19	H19, imprinted maternally expressed transcript (non-protein coding)	283120_at	283120	1,95	9,255262101	3,01E-06	0,10%
MPPED2	metallophoesterase domain containing 2	744_at	744	1,95	8,348080119	2,83E-04	1,16%
IFI6	interferon, alpha-inducible protein 6	2537_at	2537	1,96	11,51967212	7,92E-05	0,54%
SLC7A11	solute carrier family 7, (cationic amino acid transporter, y+ system) member 11	23657_at	23657	2,01	7,294256647	7,65E-05	0,53%
EMP3	epithelial membrane protein 3	2014_at	2014	2,09	7,371324685	4,76E-06	0,12%
APOL6	apolipoprotein L, 6	80830_at	80830	2,11	6,276044523	8,09E-07	0,06%
DUSP4	dual specificity phosphatase 4	1846_at	1846	2,12	6,673716905	2,51E-06	0,10%
IFIT2	interferon-induced protein with tetratricopeptide repeats 2	3433_at	3433	2,14	5,99411937	2,22E-06	0,09%
SDK2	sidekick homolog 2 (chicken)	54549_at	54549	2,16	6,856323797	9,70E-06	0,16%
AFF3	AF4/FMR2 family, member 3	3899_at	3899	2,16	8,053518591	6,80E-07	0,06%
EGR3	early growth response 3	1960_at	1960	2,16	7,449399602	6,57E-06	0,13%
CMPK2	cytidine monophosphate (UMP-CMP) kinase 2, mitochondrial	129607_at	129607	2,21	8,542190577	5,68E-06	0,13%
TGFBI	transforming growth factor, beta-induced, 68kDa	7045_at	7045	2,21	6,406009873	5,39E-04	1,65%
PARP14	poly (ADP-ribose) polymerase family, member 14	54625_at	54625	2,22	9,027314074	7,14E-06	0,14%
CAV1	caveolin 1, caveolae protein, 22kDa	857_at	857	2,23	6,684728209	3,76E-05	0,36%
MT2A	metallothionein 2A	4502_at	4502	2,23	11,38264217	3,99E-07	0,04%
BDKRB1	bradykinin receptor B1	623_at	623	2,26	7,595901607	4,00E-06	0,11%
FAM5B	family with sequence similarity 5, member B	57795_at	57795	2,33	7,990252174	2,16E-07	0,04%
TGM2	transglutaminase 2 (C polypeptide, protein-glutamine-gamma-glutamyltransferase)	7052_at	7052	2,35	7,78116388	2,88E-05	0,31%
LPAR1	lysophosphatidic acid receptor 1	1902_at	1902	2,37	6,575360477	2,56E-05	0,29%
HERC6	hect domain and RLD 6	55008_at	55008	2,39	8,716003657	1,64E-04	0,84%
AGR2	anterior gradient homolog 2 (Xenopus laevis)	10551_at	10551	2,40	7,146446502	2,06E-08	0,02%

Symbol	Description	Probe	Gene	logFC Treatment-Control	AveExpr Treatment-Control	P.Value Treatment-Control	FDR Treatment-Control
IFI16	interferon, gamma-inducible protein 16	3428_at	3428	2,45	5,317007642	6,65E-04	1,86%
TCF21	transcription factor 21	6943_at	6943	2,47	6,808045795	5,20E-06	0,12%
MUCL1	mucin-like 1	118430_at	118430	2,48	8,156771675	2,39E-08	0,02%
LOX	lysyl oxidase	4015_at	4015	2,50	6,523605374	4,87E-05	0,42%
PADI2	peptidyl arginine deiminase, type II	11240_at	11240	2,51	7,612124221	7,07E-08	0,02%
PARP9	poly (ADP-ribose) polymerase family, member 9	83666_at	83666	2,52	8,043390009	1,92E-05	0,24%
VIM	vimentin	7431_at	7431	2,57	7,657125406	1,13E-05	0,18%
CTGF	connective tissue growth factor	1490_at	1490	2,65	8,288413238	1,51E-05	0,21%
XAF1	XIAP associated factor 1	54739_at	54739	2,66	10,23470051	1,57E-04	0,82%
RSAD2	radical S-adenosyl methionine domain containing 2	91543_at	91543	2,67	7,794188724	1,61E-05	0,22%
FN1	fibronectin 1	2335_at	2335	2,68	7,430931476	7,88E-05	0,54%
OAS1	2',5'-oligoadenylate synthetase 1, 40/46kDa	4938_at	4938	2,70	9,344873561	5,70E-06	0,13%
DDX60L	DEAD (Asp-Glu-Ala-Asp) box polypeptide 60-like	91351_at	91351	2,72	8,058742044	1,48E-06	0,08%
DDX60	DEAD (Asp-Glu-Ala-Asp) box polypeptide 60	55601_at	55601	2,79	8,523992857	6,16E-06	0,13%
OAS3	2'-5'-oligoadenylate synthetase 3, 100kDa	4940_at	4940	2,80	8,997755199	1,89E-06	0,09%
CXCL12	chemokine (C-X-C motif) ligand 12	6387_at	6387	2,81	8,014471187	8,32E-08	0,02%
SCNN1A	sodium channel, nonvoltage-gated 1 alpha	6337_at	6337	2,89	7,688196305	3,01E-08	0,02%
RET	ret proto-oncogene	5979_at	5979	2,98	8,368634107	1,88E-07	0,03%
IFIT3	interferon-induced protein with tetratricopeptide repeats 3	3437_at	3437	3,06	6,634329881	5,65E-08	0,02%
ANXA1	annexin A1	301_at	301	3,10	6,803049914	6,22E-05	0,48%
LOC402778	CD225 family protein FLJ76511	402778_at	402778	3,12	7,506900476	3,35E-06	0,10%
SAMD9	sterile alpha motif domain containing 9	54809_at	54809	3,24	8,386274014	1,19E-06	0,07%
MMP2	matrix metallopeptidase 2 (gelatinase A, 72kDa gelatinase, 72kDa type IV collagenase)	4313_at	4313	3,31	7,228038706	3,45E-06	0,10%
OAS2	2'-5'-oligoadenylate synthetase 2, 69/71kDa	4939_at	4939	3,32	9,504688775	1,18E-04	0,69%
PRSS23	protease, serine, 23	11098_at	11098	3,64	7,832283105	1,20E-06	0,07%
IFI44	interferon-induced protein 44	10561_at	10561	3,78	6,601749899	1,89E-07	0,03%
IFIT1	interferon-induced protein with tetratricopeptide repeats 1	3434_at	3434	3,86	9,039040561	8,79E-06	0,15%
IFI44L	interferon-induced protein 44-like	10964_at	10964	4,22	8,988775342	5,30E-06	0,12%
SPARC	secreted protein, acidic, cysteine-rich (osteonectin)	6678_at	6678	4,53	8,432603952	6,74E-06	0,14%

Curriculum Vitae

Elke Ziegler
02.10.1981, born in Darmstadt, Germany

Papenhöhe 14, 25335 Elmshorn, Germany
elke.ziegler@gmail.com

Professional experience

2009/07 - 2012/12	Universtätsmedizin Göttingen Scientific assistant
2008/05 - 2009/05	Rheinische Friedrich-Wilhelms-Universität Bonn Scientific assistant
2007/03 - 2008/03	Sonnen-Apotheke Wolfhagen Pharmacist

Education

2009/10 - 2012/09	Georg-August-Universität Göttingen International PhD program Molecular Medicine
2010/09 - 2012/07	Verwaltungs- und Wirtschaftsakademie Kassel Graduation: Economist in Health Care (Gesundheits- und Sozial-Ökonomin (VWA))
2008/04 - 2009/03	Rheinische Friedrich-Wilhelms-Universität Bonn Graduation: Degree in Pharmaceutics (Diplom-Pharmazeutin)
2001/10 - 2005/09	Johann Wolfgang Goethe-Universität Frankfurt/Main Graduation: License to practice Pharmacy (Approbation)
1992 - 2001	Liebfrauenschule Bensheim, Gymnasium Graduation: Abitur